STUDY OF WAVE IMPACT LOADS ON COMPONENTS OF STILLING WAVE BASIN ON A VERTICAL SEAWALL

A THESIS SUBMITTED TO
THE GRADUATE SCHOOL OF NATURAL AND APPLIED SCIENCES
OF
MIDDLE EAST TECHNICAL UNIVERSITY

BY

MUSTAFA GÖKAY ALTUNBAŞ

IN PARTIAL FULFILLMENT OF THE REQUIREMENTS
FOR
THE DEGREE OF MASTER OF SCIENCE
IN
CIVIL ENGINEERING

AUGUST 2022

Approval of the thesis:

STUDY OF WAVE IMPACT LOADS ON COMPONENTS OF STILLING WAVE BASIN ON A VERTICAL SEAWALL

submitted by **MUSTAFA GÖKAY ALTUNBAŞ** in partial fulfillment of the requirements for the degree of **Master of Science** i**n Civil Engineering, Middle East Technical University** by,

Prof. Dr. Halil Kalıpçılar
Dean, Graduate School of **Natural and Applied Sciences** _____

Prof. Dr. Erdem Canbay
Head of the Department, **Civil Engineering** _____

Assist. Prof. Dr. Gülizar Özyurt Tarakcıoğlu
Supervisor, **Civil Engineering, METU** _____

Assist. Prof. Dr. Doğan Kısacık
Co-Supervisor, **Civil Engineering, IZTECH** _____

Examining Committee Members:

Prof. Dr. Ahmet Cevdet Yalçıner
Civil Engineering, METU _____

Assist. Prof. Dr. Gülizar Özyurt Tarakcıoğlu
Civil Engineering, METU _____

Assoc. Prof. Dr. Elif Oğuz
Civil Engineering, METU _____

Assist. Prof. Dr. Cüneyt Baykal
Civil Engineering, METU _____

Assist. Prof. Dr. Doğan Kısacık
Civil Engineering, IZTECH _____

Date: 24.08.2022

I hereby declare that all information in this document has been obtained and presented in accordance with academic rules and ethical conduct. I also declare that, as required by these rules and conduct, I have fully cited and referenced all material and results that are not original to this work.

Name Last name : Mustafa Gökay Altunbaş

Signature :

ABSTRACT

STUDY OF WAVE IMPACT LOADS ON COMPONENTS OF STILLING WAVE BASIN ON A VERTICAL SEAWALL

Altunbaş, Mustafa Gökay
Master of Science, Civil Engineering
Supervisor: Assist. Prof. Dr. Gülizar Özyurt Tarakcıoğlu
Co-Supervisor: Assist. Prof. Dr. Doğan Kısacık

August 2022, 107 pages

In this study, the wave pressure on components of Stilling Wave Basin (SWB) is investigated by analyzing the physical model experiment data of wave pressures for various hydrodynamic conditions. SWB is a structure that can be used for optimizing the crest height to achieve lower overtopping conditions especially in urban areas. The experiments are based on assessing the performance of SWB on a vertical seawall for which limited research exists. Wave pressure data on the seaward storm walls (both rows) and the landward storm wall behind a promanade is analyzed as individual components as well as the whole SWB structure to determine the magnitude and type of wave pressure. The comparison of wave pressure can be used to determine the effect of SWB configuration on the wave loads acting on each component. The results show that additional superstructures on the seaside of the SWB, the pressure measurement of the landward storm wall decreases remarkably. Storm wall with gaps on the seaside causes more pressure in front of the storm wall. Placing bullnoses as a superstructure on top of the storm wall causes pressure increase on seaward storm wall structure but decrease on the landward structures. The empirical formulations of Goda (2010) including maximum pressures usually

underpredict the pressures. However, the scatter is much higher for the maximum pressure dataset.

Keywords: Wave Pressure, Impact Loads, Stilling Wave Basin (SWB), Vertical Wall Breakwater, Storm Wall.

ÖZ

DÜŞEY YÜZLÜ KIYI YAPILARI ÜZERİNDEKİ DURGUN DALGA HAVUZU BİLEŞENLERİNE ETKİYEN DALGA YÜKLERİNİN İNCELENMESİ

Altunbaş, Mustafa Gökay
Yüksek Lisans, İnşaat Mühendisliği
Tez Yöneticisi: Dr. Öğr. Üyesi Gülizar Özyurt Tarakcıoğlu
Ortak Tez Yöneticisi: Dr. Öğr. Üyesi Doğan Kısacık

Ağustos 2022, 107 sayfa

Bu çalışmada, Durgun Dalga Havuzunun (DDH) bileşenleri üzerindeki dalga basıncı çeşitli hidrodinamik koşullarda gerçekleştirilen deneylerden elde edilen analiz sonuçlarına göre incelenmiştir. İlk kez Belçika kıyılarında kullanılmış olan DDH sistemi, kentsel kıyı bölgelerinde düşük dalga aşma koşulları sağlanabilmesi için kret yüksekliğini optimize etmek için tasarlanmıştır. Düşey yüzlü kıyı yapıları üzerinde durgun dalga havuzu sistemlerine ait çalışmalar literatürde sınırlı sayıdadır. Bu çalışmada, yapının denize bakan duvarları ve bir yürüyüş yolunun arkasındaki karadaki parapet üzerindeki ölçülen dalga basıncı verileri, hem bileşenler hem de bütün DDH yapısı için analiz edilmiştir. Analizler arası yapılacak karşılaştırma, DDH yapısının her bir farklı bileşene etki eden dalga basınçlarını nasıl değiştirdiğini ortaya koymuştur. Çalışmanın sonunda DDH yapısının denize bakan ve karada bulunan duvarlarının basınç ölçümlerinde dikkat çekici düzeyde düşüş gözlemlenmiştir. Denize bakan parapetin boşluklu yapıdan oluşması, parapetin önünde daha fazla basınca sebep olmaktadır. Üst yapı olarak parapetin üzerine küt burun eklenmesi denize bakan parapetin üzerinde daha çok basınca neden olurken, kara tarafında olan parapetin üzerindeki basınçta düşüşe sebep olmaktadır. Goda'nın

(2010) maksimum basınç hesabını da içeren formülleri ile hesaplanan basınçlar genellikle daha düşük sonuç vermektedir. Ancak bu çalışmada maksimum basınç verileri için varyans beklenenden çok daha yüksektir.

Anahtar Kelimeler: Dalga Basıncı, Çarpma Etkili Yükler, Durgun Dalga Havuzu (DDH), Düşey Yüzlü Dalgakıran, Parapet.

To my family and beloved ones

ACKNOWLEDGMENTS

I would like to express my sincere gratitude to my supervisor Assist. Prof. Dr. Gülizar Özyurt Tarakcıoğlu for her guidance and patience throughout the study. I could not have undertaken this process without her precious assistance, enormous contributions and unlimited encouragement. I would also like to thank Assist. Prof. Dr. Doğan Kısacık for sharing his knowledge and experience to support my study.

I would like to extend my appreciation to Assist. Prof. Dr. Cüneyt Baykal, who generously provided knowledge and guided me at the beginning of my masters study.

I would also like to extend my sincere thanks to Assist. Prof. Dr. Aslı Numanoğlu Genç who inspired me to study coastal engineering in my undergraduate education. This thesis would not be possible without her.

I am also grateful to my friends Berkay Akyol and Günay Gazaloğlu whom I shared unforgettable memories throughout my masters study.

This work is partially funded by Middle East Technical University (METU) under the grant number BAP-08-11-2015-036, Assessment of Coastal Floods in Inner Bay of Izmir and A Solution Strategy: Stilling Wave Basin.

TABLE OF CONTENTS

LIST OF TABLES

TABLES

LIST OF FIGURES

FIGURES

LIST OF ABBREVIATIONS

ABBREVIATIONS

BAP	Scientific research project
BOW	Broken Wave
BW	Breaking wave
BWLAT	Breaking wave with large air trap
BWSAT	Breaking wave with small air trap
CPS	Circular cum parabolic seawall
FSS	Flaring shaped seawall
MAE	Mean absolute error
METU	Middle East Technical University
NBW	Non-breaking wave
RMSE	Root mean square error
SBW	Slightly breaking wave
SWB	Stilling wave basin
SWL	Still-water level

LIST OF SYMBOLS

SYMBOLS

β	Wave approach angle
d_c	Depth of water
d_f	Dimension between SWL and storm wall
d_w	Depth of storm wall
Δx	Width along stilling wave basin
H	Wave height
$H_{1/3}$	Significant wave height
H_{max}	Maximum wave height
H_{s_o}	Initial significant wave height
h	Depth of water
h'	Buoyancy depth
h_b	Seaward side distance
h_s	Depth of water
L	Wave length
η^*	Wave pressure elevation
P	Wave pressure

P_u	Ultime wave pressure
ρ	Density of water
T	Wave period
Z	Placement height

CHAPTER 1

INTRODUCTION

Coastal areas are the most popular areas as they provide resources for a variety of economic and social activities. Therefore, a lot of infrastructure had been built along the shores especially in urban regions. However, roads, promenades and buildings become vulnerable areas to disasters as they are located very close to the sea and depending on the coastal protection measures available in the region. Also, climate change and its effects are increasing the vulnerability of these areas. In fact, some of these regions already experienced coastal flooding during storms which negatively effect all the activities in the region. In Figure 1.1, the coastal flooding due to overtopping in Kordon Region, Izmir is presented.

Figure 1.1: Flood caused by wave overtopping in Kordon Region, Izmir (Ozyurt Tarakcioglu et al., 2015)

Wave overtopping is the main wave-structure interaction process in the urban regions for the design of coastal protection strutuctures such as dikes and seawalls. Altough sloped structures such as dikes are commonly used around the world, vertical structures such as seawalls are usually more common in urban areas especially combined with promenades for recreational purposes. Seawalls are

impermeable and durable structures with their vertical face through the wave direction. However, the vertical wall increases the wave height due to high reflection and therefore experiences higher overtopping volumes as well wave loadings compared to sloped structures. To decrease the effect of the wave overtopping to the promenade (land behind the wall), several superstructures can be designed on the seawall such as storm walls, storm walls with bullnose, wide promenades and stilling wave basins. Stilling wave basin (SWB) is a superstructure that can be used to optimize the crest height to achieve lower overtopping conditions especially in urban coastal areas. The stilling wave basin is a structure which combines a double row of shifted storm walls (partially permeable due to gaps) on the seaside, a wide promenade and a landward storm wall (continous without gaps) as shown in Figure 1.2.

The overtopping performance of a SWB design on a vertical seawall under a range of hydrodynamic conditions are studied by Ozyurt Tarakcioglu et al. (2015), Kisacik et al. (2019) and Kisacik et al. (2022) for BAP Project 08-11-2015-036, "Assessment of Coastal Floods in Inner Bay of Izmir and A Solution Strategy: Stilling Wave Basin (İzmir İç Körfezde Yaşanan Fırtına Taşkınlarının Araştırılması ve Taşkınların Önlenmesi İçin Bir Öneri: Durgun Dalga Havuzu Modeli)". In the BAP project, SWB superstructure is investigated to reduce the overtopping and control flooding along the Kordon coast, Izmir, Türkiye. The physical modelling experiments are performed in METU Civil Engineering Department Coastal and Ocean Laboratory for optimization of SWB design and additional superstructures such as promenade and parapets with bullnose. In the project each structure and components are tested under a wide range of hydrodynamic conditions and it is resulted that the optimized SWB with bullnose is a very good alternative when crest height is constant. As part of this BAP project, wave pressure data was also measured on the components of SWB configurations to understand the wave loads during overtopping events.

Kisacik et al. (2022) compared the overtopping performance of SWB focusing on other superstructures such as storm wall on the seaside, only promenade or promenade and stormwall at the land side as an extension of BAP Project results.

They showed how the overtopping performance of SWB is improved compared to its components and the considerations to minimize the overtopping for an existing seawall.

The wave load acting on the vertical wall is another important design consideration for the stability of the structure. There exists several empricial formulas and methods to determine the wave pressure and loads along the vertical breakwaters or seawalls. However, the literature on the storm walls (crown wall in the case of breakwater), bullnoses attached to storm walls are limited especially for vertical wall structures. Type of the wave condition (breaking, non-breaking) is an important criteria for determining the wave pressures and loads. It is more complex to analyze the wave pressure under breaking waves as impulsive loads are observed that have very high pressures over a very short time. Although these pressures are exerted for a very short duration, these are the loads that cause the damage on the structure. Therefore, it is important to know the wave pressure acting on both the vertical seawall as well as the individual components of the SWB superstructure for design considerations as well as the safety of other users.

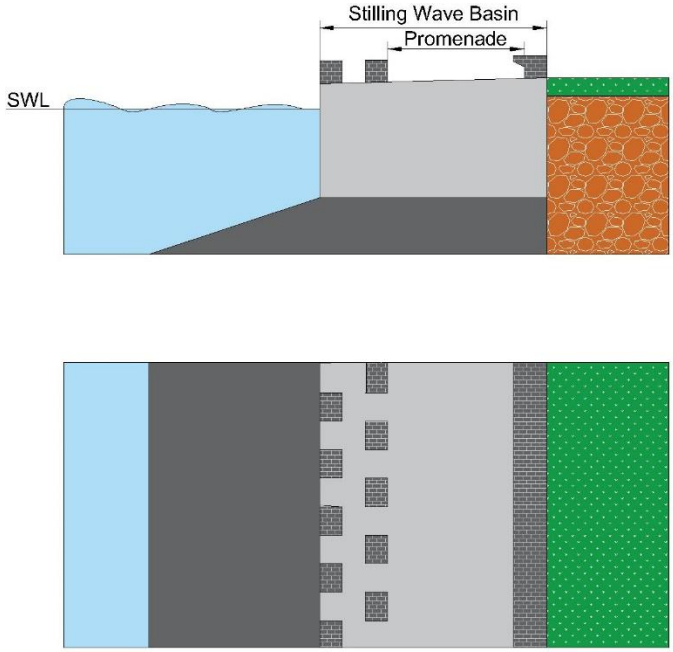

Figure 1.2: Basic descriptive figure of SWB

Using the experimental wave pressure data measured during the BAP Project 08-11-2015-036 (Ozyurt Tarakcioglu et al., 2015), this thesis evaluates the wave pressures for different combinations of SWB components and superstructures. In the BAP project, the SWB alternatives to reduce the wave overtopping and flooding along the Kordon coastal area in Izmir, Türkiye is discussed. The main aim of this thesis is to analyze wave loads on a seawall by considering wave height, wave period, wave breaking and geometry of the stilling wave basin components with help of performed experiment's data. Wave pressure data on the seaward storm walls and the landward storm wall behind a promenade are analyzed as individual components as well as the whole SWB structure to determine the magnitude and type of wave loads. Each superstructure combination was experimented with wide range hydrodynamic conditions with wide ranged different wave parameters. These analyses are discussed based on the following points:

- The wave pressure on different superstructures on a vertical seawall under a variety of hydrodynamic conditions
- The effect of bullnose on the wave pressure along the vertical seawall
- The effect of bullnose on the wave pressure on the storm wall for both seaside and landward locations
- The wave pressure on the storm wall at different locations (seaside and landward)
- The effect of gaps on the wave presssure at the storm wall at the seaside
- The effect of gaps on the wave pressure on the vertical wall
- The performance of formulation of Goda (2010) and its extension for wave pressure along the vertical seawall considering average and maximum wave pressures

Although wave pressure on the some of the superstructures studied in this thesis are studied in the literature, many of these super structures (such as promenade and storm wall, storm wall with bullnose) are located on a dike which has a sloped geometry that effects the wave characteristics significantly different than vertical seawall. Additionally, to the best of our knowledge, there exists no other study on wave

pressure measurements for SWB superstructure and its components on a vertical seawall. The available literature on similar studies are highlighted in the literature review (Chapter 2).

In Chapter 3, the experimental setup of BAP project, analysis methodology of the pressure data and the empirical equations of Goda (2010) are presented. In Chapter 4, the results of the data analysis for wave conditions and wave pressures are presented for individual setups. In Chapter 5, the effect of location of seawalls, bullnose, promenade and the gaps on the wave pressure are discussed focusing on the components of SWB. Performance of the existing formulations for vertical seawall is also presented. In Chapter 6, conclusions, summarizations, and future study recommendations are indicated. Finally, the assesment of component stability and usage of stilling wave basin in urbanized coastal areas is discussed.

CHAPTER 2

LITERATURE REVIEW

In the literature review chapter, the information related to vertical wall breakwaters, wave loadings, wave pressure definitions and previous pressure studies for the vertical wall breakwaters, wave classifications, components of the stilling wave basin (SWB) and applications of different superstructures and gaps in the literature for the stilling wave basins with vertical structures are given respectively. Also, the relations between past research and studies are stated.

2.1 Wave Loads and Pressures on Vertical Structures

Coastal structures for preventing the shorelines from storms and extreme events become more important in the recent periods of time. Besides, with the increase of the value for the urbanization in the coastal areas, these structures become obligatory. In the literature, coastal structures can divided into two based on their geometries: sloped structures and vertical structures. Wave-structure interaction along the sloped structures are different than the vertical structures (where the interaction happens quickly) changing the hydrodynamics of the wave when it reaches the superstructure or the crest of the structure. Vertical wall breakwaters or seawalls are one type of coastal protection structures that are constructed all around the planet. Moreover, the vertical breakwaters are the very often constructed type of breakwaters which face with the largest wave pressures created by biggest forces on the structure surface.

In the literature, there are several studies for designing, analyzing and discussing the vertical wall breakwaters. In the design, there are several options exist as well as the applications. When some structures have sloped structures such as dikes which are

very common to use in design, some other vertical coastal structure designs may consist of seawalls which are preferred in urban coastal areas.

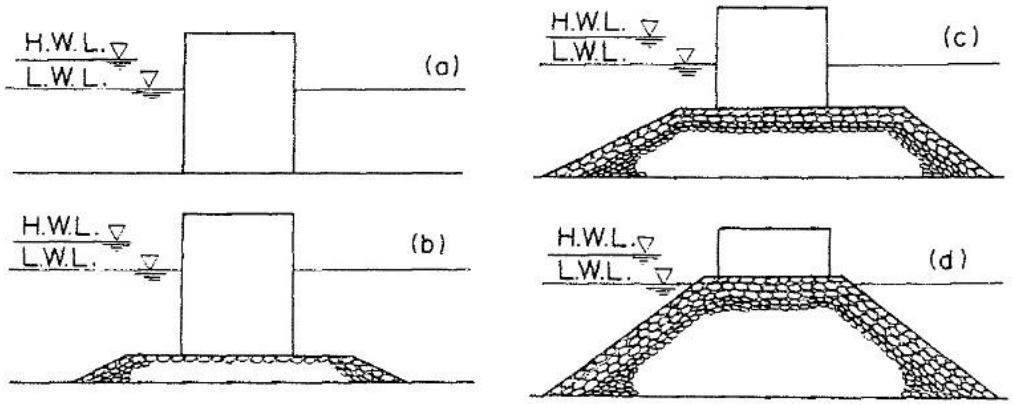

Figure 2.1: Vertical wall breakwater types (Takahashi, 2002)

Takahashi (2002) described several composite breakwaters in his study. Furthermore, he stated that "the rubblemound/rubblefoundation of composite breakwaters is vital to prevent the failure of the upright section by scouring, as well as stabilizing the foundation against the wave force and caisson weight." Also, there are some studies for the parameters of the designing vertical wall breakwaters which are wave overtopping, wave forces and wave pressure.

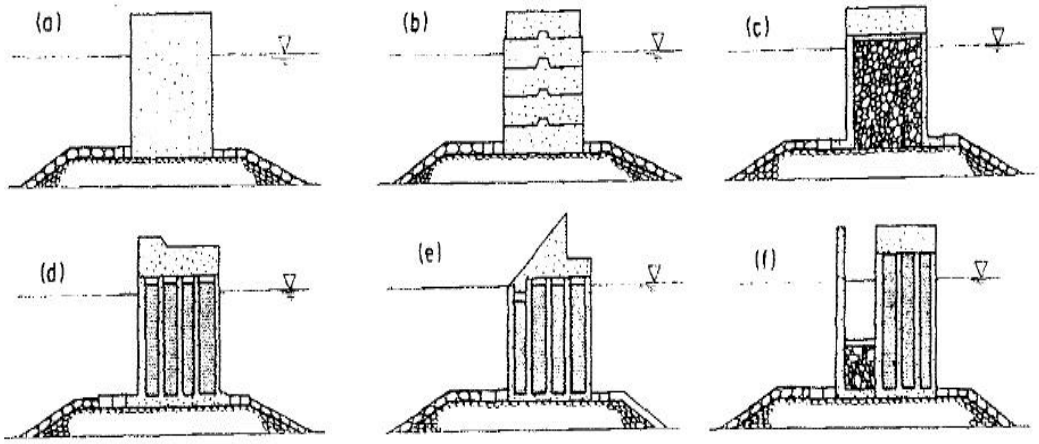

Figure 2.2: Composite breakwaters (Takahashi, 2002)

The loads acting on the vertical coastal protection structures are classified as quasi-static loads and impact loads. Quasi-static wave loads and impact wave loads are described by different researchers until today.

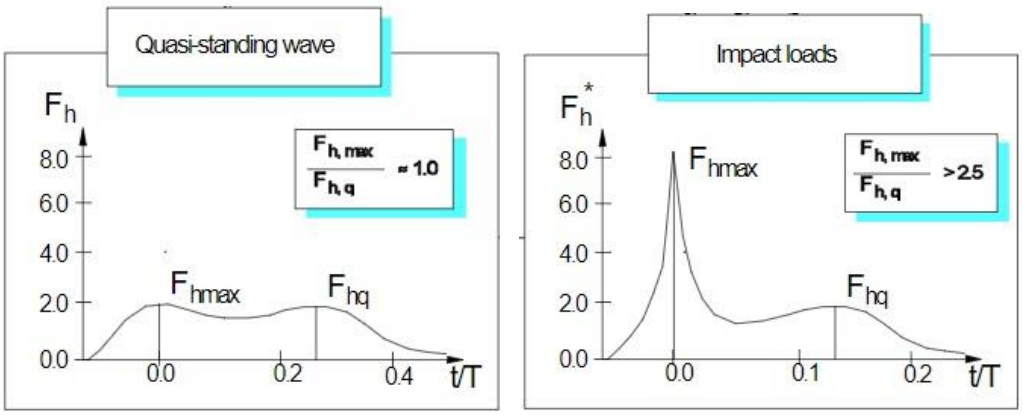

Figure 2.3: Quasi-static and impact wave definitions in PROVERBS (Oumeraci et al., 2001)

There are several formulations in the literature to calculate the wave loads. The calculation of the quasi-static wave loads have been studied by Sainflou (1928) at the beginning which uses Stokes theory. For the quasi-static loads, Sainflou (1928) suggested a full reflective model to calculate the pressure. He assumed the distribution of the pressure is linear between the surface elevation and bottom level.

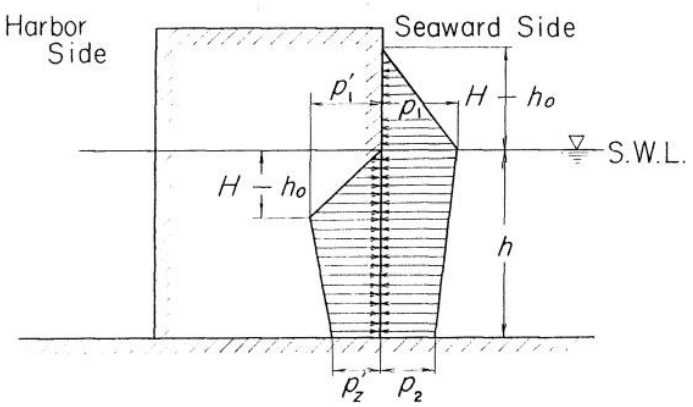

Figure 2.4: Simplified Sainflou pressure formula (Takahashi, 2002)

Further, Goda (2010) studied the formula for pressure distribution on the vertical structures by considering the wave height is taken seaward of the surf zone. Today,

commonly used method for wave loads on vertical structures is by Goda (2010). Goda (2010) studied a fourth order theory to design vertical wall breakwaters by assuming a trapezoidal pressure distribution on the structure. He contributed the literature with the formulation of the wave pressure on an upright section by considering both quasi-static and impact loads.

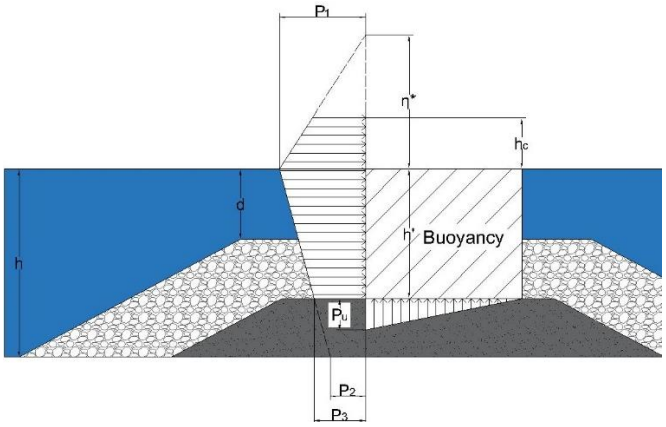

Figure 2.5: Goda pressure distribution

Impact loads are larger loads than the quasi-static loads, as can be realized by their names. Impact loads on the vertical wall breakwaters are disccussed earliest by Hiroi (1919) who searched out the wave pressure as a uniform distribution along the seawall surface.

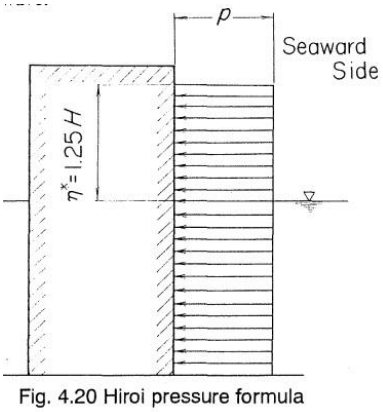

Figure 2.6: Hiroi pressure distribution (Takahashi, 2002)

Since then, the pressure studies on vertical wall breakwaters are continued till the approach of Goda (2010) became very popular in the design by suggesting relative

pressure distribution for both quasi-static and impact loads. As the history continues, the part of impact loads in Goda (2010) shaped with the contributions of Takahashi et al. (1994) by extended Goda formula.

Oumeraci et al. (1993) studied the classification of the wave loads on vertical structures in the literature and focused on the onset of breaking in front of vertical structures with respect to steepness. Their aim was determine the wave impact on the surface of vertical wall. At the end, they identified and classified the breaker types and supported their study with observations. Today, these approaches studied by Oumeraci et al. (1993) enchanted and developed by follow-up studies (Kirkgoz, 1995; Kisacik et al., 2012). On the other hand, the shape of the breakers also has a remarkable effect on the impact pressures. Time by time, different case studies has been performed to understand the relationship between wave forces and wave pressures. There are several studies performed to prove the relationship between breaker types and wave impact for seawalls. However, the major discussions are indicated by Kirkgoz (1995) and Oumeraci et al. (1993) with the help of experiments. At the end, it was seen that the wave breaking can be classified according to breaker shapes. Furthermore, "… the breaker type has an important influence on the magnitudes of impact pressures and forces." Kisacik et al. (2012) stated.

On seawalls, the shape of the front side of breaking wave has a significant consequence on the wave impact pressure. While discussing the wave pressure, one of the incontrovertible things is wave breaking. Moreover, Hattori et al. (1994) stated that "It is, therefore, reasonable to characterize the impact pressures by colliding condition of breaking waves.". Mainly, the shock pressures causes wave breaking. In the following, the pressure analysis on the breakwater with transducers started to be a topic in the literature with Hattori et al. (1994). They are the first researchers that used wave gauges for gathering data to use in their pressure study. They investigated the results with dimensionless graphs to make comments, both for the waves with air and without air. He also discussed the results of regression analysis performed to show the relationship between computational and experimental values.

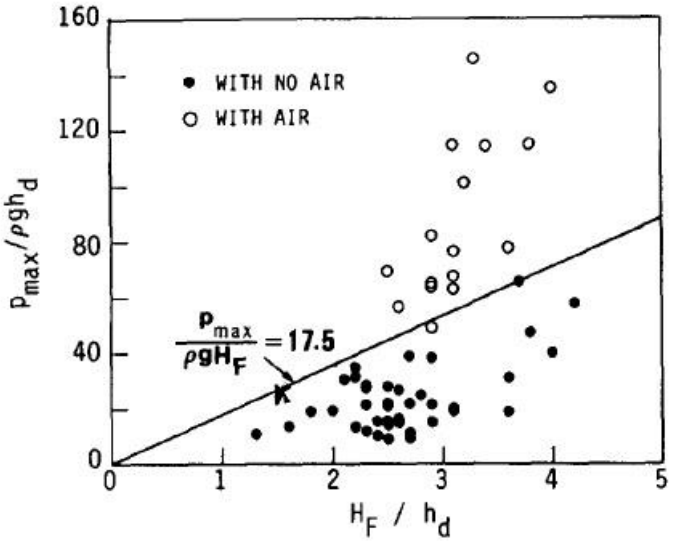

Figure 2.7: Relation between $P_{max}/\rho gh$ and H/h (Hattori et al., 1994)

Takahashi (1996) describes the types of the impulsive pressure as three different types. These are Wagner Type, Transition Type and Bagnold Type. When the angle of the wave front is larger than the curvature angle of the wave, Wagner type pressure occurs on the seawall. When β is negative, Bagnold type pressure occurs. When β is between these values, a transition type pressure acts generating an impulsive pressure similar to the Bagnold type.

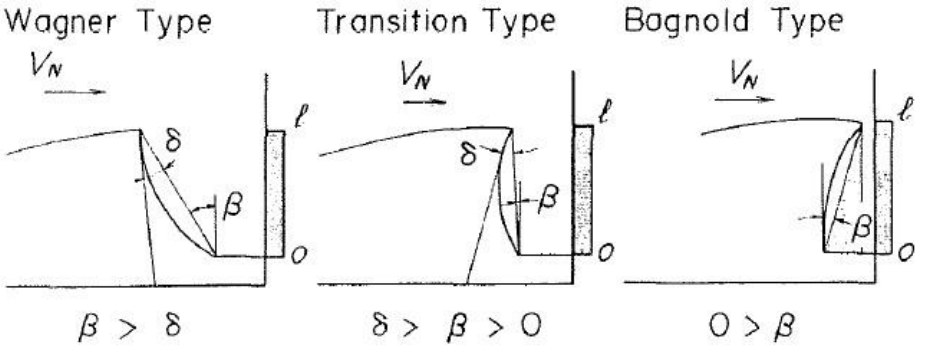

Figure 2.8: Three types of impulsive pressure (Takayashi , 1996)

After some time, Kortenhaus et al. (2001) brought a new sight to design methods for wave loading. They summarized their study with an overview of design methods for wave loading table for different waves which are quasi-static, impact and broken

waves. On the other hand, Hull & Müller (2002) investigated the impact pressure for different wave types on the seawall surface by discussing different breaker types.

Table 1: Overview of design methods for wave loading (Kortenhaus et al., 2001)

Author	Year	Pres-sures	Forces	Uplift	Comments
Quasi-Static Waves					
Sainflou	1928	yes	yes, but difficult	no	vertical wall, no berm
Miche-Rundgren	1944 1958	yes	yes	no	design curves from SPM, 1984
Goda	1985	yes	yes	yes	most-widely used design method
Impact Waves					
Hiroi	1919	yes	yes	no	vertical wall
Bagnold	1939	-	-	-	conceptual model only
Minikin	1963	yes	yes	no	sometimes incorrect dimen-sions!
Ito	1971	yes	yes	yes	
Blackmore & Hewson	1984	yes	yes	no	
Partenscky	1988	yes	not given	no	air content of wave needed
Kirkgöz	1990 1995	yes	yes	no	vertical wall only
Takahashi	1994	yes	yes	yes	extension of Goda model
Allsop et al.	1996	no	yes	yes	
Walkden et al.	1996	no	yes	no	relation of forces and rise time
Oumeraci & Kortenhaus	1997	yes	yes	yes	time-dependent approach!
McConnell	1998	no	yes	no	amendment of O&K, 1997
Hull & Müller	1998	yes	yes	no	amendment of O&K, 1997
Vicinanza	1998	yes	yes	no	amendment of O&K, 1997
Broken Waves					
SPM	1984	yes	yes	no	vertical walls only
Camfield	1991	yes	yes	no	amendment of SPM, 1984
Jensen	1984	yes	yes	yes	Crown walls
Bradbury & Allsop	1988	yes	yes	yes	Crown walls
Pedersen	1997	yes	yes	yes	Crown walls
Martín et al.	1997	yes	yes	yes	Crown walls

As a part of the design, Oumeraci et al. (2001) studied PROVERBS for vertical wall breakwaters depending on the parameters berm height, berm width and wave height with respect to wave loading. Waves are classified by using PROVERBS as if they are small waves or large waves. For vertical walls, small waves indicate quasi-standing waves and large waves indicate impact loads.

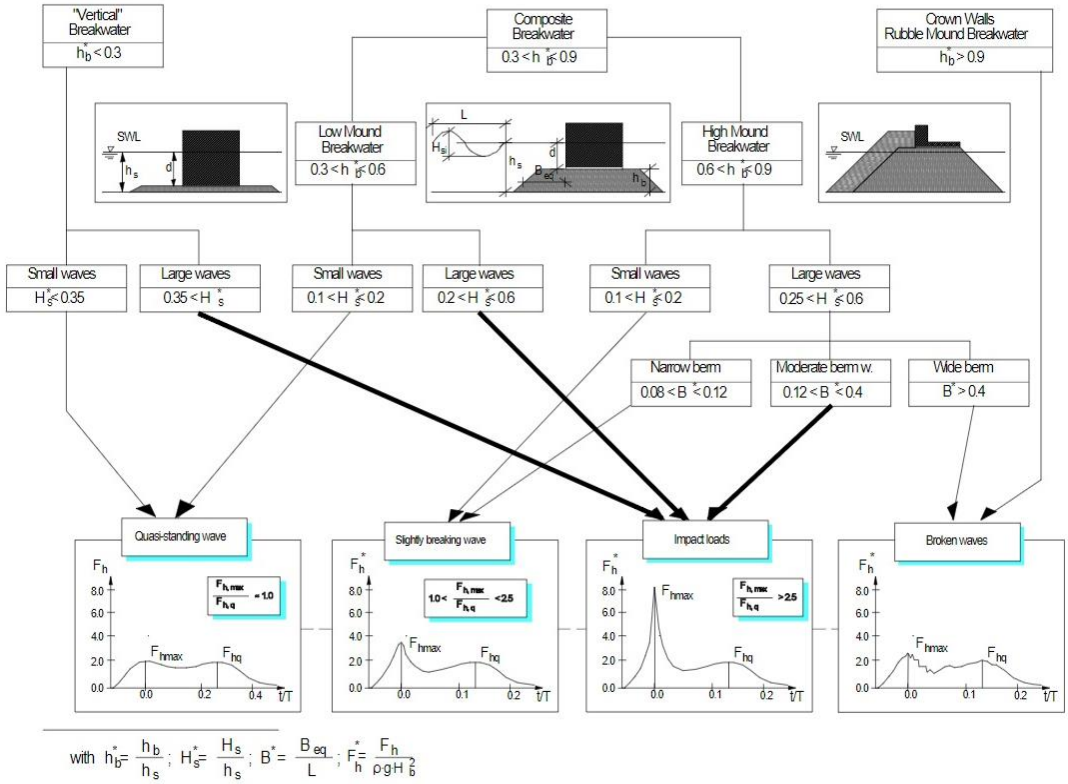

Figure 2.9: Parameter map of PROVERBS (Oumeraci et al., 2001)

In the clean experimental pressure signal, it is also possible to classify the breaking waves as Kisacik et al. (2012) stated which is developed for vertical structures by Oumeraci et al. (1993). Ravindar & Sriram (2021) performed the wave impact pressure to times history for different breaking cases from the same transducer. At the end, they obtained that they have broken waves, breaking waves with large air traps (BWLAT), breaking waves with small air trap (BWSAT), slightly breaking waves (SBW) and non-breaking waves (NBW). As performed by Ravindar & Sriram (2021), several researchers performed visual and signal based classification in their studies.

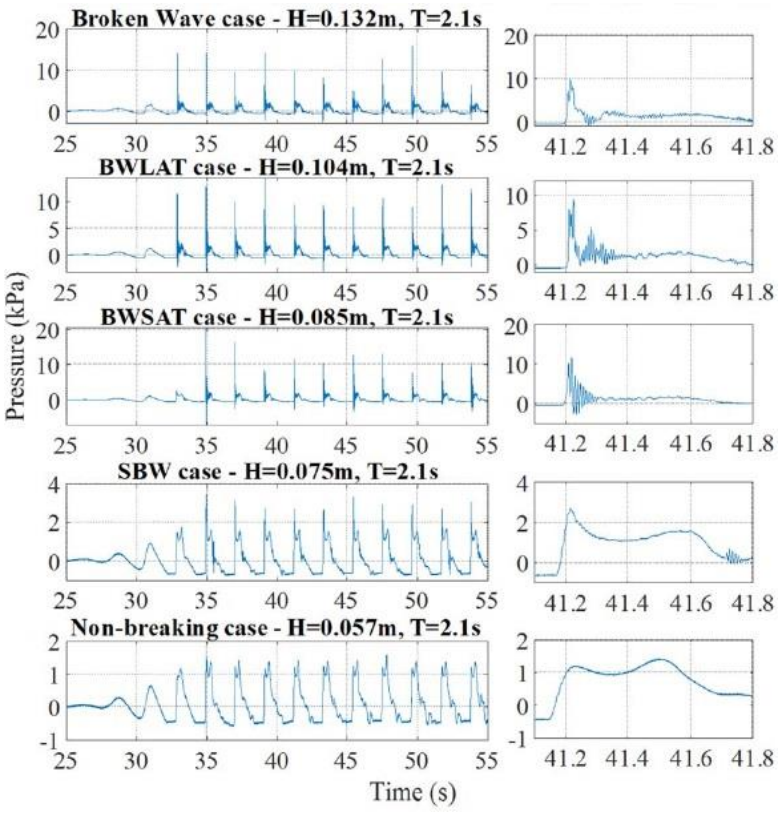

Figure 2.10: Wave impact pressure–time history for different breaking cases (Ravindar & Sriram, 2021)

In the most of the experiments to obtain the wave pressure on the structures, transducer pressure gauges had been used so far and this transducers require the knowledge of signal processing. In the literature, there are several different approaches about processing the pressure signals. Also in the literature, the signal processing part of the transducers are discussed and different approaches noted to show how the pressure values at the specific points read. First, Kirkgoz (1991) discussed the values that transducer read at some points may be unrealistic. In the other cases, it is proved that the unrealistic values of the signal are noises to be cleaned in the base signal.

Another crucial point for the pressure experiments is the nonrepeatability. Even if the waves in the experiment are regular waves, the impact pressure behaviour of the waves may varies in the experiments performed in different times. Although the directed waves from the wave generator in one test are identical, their impact

behavior pressure magnitude may vary significantly and it is possible to see various impact types in same run of the experiment. However, the nonrepeatability is a well discussed part of the topic by several researchers (Hattori et al., 1994; Kirkgoz, 1995; Kisacik et al., 2012 and Ravindar et al., 2019).

2.2 Wave Pressure and Loads on Superstructures

Changing the structural shape of the breakwater and use an additional superstructure along the seawall were the most applied and studied cases to have better results for overtopping for the coastal structures. The different types of the superstructures are discussed in different studies. However, the most focused parameter was the overtopping throughout the past years in the studies.

On storm walls, the shape of the breaking wave has a remarkably effect on the wave impact pressure. In the literature, different geometrical modifications are introduced and discussed by different researchers for storm walls. One of the firsts, Murakami et al. (1996) experimented a different type of vertical breakwater with different wave and setup conditions to show the performance of the flaring shaped vertical wall breakwater is better than the common continuous one. However, the case that Murakami et al. (1996) studied was a non-overtopping wave type of the seawall.

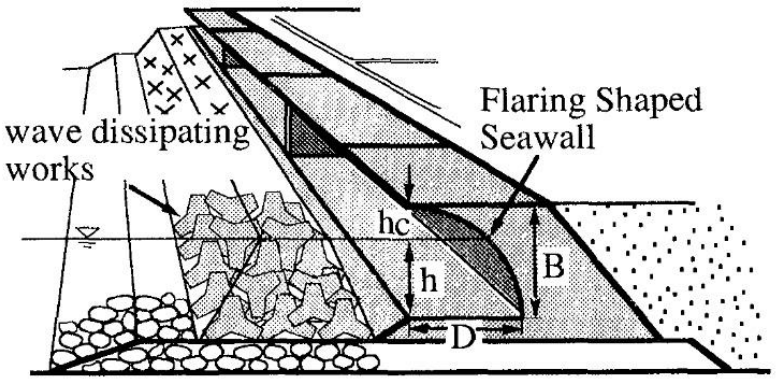

Figure 2.11: Conceptual sketch of the Flaring Shaped Seawall (Murakami et al., 1996)

A similar approach has been followed by Anand et al. (2011) by comparing different curved geometry vertical seawalls and their combination.

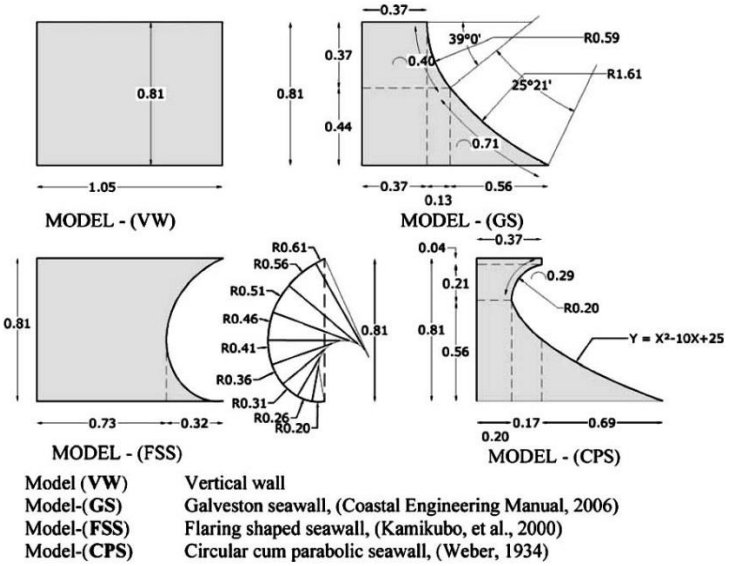

Figure 2.12: The geometry of the curved-front seawalls (Anand et al., 2011)

At the end, the evaluation showed that the two models, FSS and CPS are resulted efficient in reducing crest elevation because of recurved nature. Both the models FSS and model CPS could be used effectively. However, the model FSS was not found efficient since the shape of the model causes an increase in the run-up.

Kirkgoz (1991) examined the impact pressures with different backward sloping walls with the tests carried out at to determine the pressures and forces due to wave impact on seawalls. However, the fact that the impact pressures and their forces on parapets or any other kind of curved seawalls are more than the non-sloping ones, as Kirkgoz (1991) discussed.

One of the superstructures with efficient performance is placing additional bullnoses onto the top of the storm wall, with their common usage in Japan. In the literature, the reduction effect of the bullnoses on the wave overtopping are discussed. As an example, in the experimental study of Zanuttigh & Formentin (2018), it is found that the bullnoses decrease the wave overtopping discharge significantly.

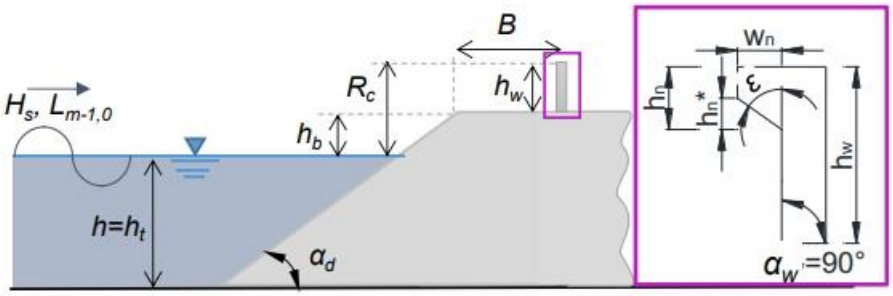

Figure 2.13: Scheme of a dike cross-section with crown wall and with bullnose, (Zanuttigh & Formentin, 2018)

On the other hand, there are some numerical studies performed to discuss the effect of the bullnoses. Molines et al. (2019) evaluated the influence of the parapets on wave overtopping on mounded breakwaters with comparison of experimental data and numerical data obtained with the software OpenFOAM. They obtained reduction in the wave overtopping discharge and recommended optimization on the bullnose design.

Recently, the wave impact effect on a vertical wall is examined by Ravindar et al. (2019) and then the impact pressure is also discussed for different size of bullnose superstructures on the seawalls accordingly by Ravindar & Sriram (2021). At the end of these studies, Ravindar & Sriram (2021) summarized "… parapets significantly reduce overtopping. In addition, for pressure and forces, parapets induce significantly higher impulsive pressure compared with a vertical wall without parapets.".

On the superstructure topic, Kisacik et al. (2019) stated "a promenade and a landward storm wall with bullnose (SWB) lead to a significant reduction of the overtopping discharge while preserving the original outline of the seawall and promenade." at the end of their study.

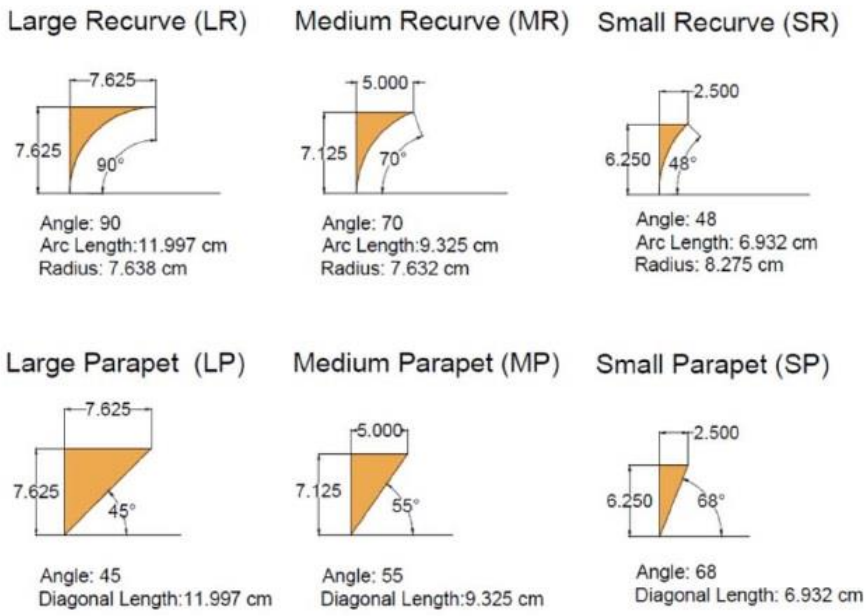

Figure 2.14: Different bullnose types for the parapets (Ravindar & Sriram, 2021)

2.2.1 Stilling Wave Basin (SWB)

Stilling wave basin (SWB) is a type of superstructure that has shifted double row and continuous storm wall at the seaward and landward of the promenade, respectively. The main reason to build a SWB superstructure along the seawall is to decrease the wave overtopping for both the promenade and land behind the landward stormwall where building a higher coastal structure is not possible because of the implications for people living close to the area. One of the pioneer studies was performed for the SWB by Geeraerts et al. (2006). The SWB superstructure in the crest exists on a seaside slope in front of a crownwall of a classical dike. In that study, the wave overtopping discharge is evaluated for both non-breaking and breaking waves.

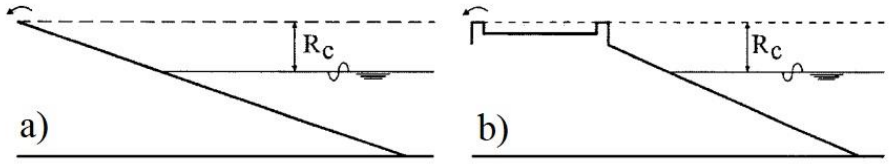

Figure 2.15: The principle sketch of **a)** classical dike and **b)** dike with SWB by Geeraerts et al. (2006)

In the study, the SWB was composed of double row storm wall, a sloped structure and landward storm wall as in the SWB definition.

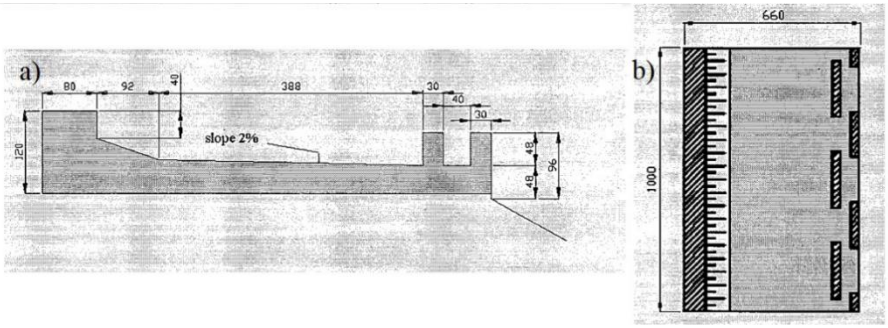

Figure 2.16: a) Side view **b)** plan view of the studied SWB (Geeraerts et al., 2006)

At the end of the investigation of Geeraerts et al. (2006), the efficiency in reducing the wave overtopping by the SWB built in the crest is presented with a comparison between results obtained from experimental data computed data.

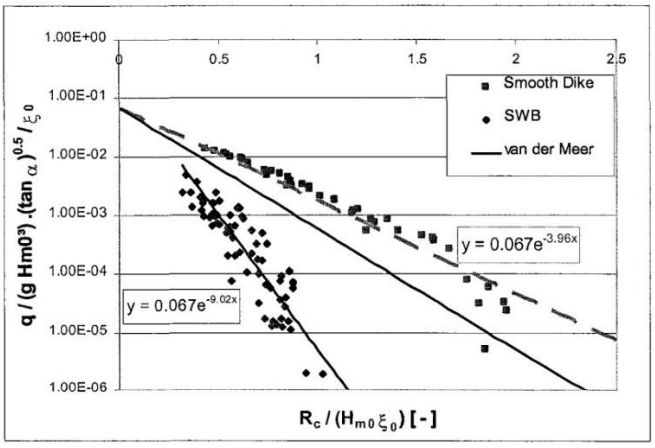

Figure 2.17: Dimensionless overtopping discharge as a function of dimensionless crest freeboard for both smooth dike and dike with SWB for breaking waves (Geeraerts et al., 2006)

Another regression analysis with the experimental results has already given in the literature for an overtopping study on the SWB as discussed by Kisacik et al. (2019). In that study, the overtopping reduction is also discussed with the experiment outputs. The discussion of Kisacik et al, (2019) are based on assessing the performance of SWB on a vertical seawall was to optimize the crest height for lower overtopping values. At the end of the study, it is stated that the modification of SWB can be an applicable alternative solution for higher overtopping conditions in highly urbanized coastal areas.

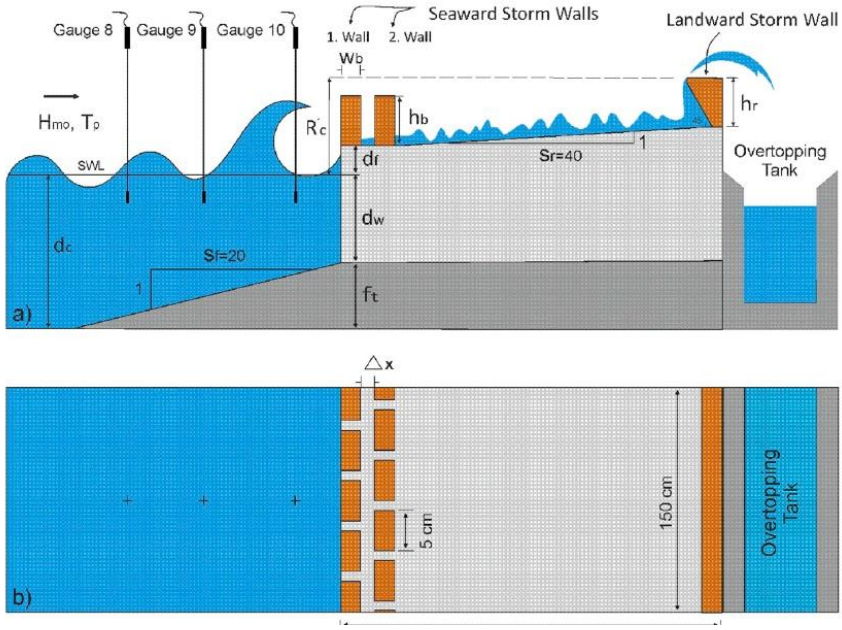

Figure 2.18: Details of the vertical seawall with SWB, **a)** side view and **b)** top view (Kisacik et al., 2019)

Kisacik et al. (2022) compared the overtopping performance of SWB focusing on other superstructures such as storm wall on the seaside, only promenade or promenade and stormwall at the land side. They showed how the overtopping performance of SWB is improved compared to its components and the considerations to minimize the overtopping for an existing seawall.

However, limited researchs exist about the SWB in the literature. Although there are several studies exist in the literature about the topics, all previous publications deal

with the applications in the crest of a rubble mound structure or structure in the crest of impermeable dikes. Most of the existent studies are focused on to investigate the performance of the SWB to reduction for the wave overtopping not wave pressure distribution among the components of SWB such as the storm walls located differently, the effect of gaps as well as promenade. Combination of storm walls with bullnose and how this might effect the pressure distribution on the second row and the landward is also not analyzed in the literature to the best of the results of the literature review. Therefore, in this study, these gaps in the literature are discussed based on the available experimental datasets.

CHAPTER 3

METHODOLOGY

In the methodology chapter, the experiment setup which was used to collect the pressure data, the methods of signal processing to obtain the maximum pressures from the experimental data, and the empricial formulas used to compare the results are given in detail.

3.1 The Experimental Setup

In this study, the wave and pressure data of the experiments that were performed for overtopping by Ozyurt Tarakcioglu et al. (2015) within the BAP Project 08-11-2015-036, "Assessment of Coastal Floods in Inner Bay of Izmir and A Solution Strategy: Stilling Wave Basin (İzmir İç Körfezde Yaşanan Fırtına Taşkınlarının Araştırılması ve Taşkınların Önlenmesi İçin Bir Öneri: Durgun Dalga Havuzu Modeli)" are used for the analysis. In the BAP project, the performance of the SWB superstructure is mainly investigated to reduce the overtopping and control flooding along the Kordon Region, Izmir. As an extension of the experimental campaign, wave pressures were measured on the components of the SWB under overtopping conditions. All the experiments of the project are performed in the Middle East Technical University Civil Engineering Department Coastal and Ocean Laboratory. In the project, each structure and components are tested under a wide range of hydrodynamic conditions. The experiment was designed to obtain the wave pressure values over a SWB structure and its components. The flume was constructed along one side of the small wave basin using glass walls as the flume wall. The layout of the experiment is shown in the Figure 3.1.

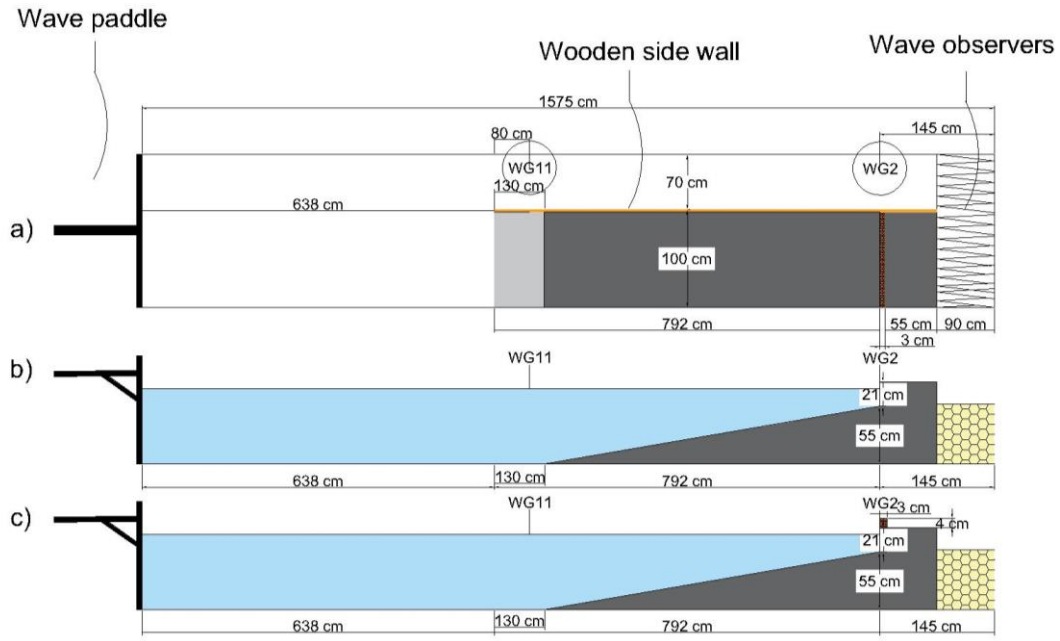

Figure 3.1: The flume model set-up. **a)** top view **b)** side view without storm wall **c)** side view with storm wall

The constructed wave flume is 15.75m long and 1.7m wide. To perform the experiments, another inner channel had been constructed in the flume with the help of a wooden partition wall. The regular wave generator was having a frequency between 0.05 Hz and 2.0 Hz by pushing the wave paddle. The model was placed at 14.3m away from the wave generator. Wider partition had the vertical wall and the super structure(s) on which the pressure data was collected. The smaller partition had only the bed slope until the location of the structure. Then the channel bed was left as horizontal without any structure. This partition was used to measure the wave data using two resistant type wave gauges, gauge 2 and gauge 11. Gauge 2 is placed just at the location where the sea wall is placed in the second channel to the measure the wave characteristics in front of the seawall. On the other hand, gauge 11 is placed at the 80 cm away from the beginning of the side wall and with the aim of measuring the wave characteristics on the deep water (before the wave transformation along the slope). The model was created with the scale 1:16 based on the scaling studies with the hydraulic boundaries of Kordon, Izmir as the BAP project studied by Ozyurt Tarakcioglu et al. (2015).

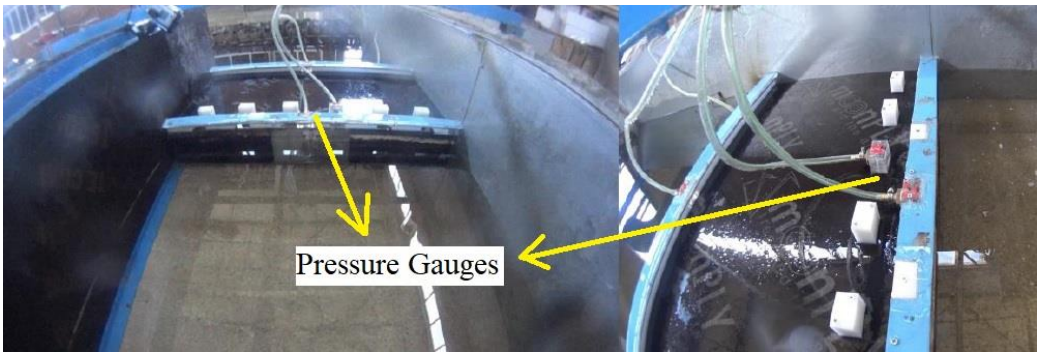

Figure 3.2: Section model

In this study, 7 of 11 setups used in the overtopping studies are investigated which are setup 1,2,4,6,7,8 and 11 of the experiment. In the experiment, 20 different regular waves were generated with six different water depths. The hydrodynamic conditions matrix is presented in Table 2.

Table 2: Experiment hydrodynamic conditions

Test (wave)	d_c (m)	d_w (m)	d_f (m)	H_{s0} (m)	$T_{m-1,0}$ (s)
1	0.600	0.200	0.010	0.081	1.26
2	0.581	0.181	0.029	0.075	1.26
3	0.563	0.163	0.047	0.069	1.22
4	0.544	0.144	0.066	0.067	1.26
5	0.600	0.200	0.010	0.088	1.37
6	0.581	0.181	0.029	0.085	1.50
7	0.563	0.163	0.047	0.083	1.33
8	0.544	0.144	0.066	0.076	1.45
9	0.525	0.125	0.085	0.071	1.37
10	0.581	0.181	0.029	0.104	1.61
11	0.563	0.163	0.048	0.092	1.61
12	0.544	0.144	0.066	0.084	1.61
13	0.525	0.125	0.085	0.076	1.61
14	0.506	0.106	0.104	0.075	1.72
15	0.563	0.163	0.047	0.094	1.72
16	0.544	0.144	0.066	0.090	1.66
17	0.525	0.125	0.085	0.084	1.66
18	0.506	0.106	0.104	0.080	1.66
19	0.563	0.163	0.048	0.105	1.72
20	0.544	0.144	0.066	0.098	1.79

The representative depths in the parameters are shown in the setup figures, where d_c is the water depth, d_w is the depth of stormwall and d_f is the vertical distance between promenade and still-water level (SWL). The wave generator was prepared to generate these deep water wave heights and periods.

The pressure measurements of the experiment are obtained by four Kistler 601CBA250 piezoelectric sensors. The data acquisition system by Kistler is also used to collect the data in bars. The system can measure the pressure up to 250 bar and 62.5 kHz. For the experiments, the data was collected at 12.5kHz to optimize the file size based on sensitivity trials focusing on the maximum pressure. The system was also set for 5 bar as the maximum pressure to increase the accuracy of the measurements. These sensors are placed at different locations for each setup. The distribution of the pressure gauges is presented in the setup figures.

The model was also equipped with two high definition video cameras to collect information on wave breaking and flow behavior over the superstructures.

3.1.1 Superstructure Setups

In this study, seven different superstructure setups are investigated to understand the effect of the wave pressure on the components of stilling wave basin by measuring the pressure at different places. With these seven different setups, discussions are made and the results are analyzed and investigated.

In the setups, four different pressure gauges had been placed on the vertical wall (along y axis), on the storm walls at different locations along x axis based on the configuration of the superstructure (Figure 3.3 and Table 3). z0 represents the base of the vertical seawall (end of the slope) and can be taken as 0cm. Δx is 0 when the sensors are located on the vertical wall.

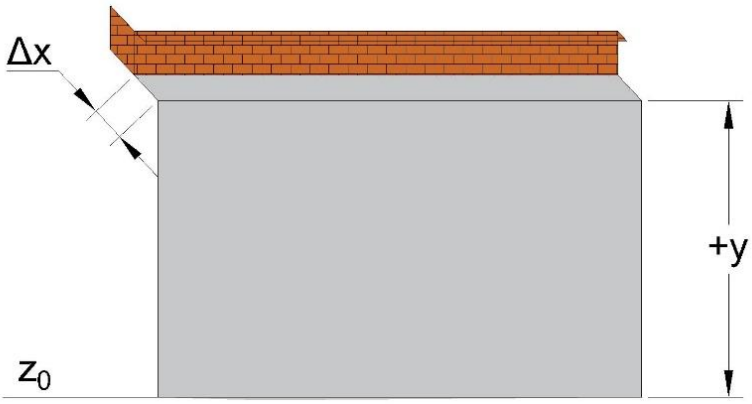

Figure 3.3: Vertical wall dimensions representative figure

Table 3: Vertical wall dimensions

	SETUP 1			
	Gauge 27	Gauge 28	Gauge 29	Gauge 30
Δx (cm)	0	0	0	0
y (cm)	23	23	23	19
	SETUP 2			
	Gauge 27	Gauge 28	Gauge 29	Gauge 30
Δx (cm)	0	0	0	0
y (cm)	23	23	23	19
	SETUP 4			
	Gauge 27	Gauge 28	Gauge 29	Gauge 30
y (cm)	23	23	23	23
Δx (cm)	4	0	50	0

Table 3: Vertical wall dimensions (cont'd)

	SETUP 6			
	Gauge 27	Gauge 28	Gauge 29	Gauge 30
y (cm)	23	23	23	23
Δx (cm)	4	0	50	0
	SETUP 7			
	Gauge 27	Gauge 28	Gauge 29	Gauge 30
Δx (cm)	0	0	0	0
z0 + y (cm)	23	23	23	19
	SETUP 8			
	Gauge 27	Gauge 28	Gauge 29	Gauge 30
Δx (cm)	0	0	0	0
z0 + y (cm)	23	23	23	19
	SETUP 11			
	Gauge 28	Gauge 29	Gauge 30	Gauge 27
Δx (cm)	0	0	0	0
z0 + y (cm)	11	15	19	23

In the Figure 3.4, the constant dimensions related to the components are provided. The distance between two storm walls is 4cm, width of each storm wall unit is 3 cm, gap width is 5cm, height of the storm walls (with or without bullnose) is 4 cm. the promenade width is also kept constant as 50cm.

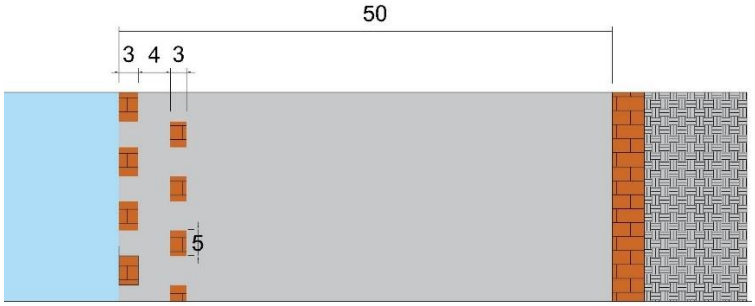

Figure 3.4: Representative top view figure of constant SWB dimensions in cm

The summary of the features of the superstructure setups are in the following Table 4.

Table 4: Superstructure setup features

Setup Features Table	
Feature	**Setup**
Continuous seaward storm wall	Setup 11
Seaward storm wall with gaps	Setup 1
Seaward storm wall with gaps and bullnose	Setup 2
Promenade + continuous landward storm wall	Setup 7
Promenade + continuous landward storm wall with bullnose	Setup 8
Seaward storm wall with gaps + promenade + continuous landward storm wall	Setup 6
Seaward double row storm wall with gaps and bullnose in the first row + promenade + continuous landward storm wall	Setup 4

The results of the pressure data analyses are discussed and compared within cases by considering the features of these setups. The features of the setups can also be seen in the setup figures. In addition, pressure gauge 30 is placed at the same location on the vertical seawall as shown in each setup figure in every setup.

3.1.1.1 Setup 1

Setup 1 has only one seaside storm wall right on top of the vertical seawall. The storm wall has horizontal gap in between the units (Figure 3.5 and 3.6). The pressure gauges 27, 28 and 29 are placed on the frontside of the storm wall with one gap in between (Figure 3.7). In Setup 1, there is no superstructure is placed at landward.

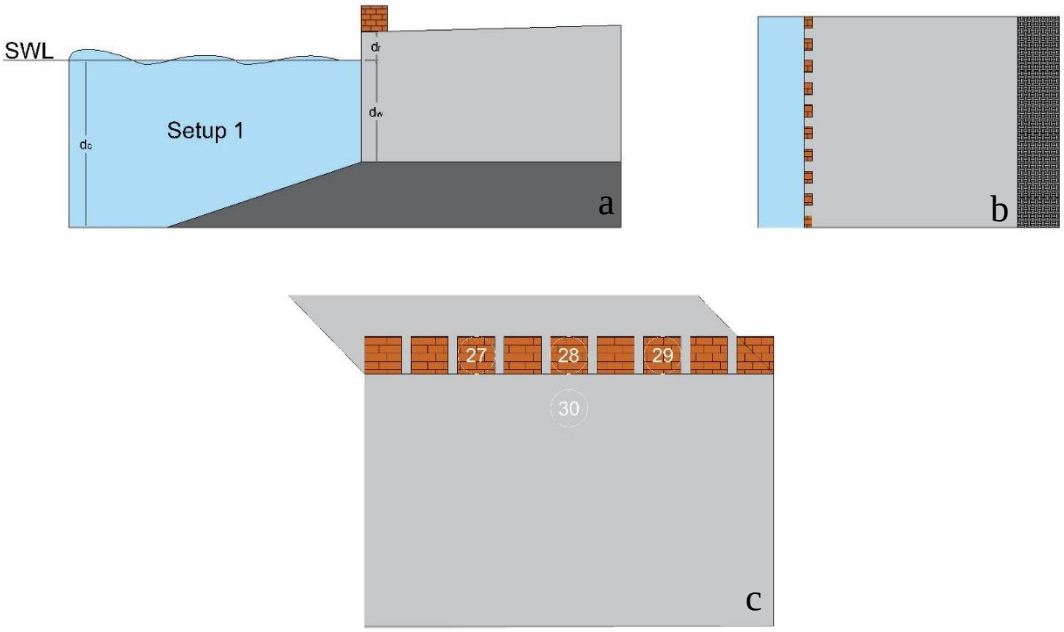

Figure 3.5: Setup 1, **a)** side view **b)** top view and **c)** front view

Figure 3.6: Experimental set-up of setup 1, front view

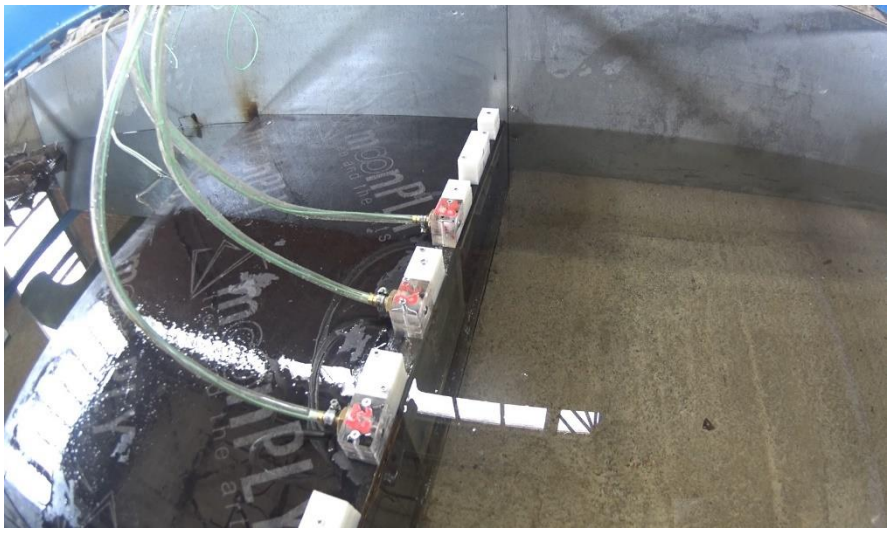

Figure 3.7: Experimental set-up of setup 1, side view

3.1.1.2 Setup 2

Setup 2 is very similar to Setup 1. Setup 2 also has horizontal gap along the seaward storm wall (Figure 3.8) The superstructure has a continuous bullnose over the gaps and the storm wall as can be seen in the Figure 3.9. The pressure gauges 27, 28 and 29 are placed on the frontside of the seaward storm wall with one gap in between (Figure 3.9). In Setup 2, there is no superstructure is placed at landward.

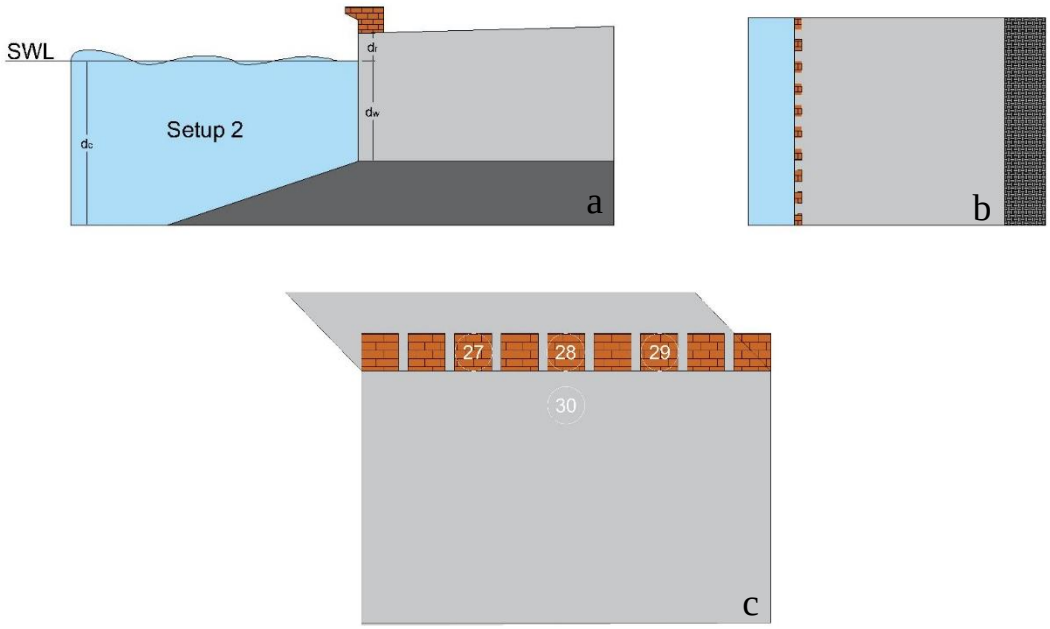

Figure 3.8: Setup 2, **a)** side view **b)** top view and **c)** front view

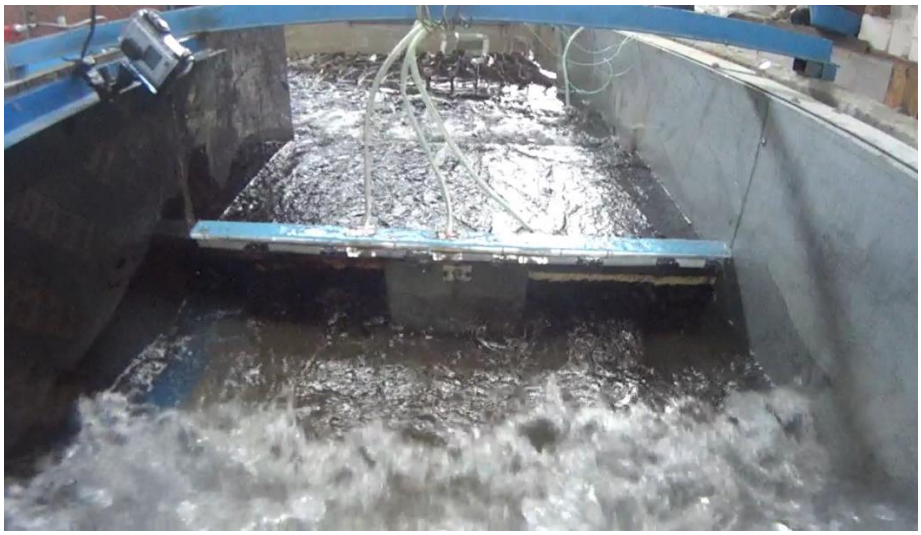

Figure 3.9: Experimental set-up of setup 2, front view

3.1.1.3 Setup 4

Setup 4 has horizontal gap between the seaward storm walls for both first and second rows. On the other hand, Setup 4 has a continuous landward storm wall behind the promenade. Furthermore, the first row of the seaward storm walls and landward

storm wall has bullnose superstructure, as can be seen in the Figure 3.10 and Figure 3.11. Pressure gauge 28 is placed on the frontside of the first seaward storm walls, pressure gauge 27 placed on the front side of the second row storm wall and pressure gauge 29 is place on the front side of the landward storm wall.

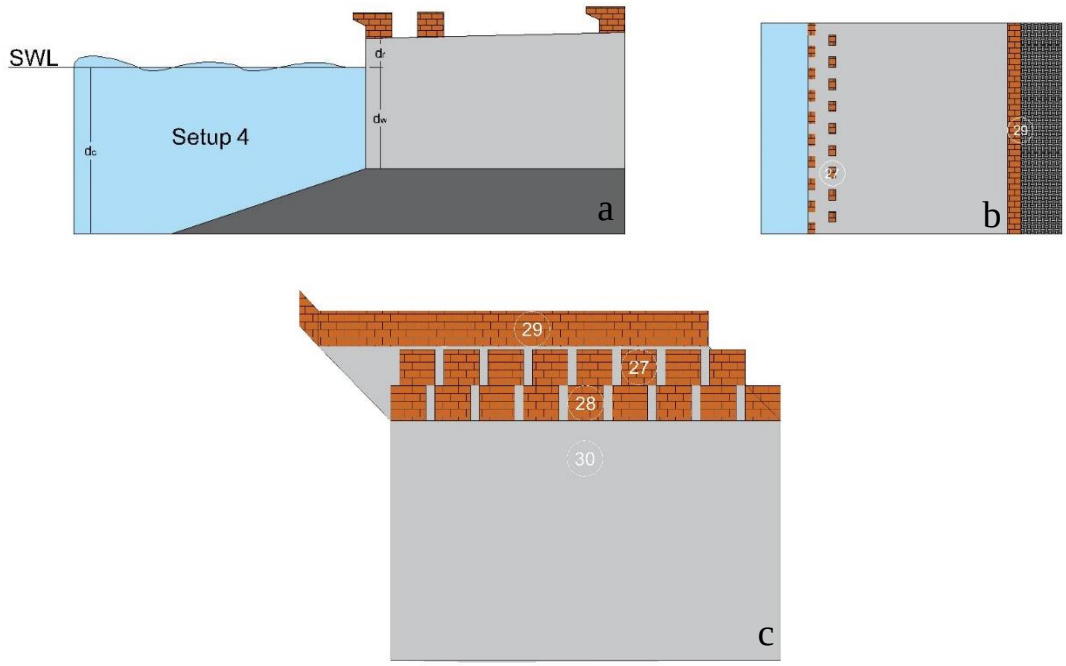

Figure 3.10: Setup 4, **a)** side view **b)** top view and **c)** front view

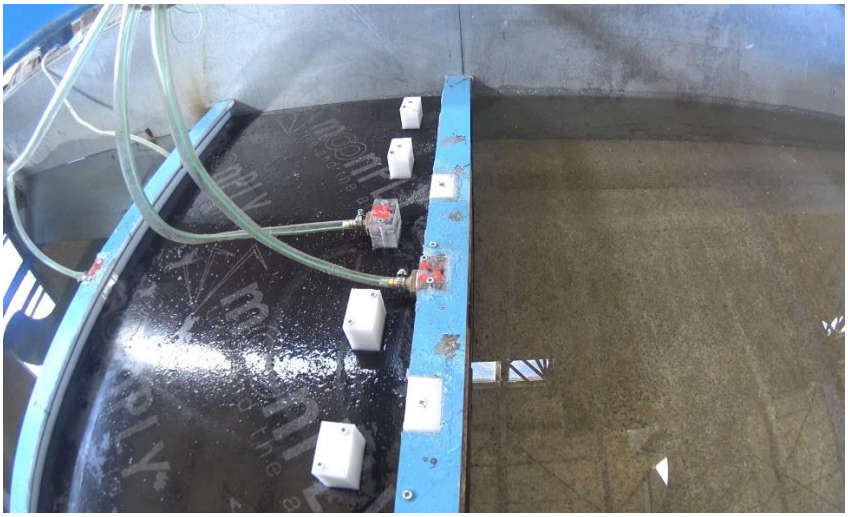

Figure 3.11: Experimental set-up of setup 4, side view

3.1.1.4 Setup 6

Setup 6 is very similar to Setup 4. Setup 6 also has horizontal gap between the seaward storm walls for both first and second rows. On the other hand, Setup 6 has a continuous landward storm wall without gap. Different to Setup 4, Setup 6 do not have any bullnose structure over the storm walls. Pressure gauge 28 is placed on the frontside of the seaward storm walls, pressure gauge 27 placed on the front side of the second row storm wall and pressure gauge 29 is place on the front side of the landward storm wall.

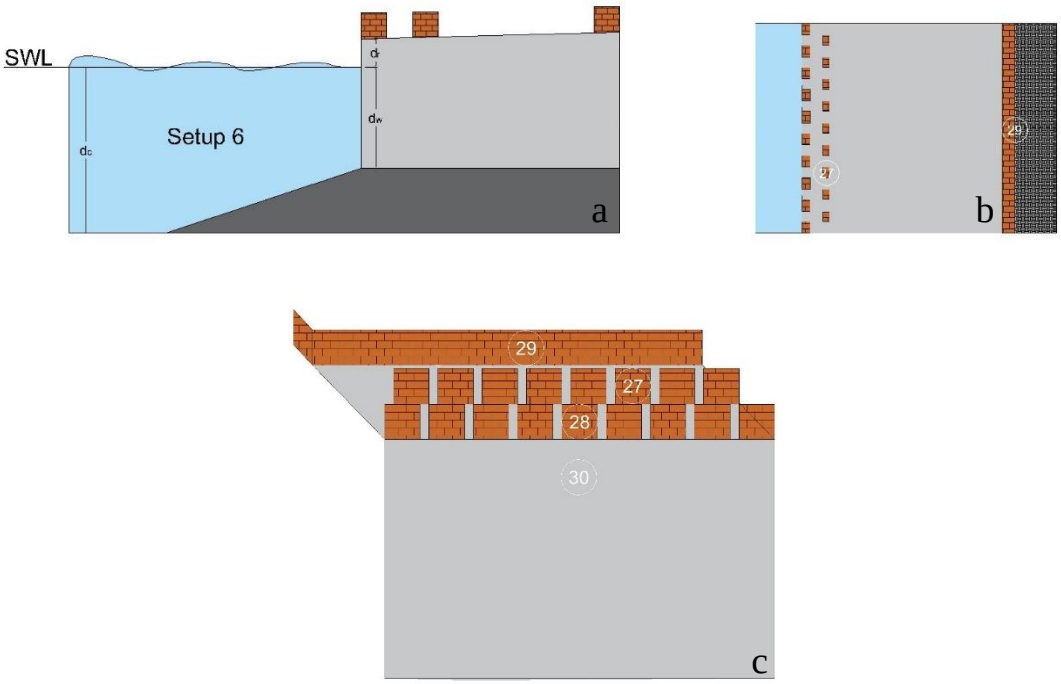

Figure 3.12: Setup 6, **a)** side view **b)** top view and **c)** front view

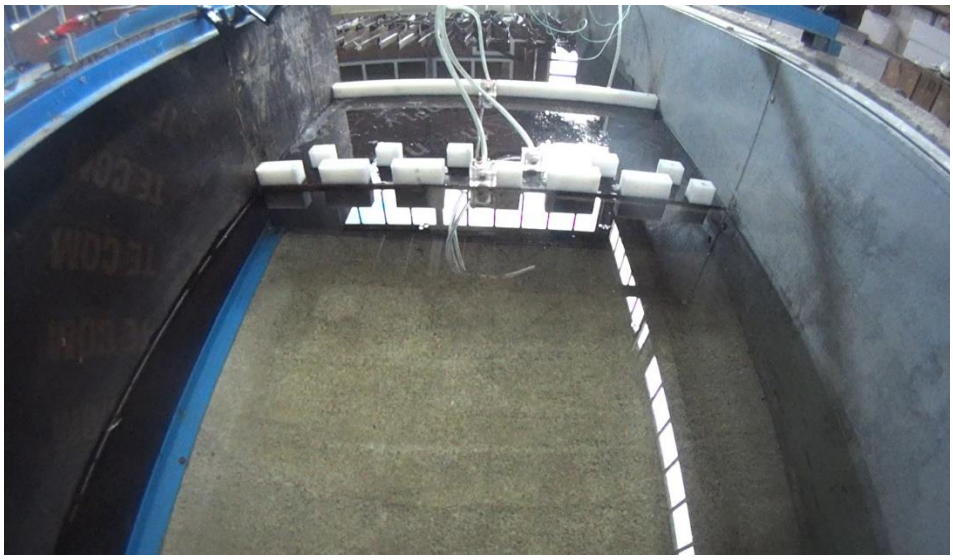

Figure 3.13: Experimental set-up of setup 6, front view

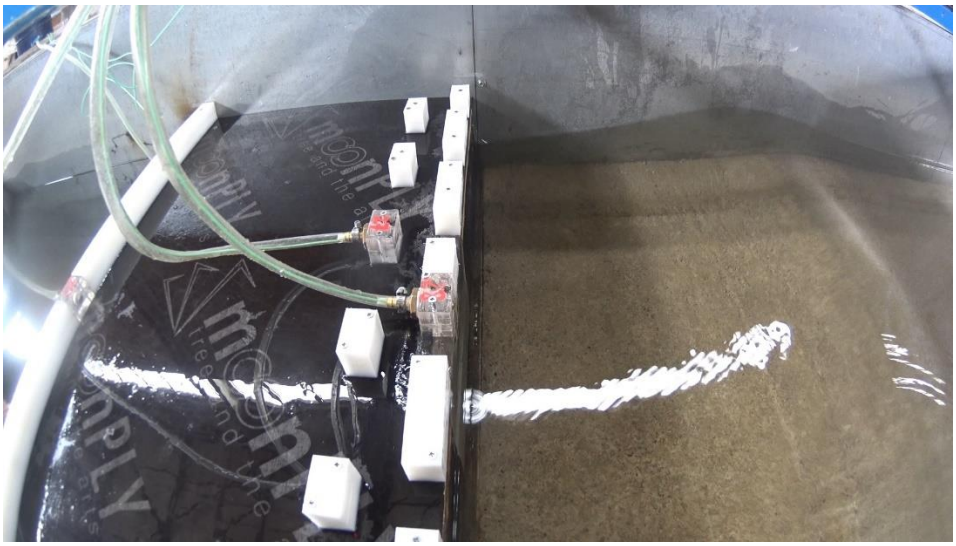

Figure 3.14: Experimental set-up of setup 6, side view

3.1.1.5 Setup 7

Setup 7 has a continuous storm wall at the landward side behind the promenade. The storm wall also does not have any bullnose superstructure. The pressure gauges 27, 28 and 29 are placed on the frontside of the landward storm wall. In Setup 7, there

is no superstructure is placed at seaward as can be seen in experimental set-up picture, Figure 3.16.

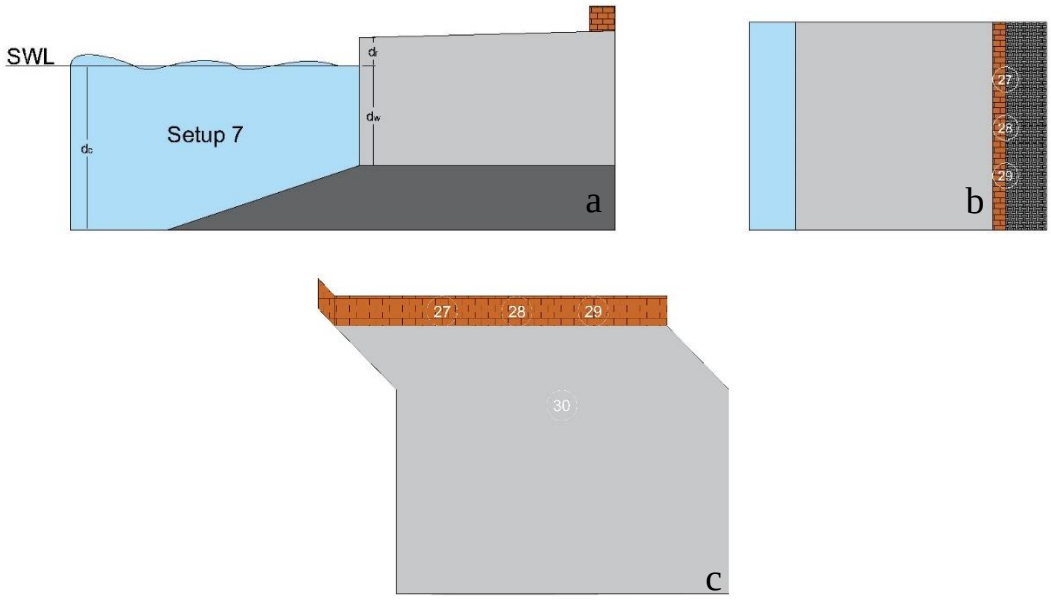

Figure 3.15: Setup 7, **a)** side view **b)** top view and **c)** front view

Figure 3.16: Experimental set-up of setup 7, front view

3.1.1.6 Setup 8

Setup 8 has a continuous storm wall at the landward side behind the promenade and the storm wall has bullnose as can be seen in the Figure 3.17. The pressure gauges

27, 28 and 29 are placed on the frontside of the landward storm wall. In Setup 8, there is no superstructure is placed at seaward as can be seen in the experimental set-up picture, Figure 3.18.

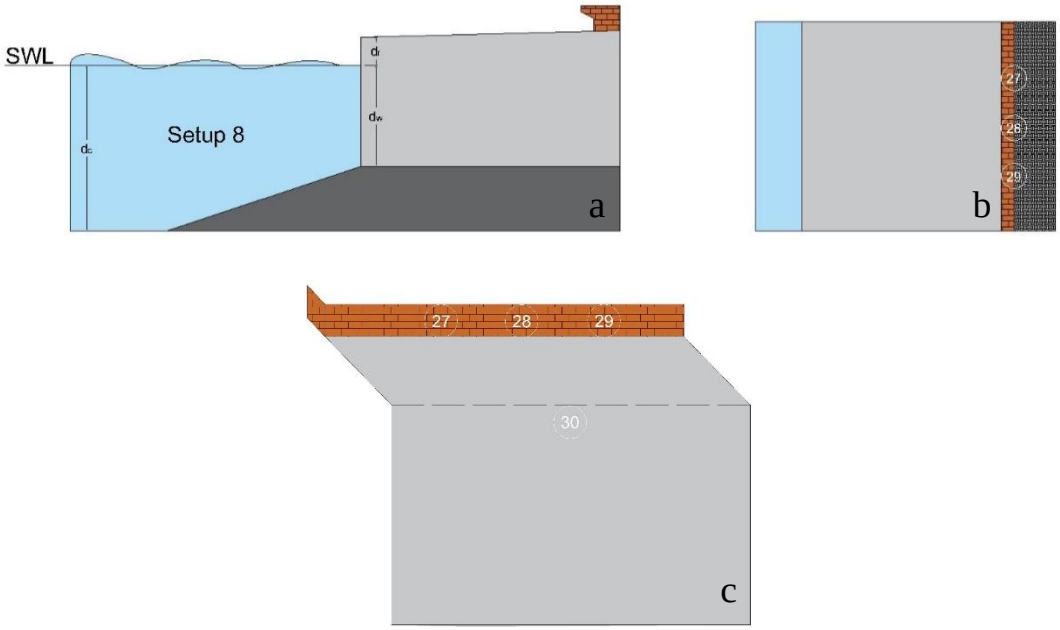

Figure 3.17: Setup 8, **a)** side view **b)** top view and **c)** front view

Figure 3.18: Experimental set-up of setup 8, front view

3.1.1.7 Setup 11

Setup 11 has a storm wall at the seaward without any gap (continuous wall) which also represent the existing seawall of Kordon, Izmir. The whole structure can be considered as the vertical seawall. All the pressure gauges are placed on the frontside of the seaward storm wall along the wall based on the water levels tested in the experiments. In Setup 11, there is no superstructure is placed at landward as well as no bullnose over the storm wall. This setup was used to analyze the performance of empirical pressure formulas along the vertical coastal structures.

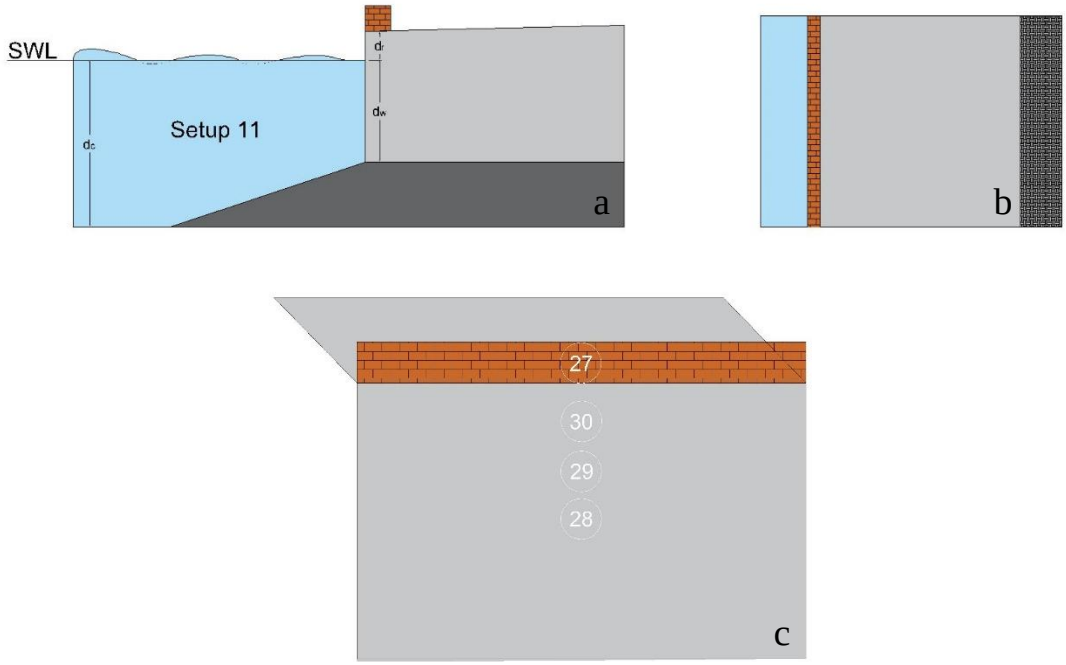

Figure 3.19: Setup 11, **a)** side view **b)** top view and **c)** front view

Figure 3.20: Experimental set-up of setup 11, side view

3.2 Data Analysis

In this part, the processes and procedures that followed while performing the analyzes of the experimental data are given. While performing the analyzes, the software MATLAB was used.

3.2.1 Wave Height and Period

In this study, the wave heights and peroids are also determined with the experimental data that obtained from the experiment. Data measured by the two resistant type wave gauges are converted into timeseries of water level measurements. This data was collected at the smaller section of the setup where there was no vertical wall or superstructures. Data was collected both at deep water conditions (in front of the slope) as well as at the end of the slope (at the depth of the structure). To find out the wave height and period, data was collected during one experiment as the wave generator used the same input and the waves generated were regular waves. Therefore, it is assumed that similar waves are generated for the rest of the experiments.

The water level data (Figure 3.21) was converted in to wave profile data considering the mean water level of the experiments (Figure 3.22). Then, wave heights and periods of individual waves are determined for both gauges using zero upcrossing method with MATLAB.

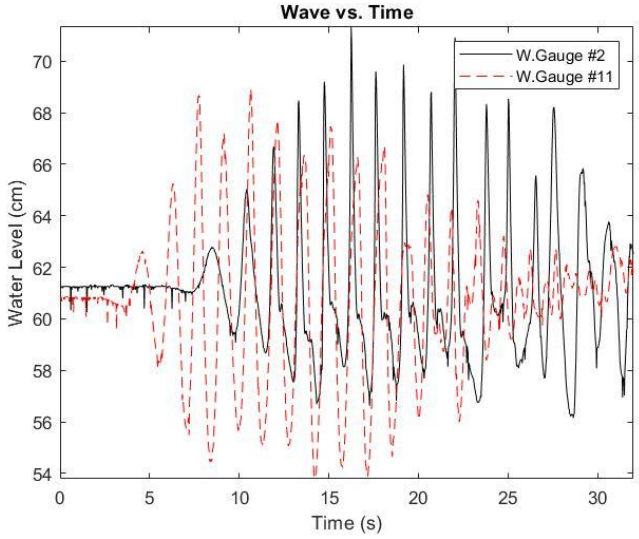

Figure 3.21: An example of water level measurement for wave gauges gauge 2 and gauge 11 at the same time

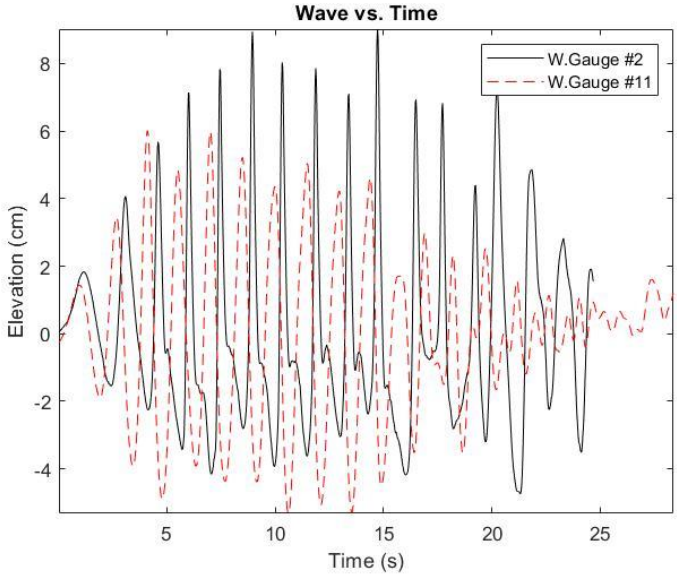

Figure 3.22: The comparison for measured elevations for gauge 2 and gauge 11

Zero up-crossing is a commonly used method in the wave analyzes, especially in short-term wave analyzes. This method contains indicating the reference points, indicating the elevation difference between reference points, indicating the time interval for the first full-wave and carrying out the wave height to obtain the wave period parts.

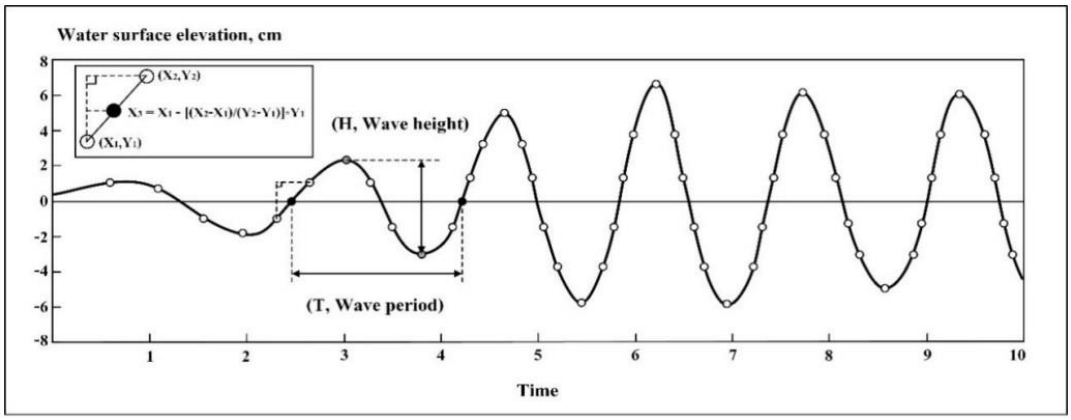

Figure 3.23: Zero up-crossing analysis method (Viriyakijja & Chinnarasri, 2015)

For the analysis of the wave and pressure measurements, only the first four waves are analyzed. The reason of this was the reflection and reflection might happen due to the size of the wave flume that experiment had been performed. By taking into account only the first 4 waves, it is aimed to neglect the events caused by reflection, refraction or other kind of wave flume caused situations. Although the first wave is usually a smaller wave when the wave is not fully developed, the pressure data was already collected for each individual wave. As the pressure analysis was performed wave by wave (not for a representative wave height), inclusion of these smaller waves provided a dataset for nonbreaking wave conditions which enhanced the overall experiment range.

3.2.2 Wave Classification

To help to understand the behavior of the waves in front of the structure, a wave classification has been performed. The waves are investigated for their types which

are non-breaking waves, slightly breaking waves, breaking waves and broken waves. For the classification of the waves, the wave pressure signals are evaluated and compared to the classification schemas in the literature such as Ravindar & Sriram (2021)

Figure 3.24 shows an example of non-breaking wave condition especially for the first three waves. As can be seen from the figure, the pressure changes follow the wave height change over the pressure sensor. The change is gradual and happens during the whole period of the wave.

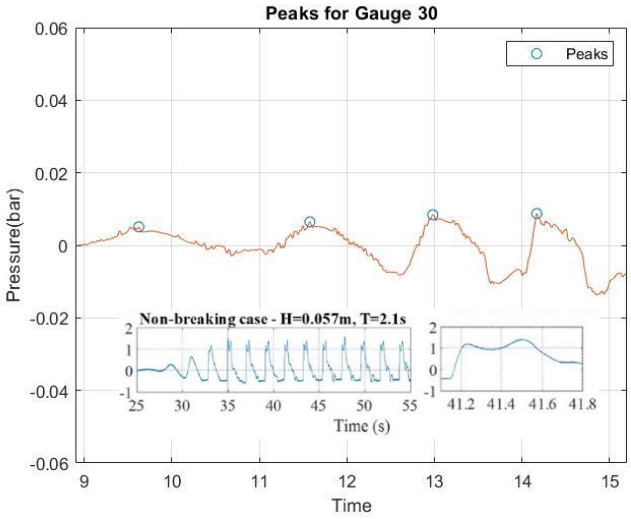

Figure 3.24: Non-breaking waves, setup 11 wave 1 gauge 30 compared with Ravindar & Sriram (2021)

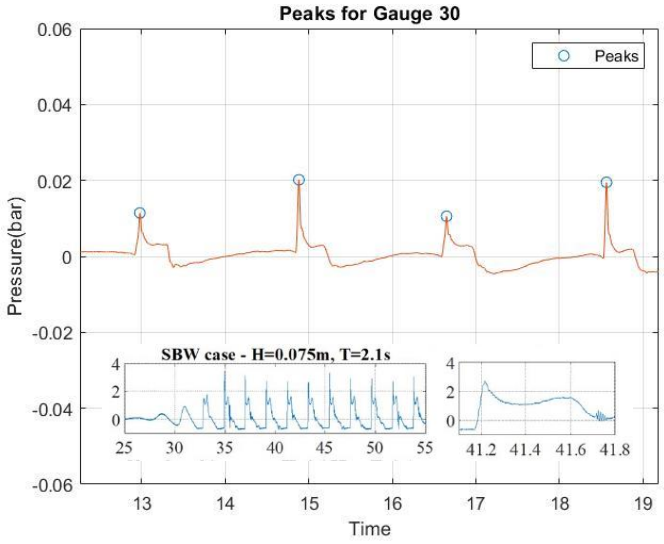

Figure 3.25: Slightly breaking waves, setup 4 wave 16 gauge 30 compared with Ravindar & Sriram (2021)

Figure 3.25 presents a slightly breaking example. As can be seen in the figure, there are slight wave breakings for all 4 waves throughout the pressure signal.

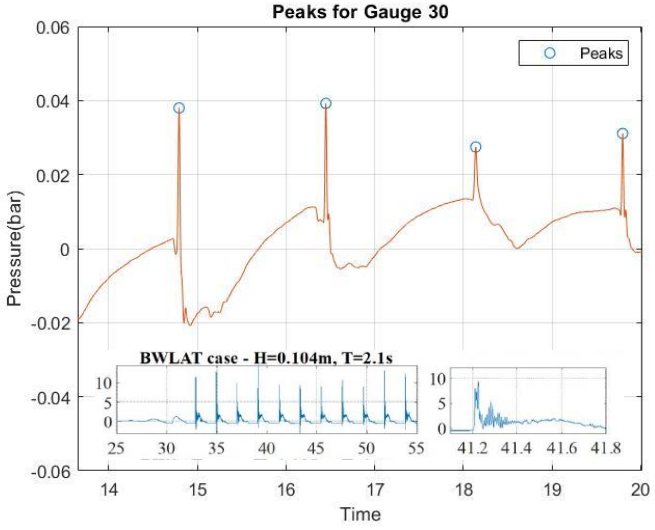

Figure 3.26: Breaking waves, setup 2 wave 20 gauge 30 compared with Ravindar & Sriram (2021)

Figure 3.26 shows an example of breaking wave condition with the comparison between this study and Ravindar & Sriram (2021) especially for the first two waves.

As can be seen in Figure 3.26, the pressure changes for the waves are fits with the pattern of BWLAT example of Ravindar & Sriram (2021).

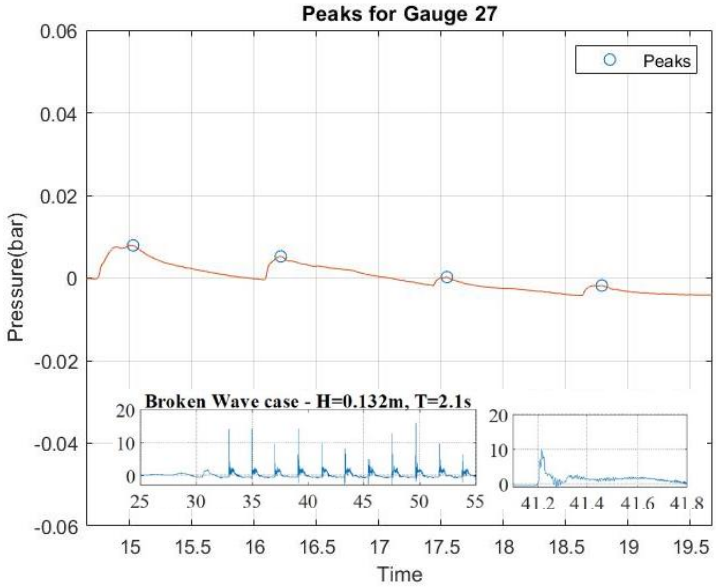

Figure 3.27: Broken waves, setup 7 wave 18 gauge 27 compared with Ravindar & Sriram (2021)

In the Figure 3.27, the comparison of the broken waves with an example this study and Ravindar & Sriram (2021) presented. In this study, the waves broken throughout the SWB reach to the pressure sensors placed in front of the landward storm wall, observed as small pressures changes in the signal.

Additionally, the waves are controlled as per their breaking status following PROVERBS classification based on Oumeraci et al. (2001). This classification means if the loading is a quasi-static load or impact load by controlling if they are small waves or large waves based on ratio of wave height at the structure to water depth in front of the structure.

Small waves, $H_s/d < 0.35$ (3.1)

Large waves, $H_s/d > 0.35$ (3.2)

Small waves generates quasi-standing wave conditions (non-breaking) where as large waves generate impact loads on the structure.

3.2.3 Pressure Signals and Noise Processing

The pressure sensors that used in the experiment recorded the pressure signals. The sensors were already calibrated therefore no additional calibration process was applied. Data was sampled at 12.5kHz. Many of the recorded signals were noisy. To have a proper signal to examine and evaluate the maximum pressure straightly, the noise in the signal had to be cleaned accurately. For this purpose, the signal processing for the pressure signals is used.

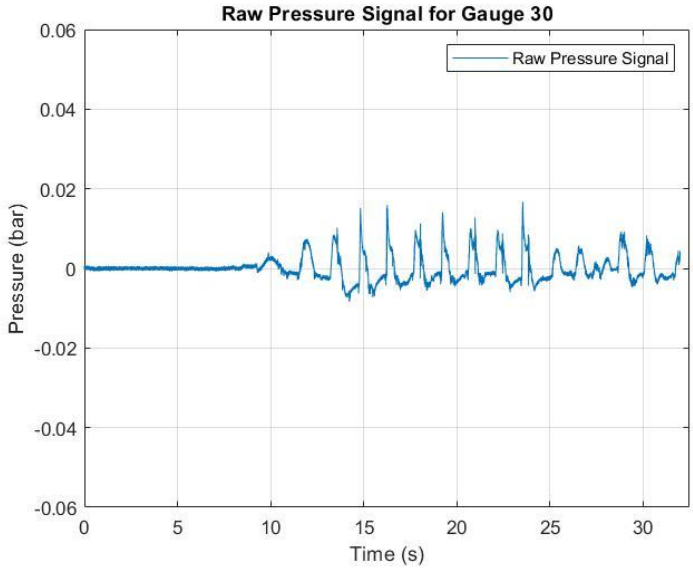

Figure 3.28: An example of raw pressure signal

While performing the noise cleaning operation in the signal, MATLAB's Signal Processing Tools' functions are tried. First, Fast Fourier Transform (FFT) is used to have clean signal with coefficients and power spectrum. However, the manual operation of the indices and losses in the pressure signal showed that FFT is not the best way to clean the noises in the signal for this study. Furthermore, detrending and polynomial fitting functions are tried but higher polynomial degrees cause losses in the peak pressures and not cleaned signals by polyfit function of MATLAB are limited to use this approach. At the end, Butterworth function is used to obtain the exact frequency interval without noises since the results of the noise processing are

better than the other approaches. The loss in the peaks after detrending can be seen in the Figure 3.29.

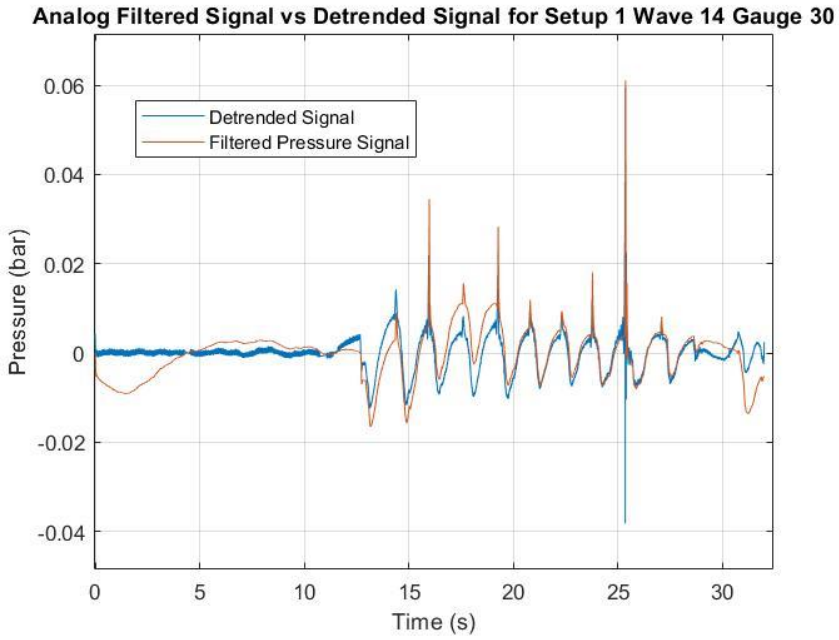

Figure 3.29: Analog filtered signal vs detrended signal for setup 1 wave 14 gauge 30

In Butterworth, the design of the filtering separates into 2 different ways: Digital and analog. In this study, the analog filtering of Butterworth function is used which designs the lowpass order in order to cutoff the angular frequency which transferred from Butterworth function of MATLAB for the filter response. In the application of the Butterworth function in MATLAB, the inputs are lowpass order and cutoff frequency. Also, the sampled frequency of the data should be defined. In this study, the design applied for a 6^{th} order lowpass filter and the normalized cutoff frequency is applied from 30 Hz for data sampled at 12500 Hz. The filter properties were determined through trial and error process such that the loss in the signal for the maximum values were as minimal as possible for the first four waves which are used in the analysis and discussions.

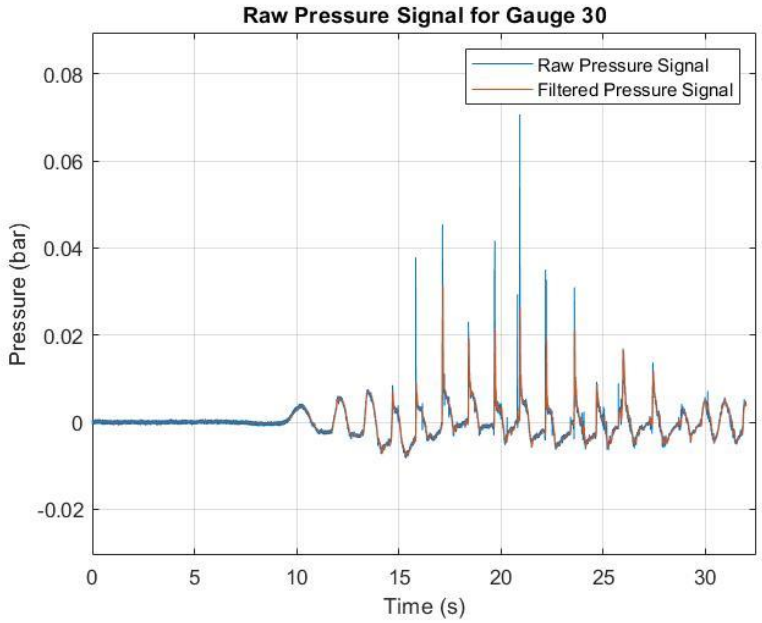

Figure 3.30: An example of filtered and smoothed pressure signal compared to raw pressure signal (the first four signals are used in the analysis)

3.2.4 Maximum Pressure Values

The noise filterin was performed for the whole timeseries of the pressure data for each experiment (setup and hydrodynamic conditions). Therefore, the pressure data set for one setup included 20 different hdydorynamic conditions and 4 pressure sensors which was 80 different time series data for each dataset. However, the analysis was performed wave by wave basis and the first four waves were considered due to reflection. This meant that the first four pressure measurements were analyzed to determine maximum wave pressures. Therefore, 320 pressure data was determined for one dataset which means a total of 7*320 (2240) pressure data was determined from the measured timeseries.

To determine the pressure measurements corresponding to each wave, first, the data obtained from the pressure sensor are defined as inputs in the MATLAB and the time interval of first 4 waves observed in the pressure signal are determined for each sensor. Further, the determined time interval is used to obtain the exact values of the

pressure in the specific times. At the end, the peak pressure values of the waves are automatically derived by peak function of MATLAB. The filtered signal is used for the determination of peak pressures.

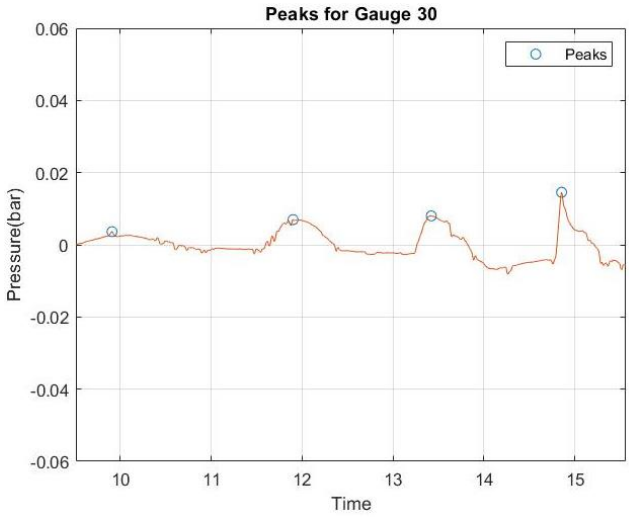

Figure 3.31: An example of indicated peaks on pressure signal for first 4 waves

3.3 Wave Pressure Equations by Goda (2010)

There are different approaches exist in the literature about the calculation of wave pressure distribution on the vertical wall breakwaters. In this thesis, approach by Goda (2010) is used to assess the performance of empirical methods used in the design of vertical structures. Goda (2010) formulas are widely used in the design of vertical wall structures and are valid for both breaking and non-breaking conditions.

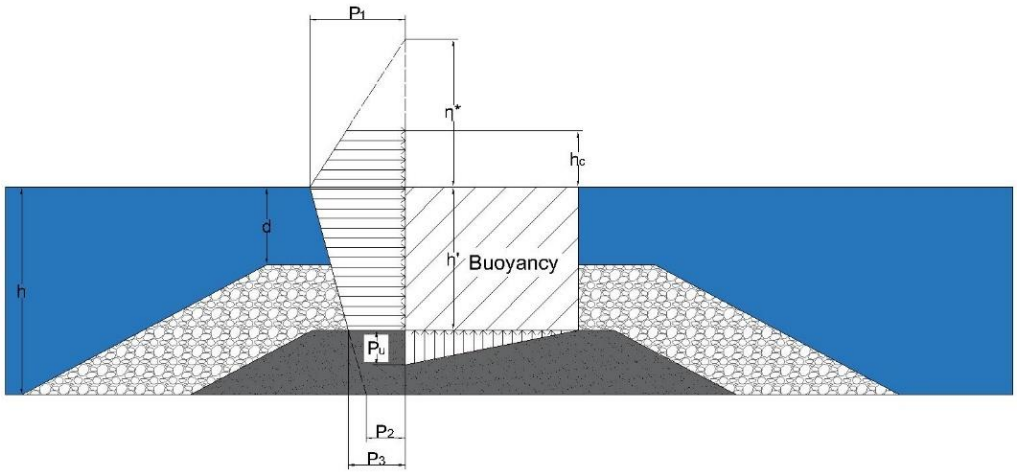

Figure 3.32: Distribution of wave pressure on an upright section of a vertical breakwater (Goda, 2010).

The wave pressure formulas for the upright sections are in the following. Elevation of the exerted wave pressure is:

$$\eta^* = 0.75(1 + \cos\beta)H_{max} \tag{3.3}$$

for the case that β annotates the wave approach angle which is taken as zero in all of the calculations since the experiment's wave approach angle was zero in all cases by directed waves by wave generator. However, the wave direction might be rotated up to 15° from the principal wave direction as stated in Goda (2010). The reason of this is the design wave approach angle has been used in the breakwater designs for the Japan coasts is referring this statement. After the clarification of the wave approach angle, the following equation finds the pressure on the front of a vertical wall.

$$P_1 = \frac{1}{2}(1 + \cos\beta)(\alpha_1 + \alpha_2\cos^2\beta)\rho g H_{max} \tag{3.4}$$

$$P_2 = \frac{P_1}{\cosh(\frac{2\pi h}{L})} \tag{3.5}$$

$$P_3 = \alpha_3 P_1 \tag{3.6}$$

where

$$\alpha_1 = 0.6 + \frac{1}{2}\left[\frac{(\frac{4\pi h}{L})}{\sinh(\frac{4\pi h}{L})}\right]^2 \quad (3.7)$$

$$\alpha_2 = \min\left\{\frac{h_b - d}{3h_b}\left(\frac{H_{max}}{d}\right)^2, \frac{2d}{H_{max}}\right\} \quad (3.8)$$

$$\alpha_3 = 1 - \frac{h'}{h}\left[1 - \frac{1}{\cosh(\frac{2\pi h}{L})}\right] \quad (3.9)$$

and where h_b represents the distance of $5H_{1/3}$ seaward side of the seawall. Another crucial equation is the uplift pressure.

$$P_u = \frac{1}{2}(1 + \cos\beta)a_1 a_3 \rho g H_{max} \quad (3.10)$$

Although Goda (2010) is valid for both non-breaking and breaking conditions, in this study, these equations are only used to determine the pressure for non-breaking datasets of the experiments. The pressure analysis for the impact loads conditions (breaking waves) provided the maximum pressure measured by the sensor. Therefore, for those datasets, the modified version of Goda (2010) formula proposed to calculate the maximum impulsive pressure is used. In this case, the formula for P_1 is modified by Goda (2010) as below.

$$P_1 = \frac{1}{2}(1 + \cos\beta)(\alpha_1 + \alpha^* \cos^2\beta)\rho g H_{max} \quad (3.11)$$

where

$$\alpha^* = \max\{\alpha_1, \alpha_I\} \quad (3.12)$$

$$\alpha_I = \alpha_{IH}\alpha_{IB} \quad (3.13)$$

and

$$\alpha_{IH} = \min\left\{\frac{H}{d}, 2.0\right\} \quad (3.14)$$

$$\alpha_{IB} = \begin{cases} \cos\delta_2/\cosh\delta_1, & \delta_2 \leq 0 \\ 1/\cosh\delta_1\cosh^{1/2}, & \delta_2 > 0 \end{cases} \quad (3.15)$$

$$\delta_1 = \begin{cases} 20\delta_{11}, & \delta_{11} \leq 0 \\ 15\delta_{11}, & \delta_{11} > 0 \end{cases} \quad (3.16)$$

$$\delta_2 = \begin{cases} 4.9\delta_{22}, & \delta_{22} \leq 0 \\ 3.0\delta_{22}, & \delta_{22} > 0 \end{cases} \quad (3.17)$$

$$\delta_{11} = 0.93\left(\frac{B_M}{L} - 0.12\right) + 0.36\left(0.4 - \frac{d}{h}\right) \quad (3.18)$$

$$\delta_{22} = -0.36\left(\frac{B_M}{L} - 0.12\right) + 0.93\left(0.4 - \frac{d}{h}\right) \quad (3.19)$$

In the formulas, the berm width over wavelength ($\frac{B_M}{L}$) is required for δ_{11} and δ_{22}. However, in this study, the berm width is zero which means that there is no sloped structure constructed in front of the vertical wall breakwater in the experiment. This case effects the whole design study of vertical wall breakwater starts with 3.18 and 3.19. As mentioned in the literature review part, there are limited research exist about the vertical seawall without dike in the front. With this study, it is also aimed that contribute to the literature for the vertical breakwaters without significant berms (pure vertical breakwater).

CHAPTER 4

RESULTS

In this chapter, the results of anaysis of the wave and pressure measurements are presented. Although the measured pressure unit was bars, that unit converted to kilopascals (kPa) for all discussions. Density of water is assumed as 1000 kg/m^3 and the gravity is considered as 9.81 m/s^2.

4.1 Wave Characteristics

Following the zero-upcrossing methodolgy wave heights and periods of the first 4 measurements of each timeseries representing the hydrodynamic conditions are presented in this section. The data is provided in the Appendix and as a dataset. The wave characteristics are determined for both gauge 2 located infront of the structure after the wave transformation as well as gauge 11 located before the slope showing the deep water conditions.

As can be seen in the Figure 4.1, most of the analyzed wave heights having a value between 0.05 and 0.1m for gauge 2, which is located in front of the seawall. On the other hand, the distribution of the wave height values for gauge 11 is different. Since the placement of the gauge 11 is in deep water, the wave heights are distributed different than gauge 2, as can be seen in the Figure 4.2. These results show that wave transformation had a significant impact on the wave characteristics which exerted the pressure on the structure. Therefore, in the discussions and dimensionless analysis, the wave height from gauge 2 is used.

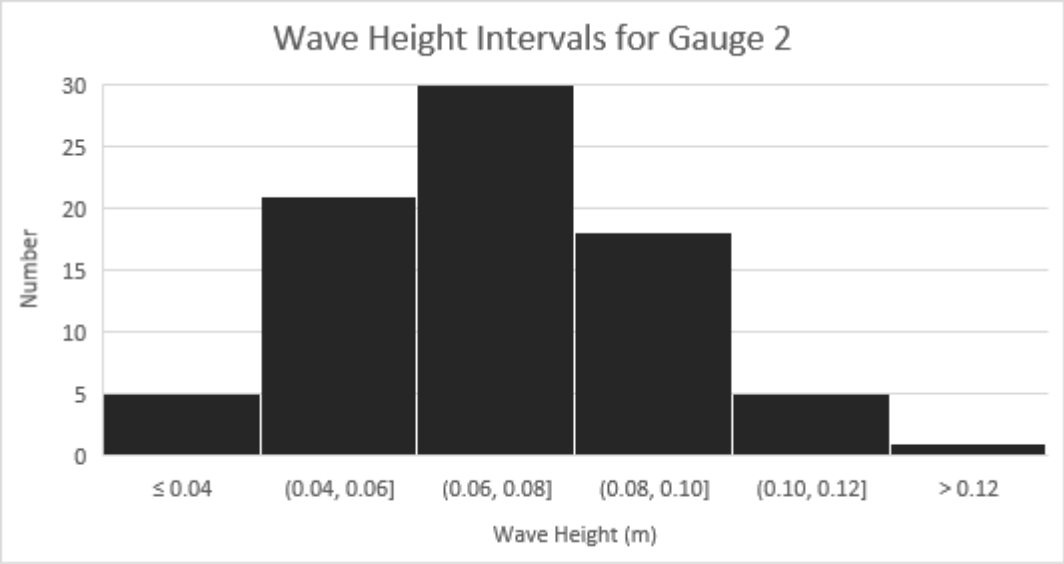

Figure 4.1: Wave height intervals for gauge 2

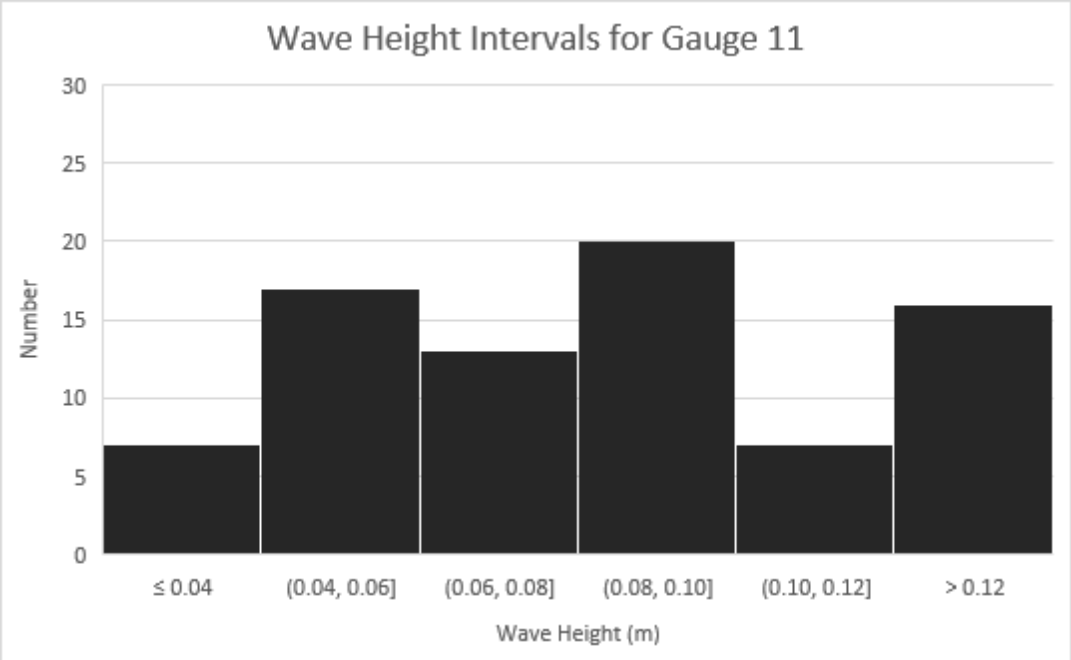

Figure 4.2: Wave height intervals for gauge 11

Similar to wave heights, wave periods are also determined for both gauges. As can be seen in the Figure 4.3, the wave periods are mostly distributed between 1.32 and 1.65 seconds for gauge 2. In the Figure 4.4, it can be seen that the wave period

distribution has slightly larger values than gauge 2. This shows that wave period was also affected by the wave transformation although not as significant as wave height.

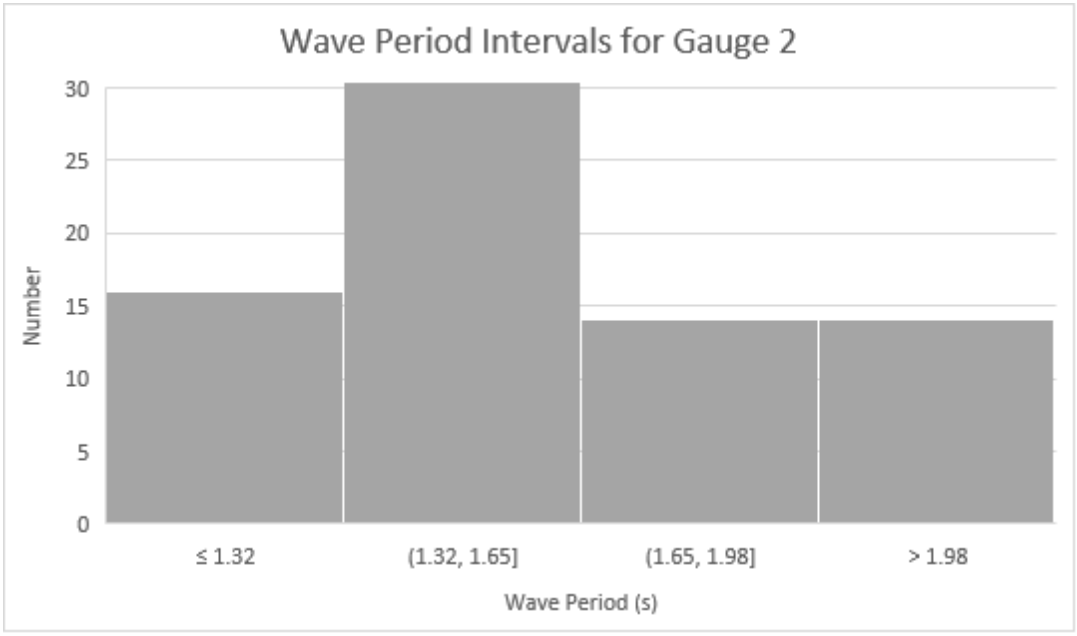

Figure 4.3: Wave period intervals for gauge 2

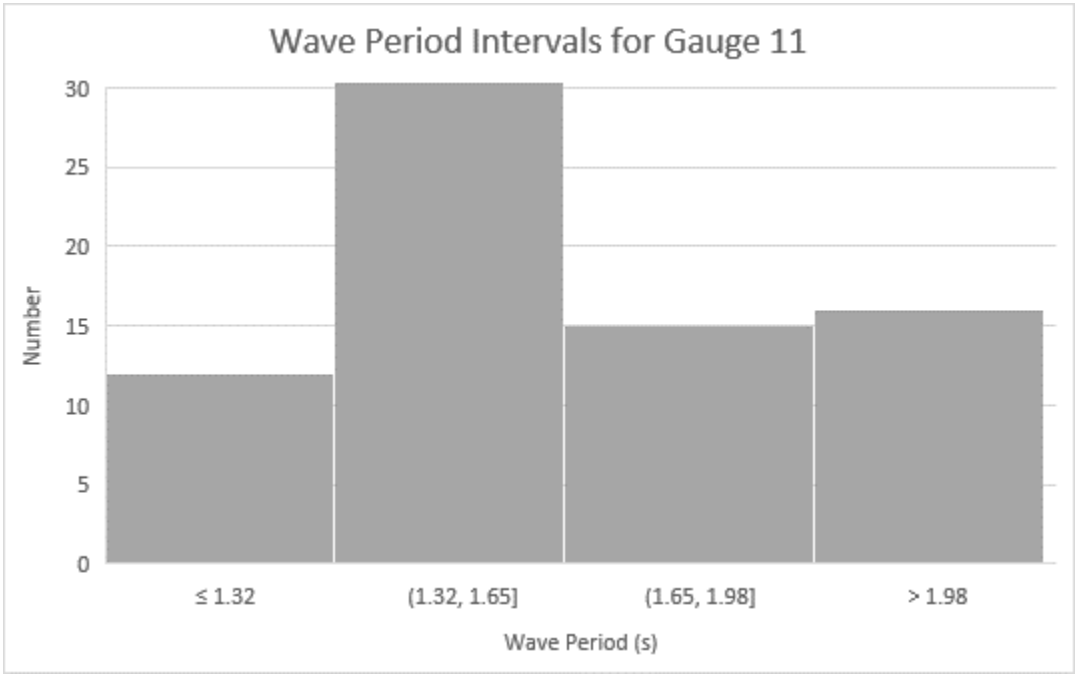

Figure 4.4: Wave period intervals for gauge 11

The wave classification based on PROVERBS showed that majority of the waves in the experiments generated impact loadings as they are classified as `large waves`. In the Figure 4.5, the distribution of the quasi-static loadings and impact loadings for the experiment is represented. Wave height performed as small waves caused quasi-static loads and large waves caused impact loads. Most of the quasistatic loads were caused by the first wave which is actually the developing wave by the generator.

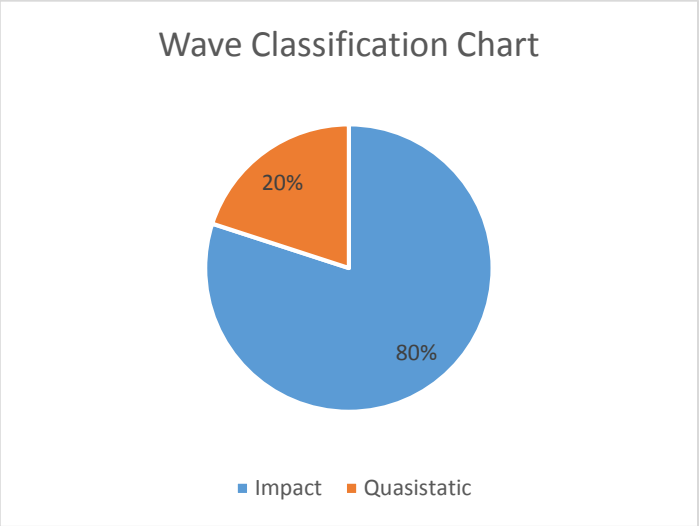

Figure 4.5: Wave Classification Chart

The wave classification based on pressure signal depicting the type of wave breaking is also performed as described in the methodology chapter. The waves that fit the pattern of the Figure 3.24 for first 4 waves are noted as non-breaking waves (NBW), fits Figure 3.25 are slightly breaking wave (SBW), fits Figure 3.26 are breaking wave (BW) and fits Figure 3.27 are noted as broken waves (BOW). In some cases, the problematic or out of ordered signals could not be evaluated. The amount of these signals is 11% of the total data. Also in the most cases, the first 4 wave's classifications for breaking case differ. In those cases, some of the waves are classified started from a NBW and then went to SBW, sometimes even directly went to BW throughout the signal. The distribution of the wave breaking classification is presented in the Figure 4.6.

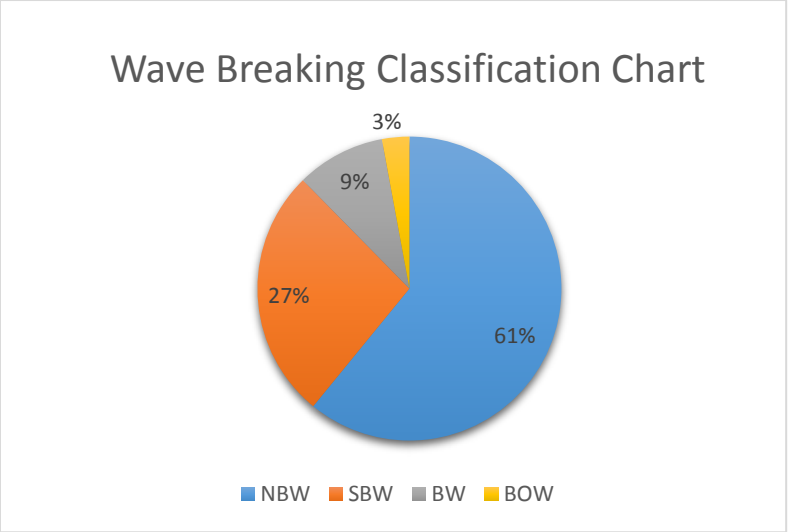

Figure 4.6: Wave breaking classification chart for all setups for gauge 30

4.2 Maximum Wave Pressures

The results of the maximum wave pressure data for each setup are presented as graphs with dimensionless parameters, H/hs vs $P/\rho gH$. In the dimensionless analysis, h_s represents the depth of water, which is indicated as d_w in the model scale of the experimental setups. By using the dimensionless parameters, the pressure results can be discussed independent of two main hydrodynamic conditions, water depth and wave height. Additionally, by using H/hs , the dataset can also be discussed following the wave classification of PROVERS which helps to understand the load type represented by the maximum pressure value. In the maximum pressure graphs, the wave classification boundary for the PROVERBS, Oumeraci et al. (2001) is presented with a red line on the 0.35. In that case, the H/hs values below the red line are quasi-static and H/hs values above the redline are impact pressures.

The results will be presented in the order of common vertical seawall (Setup 11), sea side storm walls (Setup 1 and 2), land side storm walls (Setup 7 and 8) and stilling wave basin configurations (Setup 4 and 6) to show the changes in the pressure with respect to changing of configurations as well as components.

For Setup 11 which is the conventional vertical seawall, the larger pressure values are measured at Gauge 27 which is located on the storm wall where most of the waves break when they break at the structure. Gauge 28 which is located at the very bottom measured the lowest pressures most of the time which is expected based on the pressure distribution graphs of Goda (2010). Majority of the pressure data is less than 0.005 for these wave conditions. The maximum pressure is also measured by Gauge 30 and even Gauge 29 probably due to water level changes. To understand the pressure distribution on the vertical wall, Figure 4.7 is provided.

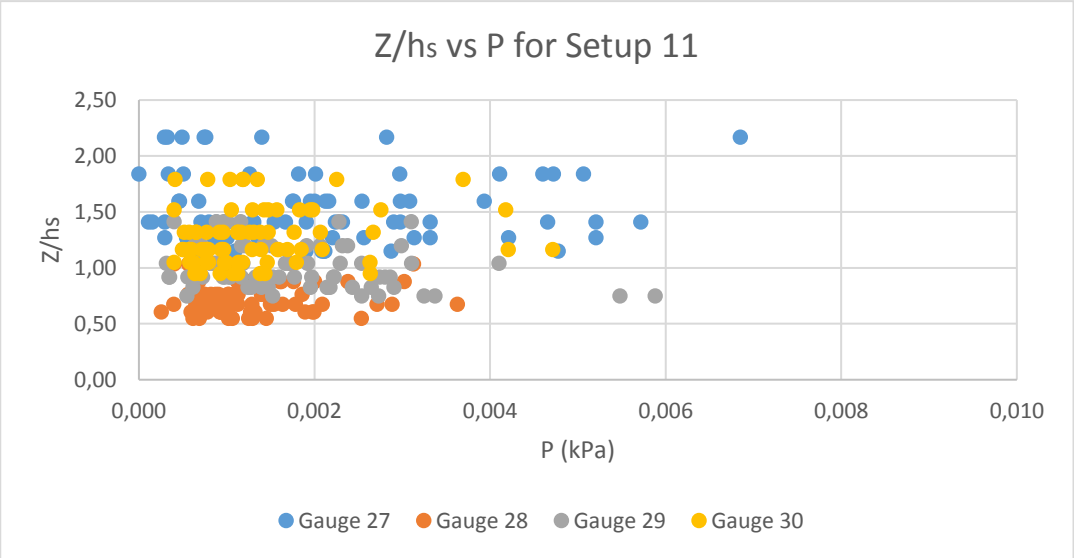

Figure 4.7: Z/hs vs P for All Gauges of Setup 11

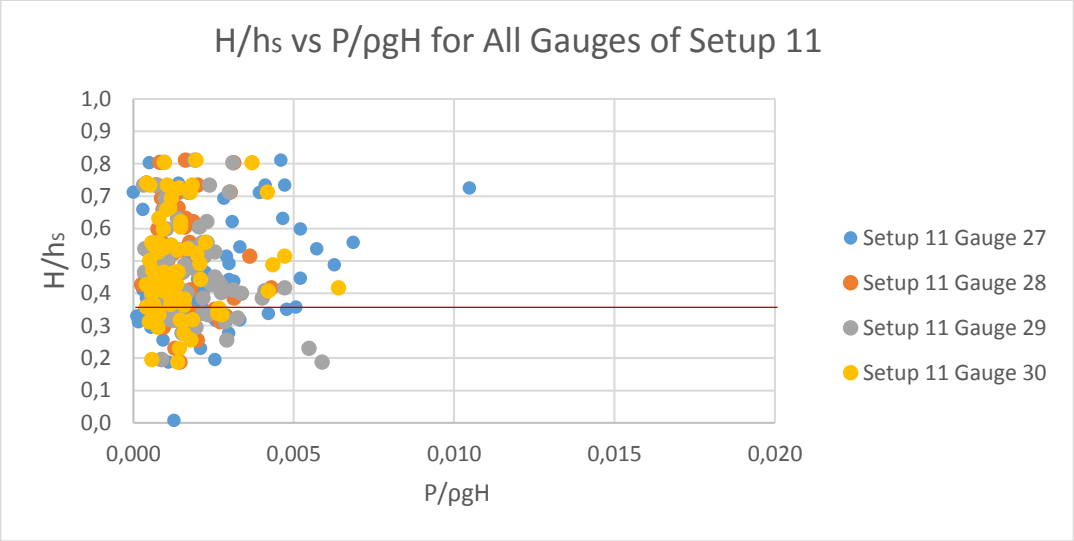

Figure 4.8: H/hs vs P/ρgH for All Gauges of Setup 11

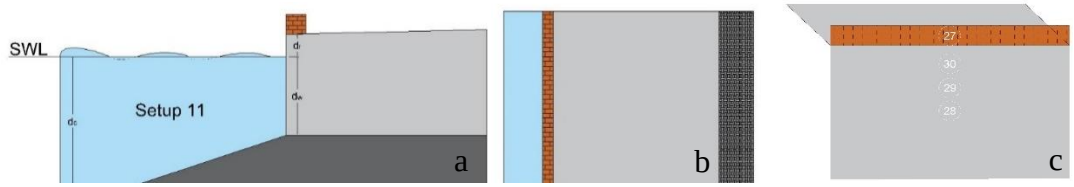

Figure 4.9: Setup 11, **a)** side view **b)** top view and **c)** front view

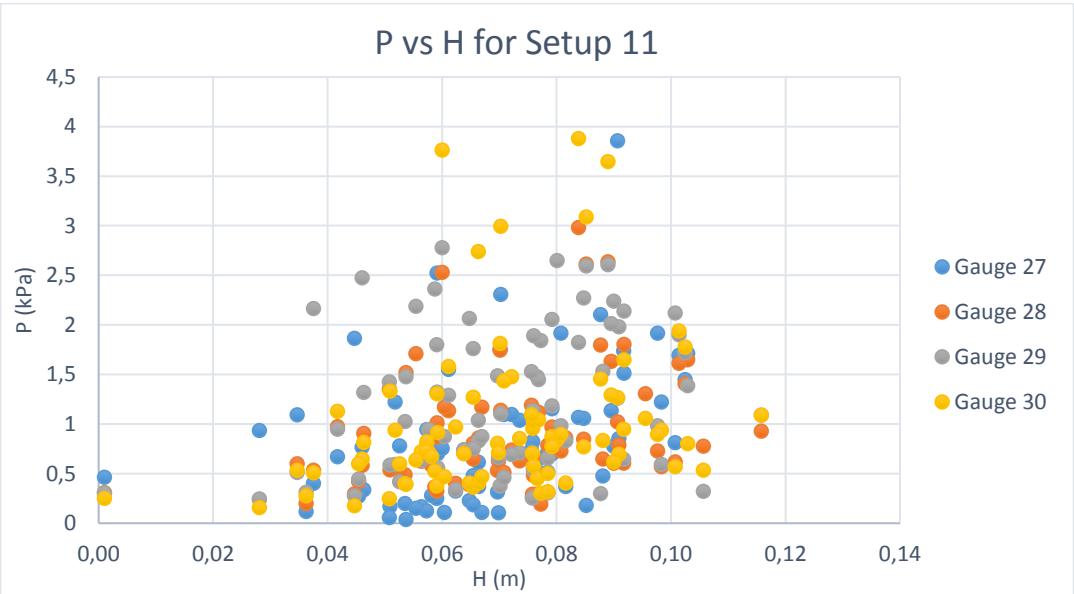

Figure 4.10: P vs H for All Gauges of Setup 11

In the setup 1, the three sensors are placed on the storm wall with gaps whereas sensor 30 is located on the wall. It can be seen in Figure 4.7 that the gauges placed in front of the storm wall are having larger pressure values compared to gauge 30. This result is similar to Setup 11 where the gauge on the storm wall measured higher pressure values. Among the three gauges that are located on the similar level, the pressures are also similar to each other with small variations. This is expected as the sensor size is small and randomness of the wave breaking which influences the impact pressures. Compared to Setup 11, the wave pressure values are slightly higher.

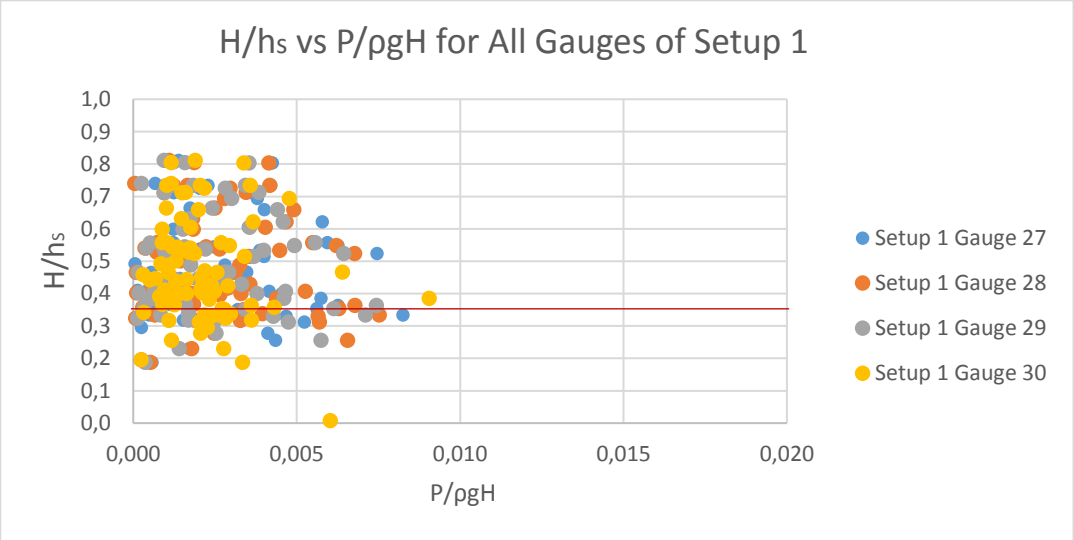

Figure 4.11: H/hs vs P/ρgH for All Gauges of Setup 1

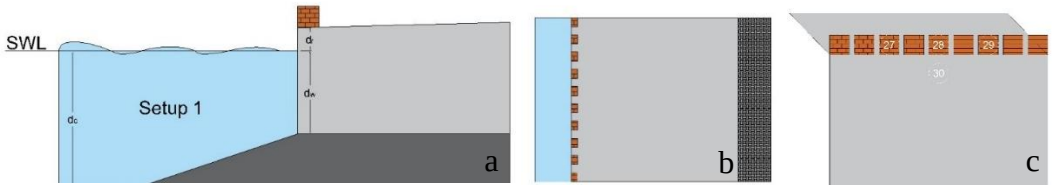

Figure 4.12: Setup 1, **a)** side view **b)** top view and **c)** front view

In the setup 2, there is a continuous bullnose over the storm wall. The pressure values measured on the storm wall via the three sensors under the bullnose are larger and the scatter is also more significant. The pressure measured by sensor 30 is also

slightly larger than the previous setups. Much higher pressure values are measured for H/hs <0.35.

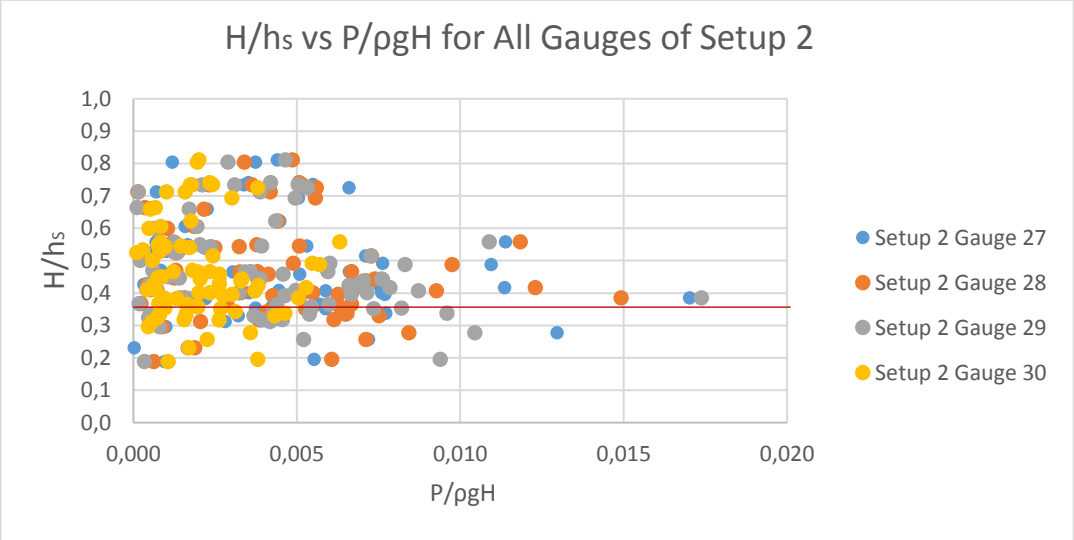

Figure 4.13: H/hs vs P/ρgH for All Gauges of Setup 2

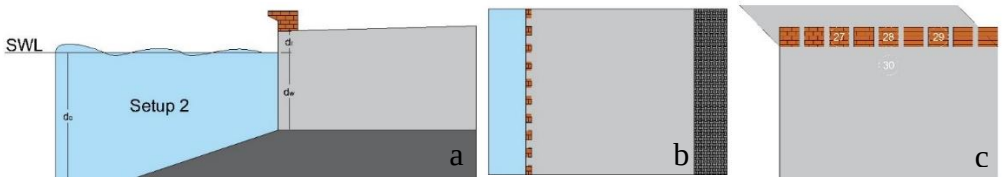

Figure 4.14: Setup 2, **a)** side view **b)** top view and **c)** front view

In the setup 7, since there is no superstructure or any component placed in seaward side. The sensors are located on the landward storm wall which is continuous. The wave passes over the promenade to reach the landward storm wall. The pressure data distribution is similar to Setup 2 such that larger pressure is measured on the storm wall and for lower values of H/hs. However, this is an interesting result because as the initial wave-structure interaction occurs at the seawall (gauge 30) however the wave that crosses across the promenade exerts larger pressure. The same storm wall located at the seaside actually in under lower pressure.

Nevertheless, most of the waves approaching to the vertical wall are non breaking or slightly breaking waves. This means the wave tends to break but the water level at the wall accelerates fast and results in an incomplete breaking due to the presence of the wall. Therefore, horizontal impact forces are measured rather small at the wave on Gauge 30. However, vertical acceleration results in larger tangential forces those cannot be recorded by the used pressure sensors. After overtopping happened on the seaward storm wall, the water is a horizontal jet or bore with a horizontal velocity that can produce high impact pressure on the vertical landward storm wall (Gauges 27-29).

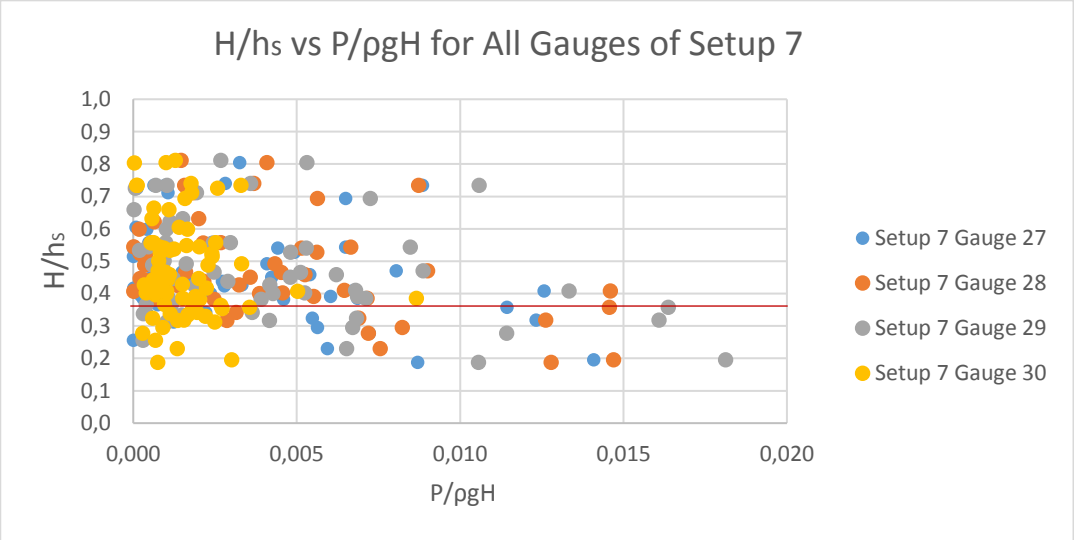

Figure 4.15: H/hs vs P/ρgH for All Gauges of Setup 7

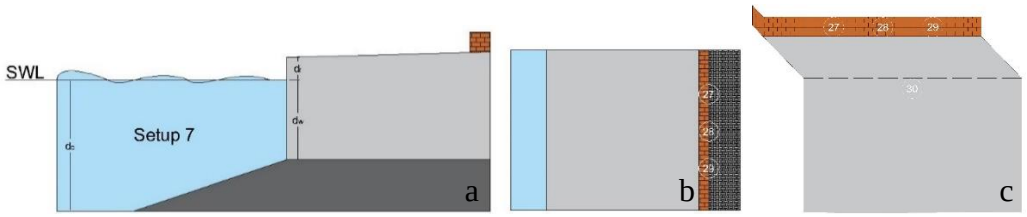

Figure 4.16: Setup 7, **a)** side view **b)** top view and **c)** front view

The situation for reading the pressure values is very close between setup 7 and setup 8. Again it is difficult to say one of them is having bigger values than the others

between the landward pressure gauges. However, they are bigger than pressure gauge 30.

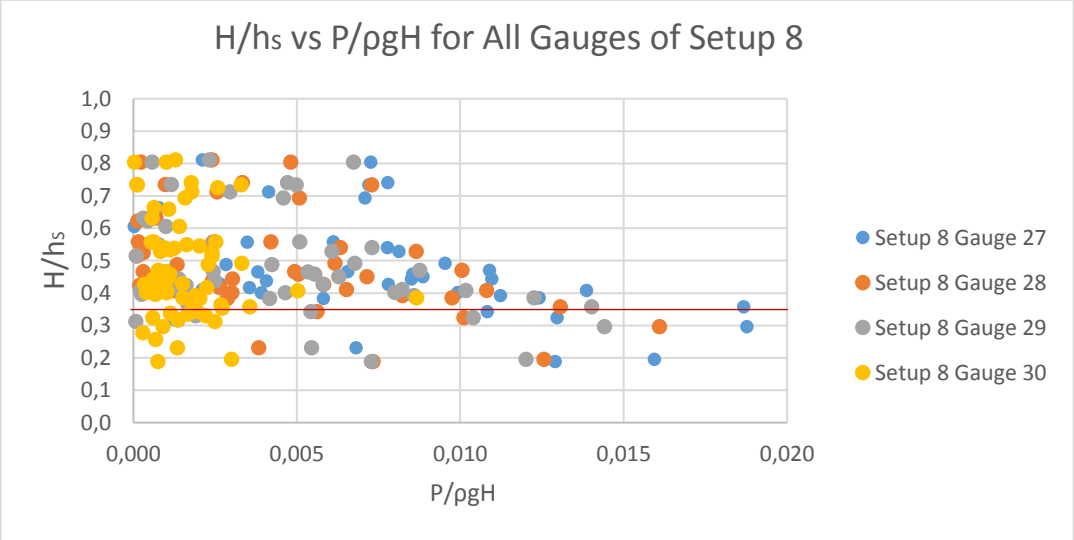

Figure 4.17: H/hs vs P/ρgH for All Gauges of Setup 8

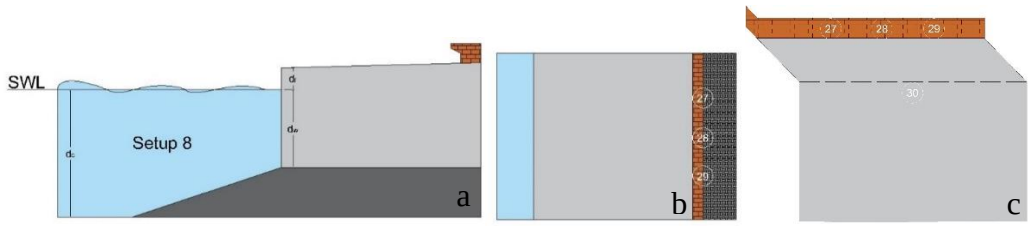

Figure 4.18: Setup 8, **a)** side view **b)** top view and **c)** front view

In the setup 6, the pressure distribution for the pressure sensors is similar top setup 4. The pressure gauge 28 which is located in front of the storm wall is having the biggest read pressure values.

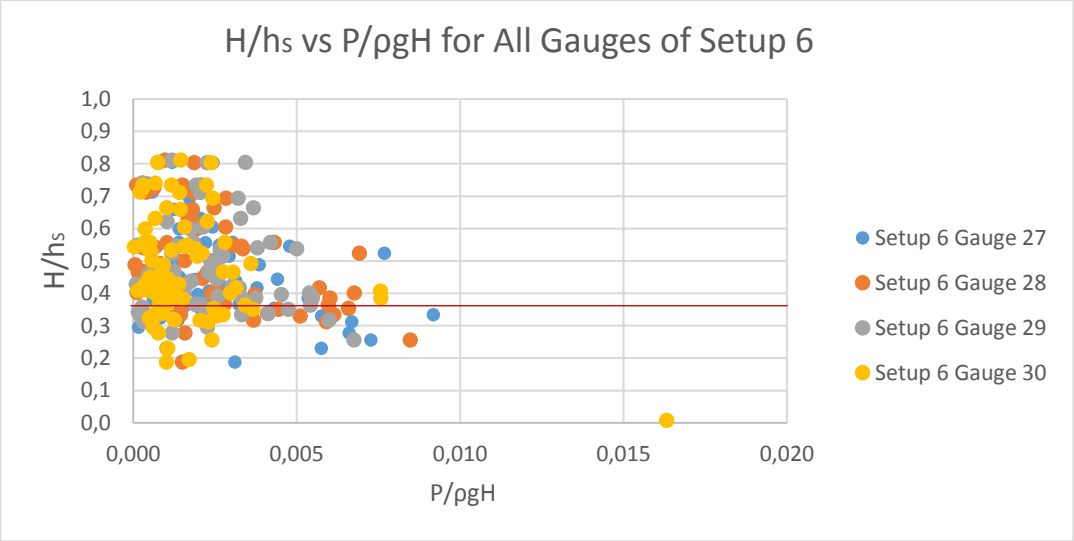

Figure 4.19: H/hs vs P/ρgH for All Gauges of Setup 6

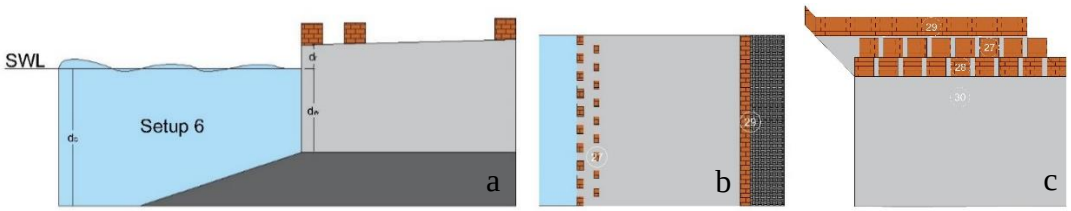

Figure 4.20: Setup 6, **a)** side view **b)** top view and **c)** front view

For the setup 4, it can be easily seen that the pressure gauge 28 which is located in front of the storm wall and above the seawall is having the biggest pressure values. Since the other pressure gauge located at the beginning and at the end of the promenade, their pressure values are not remarkably more than pressure gauge 30.

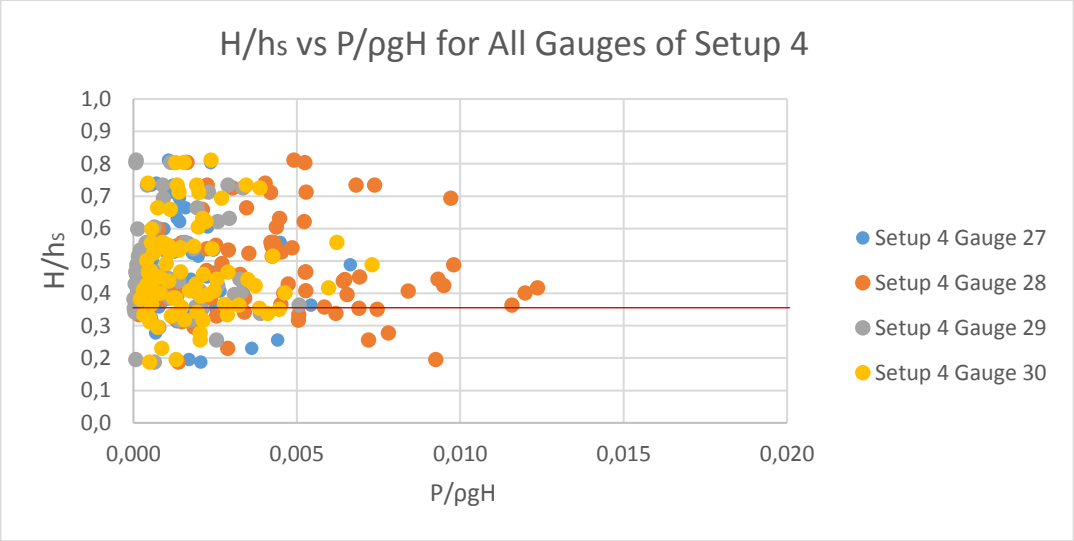

Figure 4.21: H/hs vs P/ρgH for All Gauges of Setup 4

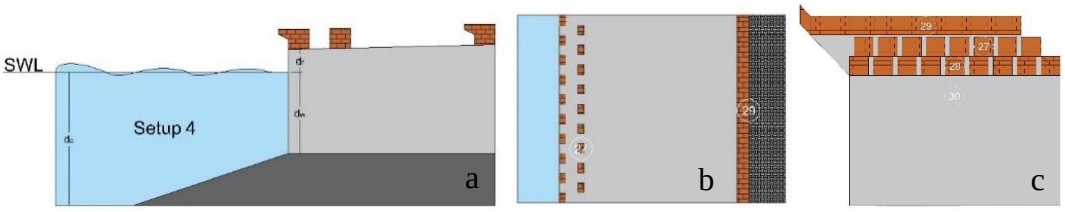

Figure 4.22: Setup 4, **a)** side view **b)** top view and **c)** front view

CHAPTER 5

DISCUSSIONS

In this chapter, the discussions are presented in detail to present how wave pressure changes on components of SWB based on the results shown in Chapter 4. Seven different cases presented in this chapter corresponds to the research questions proposed in Introduction. Due to limited geometry of SWB tested in the experiments, the discussions focus on the general trends of changes of wave pressure, not formulation for quantitive values of pressure. The general trends help to design components as well as configuration of superstructures on a vertical seawall.

5.1 Case 1 – Evaluation of the Wave Pressure on the Vertical Seawall Based on Different Storm Wall Configurations

In the case 1, the behaviour of the wave pressure on the vertical wall under different storm wall configurations is discussed. For this purpose, the effect of following stilling wave basin components are examined: seaward storm wall (single row with gaps), landward storm wall and continuous seaward storm wall is examined in their setups. The pressure gauge 30 which is located in same place for every setup, at the front side of the storm wall is evaluated.

Figure 5.1 shows the wave pressure with respect to relative wave height in dimensionless manner. If the superstructure configuration had no impact on the pressure distribution along the vertical wall, the pressure values were expected to be similar to each other for all three setups. This is true for most of the dataset within up to 0.002. However, it is clearly observed that more data is placed for Setup 1 (seaward storm wall with gaps) for higher pressure values compared to Setup 7 (no structure on top of vertical wall) and Setup 11 (continuous seaside storm wall). Setup 7 again provides slightly higher pressure values for Gauge 30 compared to Setup 11.

The difference between Setup 7 and Setup 11 is crest height where the lower crest height could increase the wave pressure due to larger volumes are being overtopped. The difference between Setup 11 and Setup 1 is the gap configuration of Setup 1. The gaps change the flow dynamics of overtopping flow where along the gaps, the flow behaves like a jet. This process could increase the pressure exerted on the vertical wall. However, detailed experiments are required to have an accurate discussion. Also, the red line drawn at 0.35 presents that the quasi-static and impact load boundary according to Oumeraci et al. (2001). Here, H/h_s values greater than 0.35 are impact values.

To sum up, the configuration of the superstructure can increase the measured pressure exerted on the vertical wall, the increase could be more when storm wall is a gapped section.

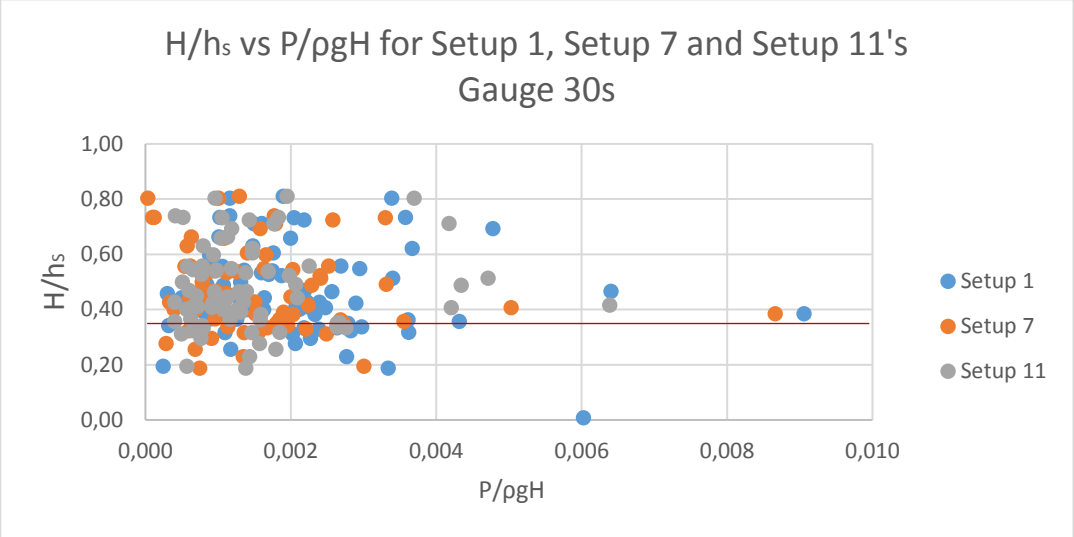

Figure 5.1: H/hs vs P/ρgH for setup 1, setup 7 and setup 11's gauge 30

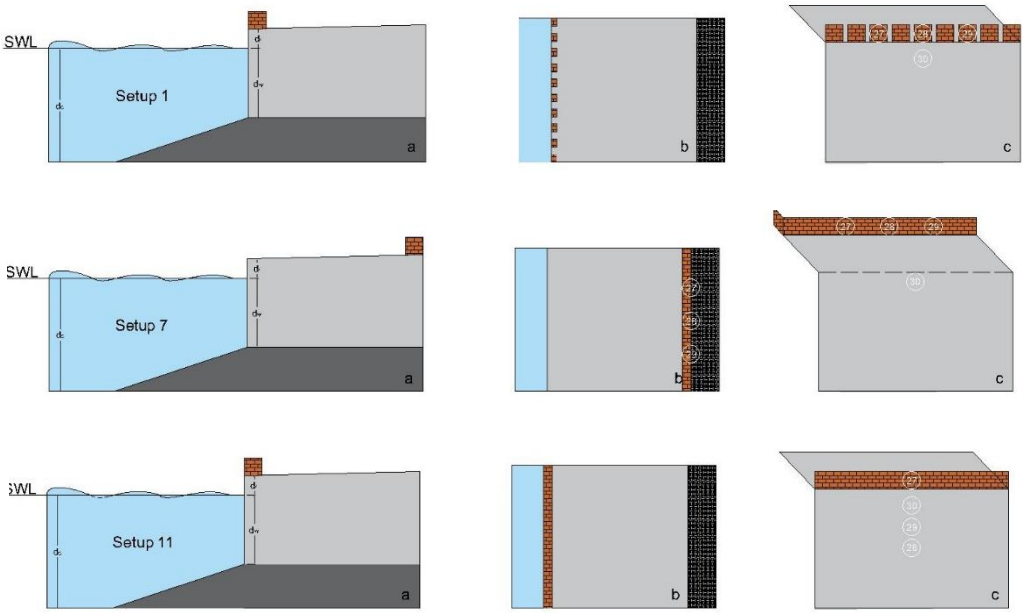

Figure 5.2: Setup 1, setup 7 and setup 11, **a)** side view **b)** top view and **c)** front view

5.2 Case 2 – Discussion of the Gap Configuration on the Wave Pressure of Storm Wall at the Seaward Side

The discussion of Case 1 is extended as in Figure 5.3 with gauge 28 of both seaward structures, which is located on the storm wall of the continuous (Setup 11) and gapped configuration (Setup 1). With the help of this extension, the comment that the gapped section causes more pressure on the front side of the storm wall, is much clearly demonstrated with higher pressure values measured for the same location located between gaps (Setup1).

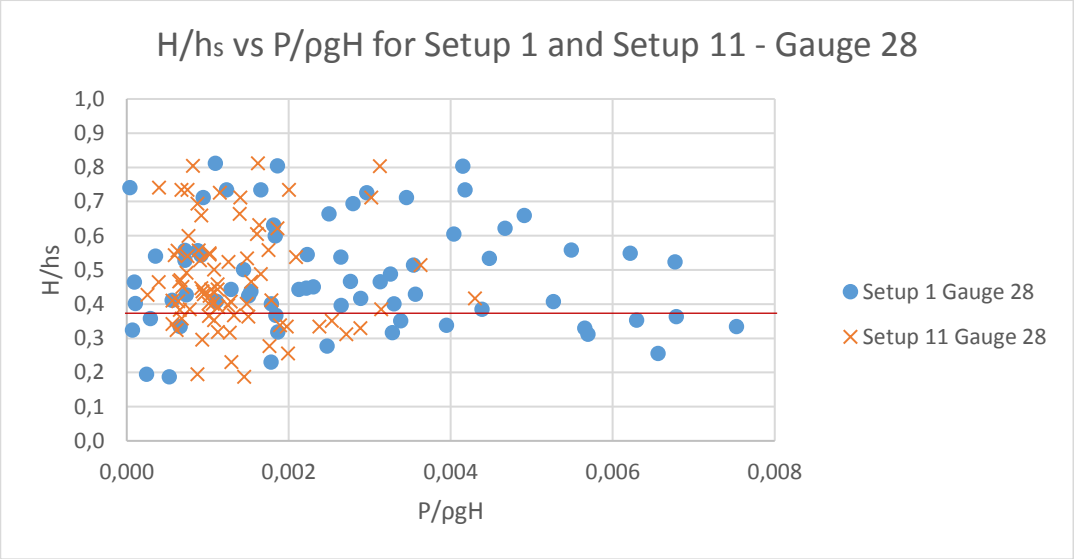

Figure 5.3: H/hs vs P/ρgH for setup 1 and setup 11's gauge 28

As also can be seen in Figure 5.4 and 5.5, it is possible that the jet behavior along the gaps increases the pressure exerted on the storm wall component. The trend is much significant for lower water levels based on the experimental data.

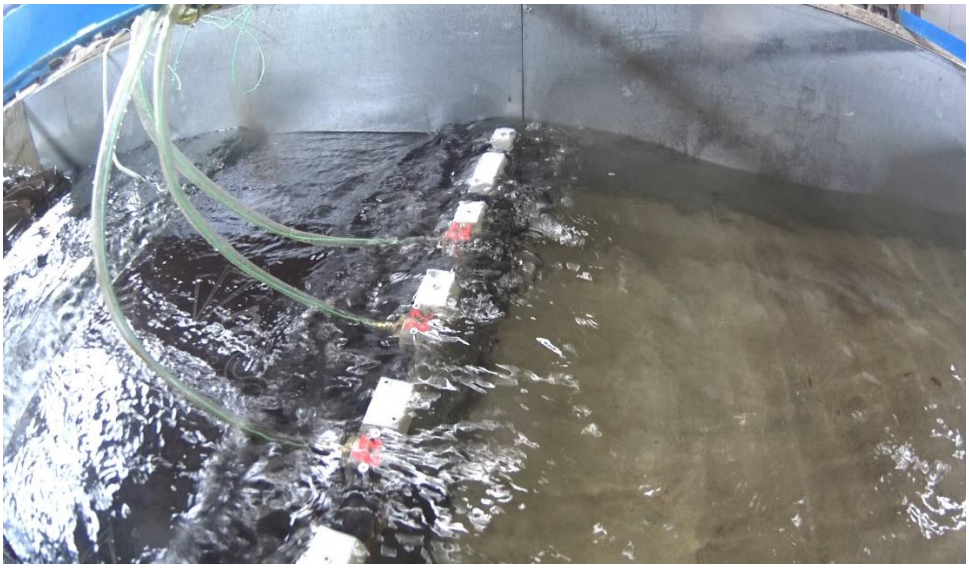

Figure 5.4: During the experiment of setup 1 wave 1 (H_{s0} = 0.081m and $T_{m-1,0}$ = 1.26s)

Figure 5.5: During the experiment of setup 11 wave 1 (H_{s0} = 0.081m and $T_{m-1,0}$ = 1.26s)

5.3 Case 3 – Discussion of the Bullnose Effect at the Seaward Side

To continue the discussion for the seaward side, bullnose effect is discussed in this case. Between the setups, gapped section structure without bullnose (setup 1) and with bullnose (Setup 2) is evaluated for gauge 28 to show the pressure change on the storm wall. As the location of the gauges are exactly the same, the graphs are drawn for the dimensionless parameter Z/hs to reflect the water depth effect (sensor is closer to water level or not). In the graphs, the unit Z represents the vertical distance for the gauge from the base of the seawall.

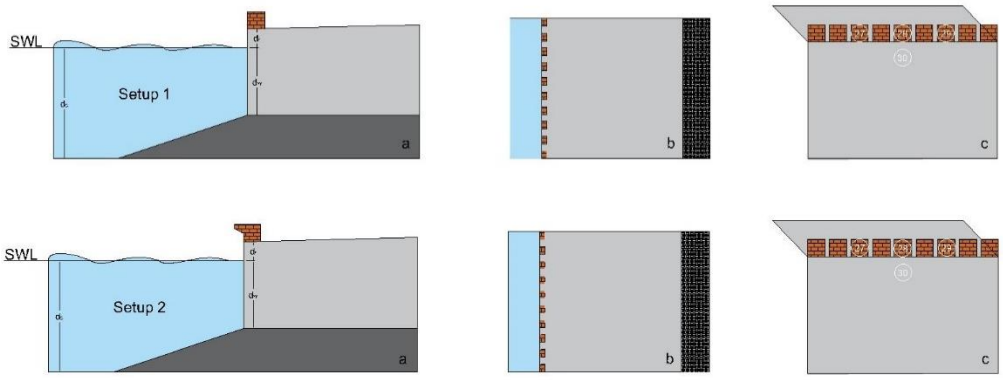

Figure 5.6: Setup 1 and setup 2, **a)** side view **b)** top view and **c)** front view

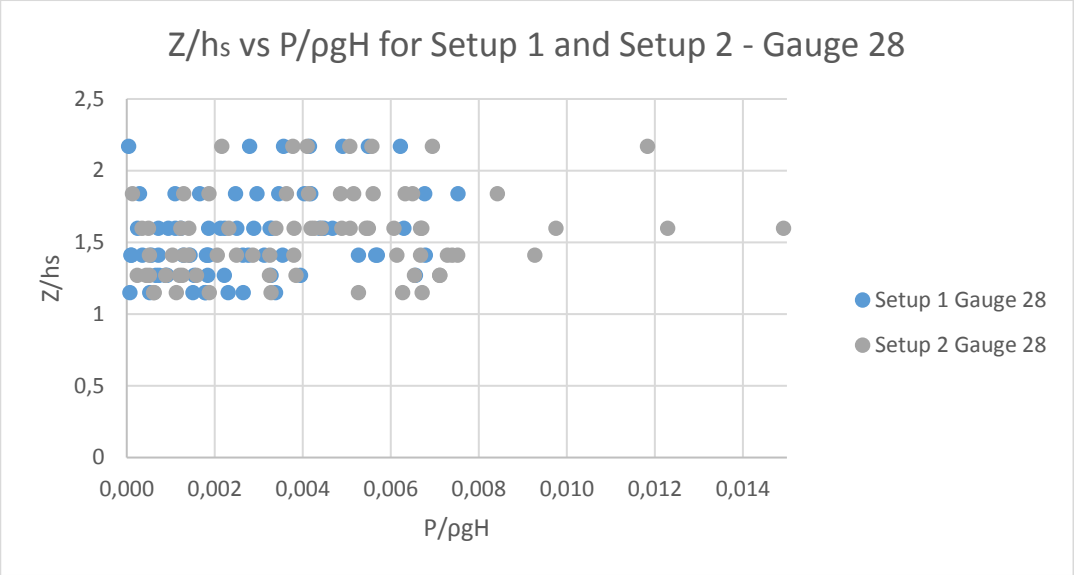

Figure 5.7: Z/hs vs P/ρgH for setup 1 and setup 2's gauge 28

Although some outlier values are exist, the presented figures Figure 5.7 and Figure 5.8 shows that the bullnose at the top of the superstructure increases the pressure on the front side of the storm wall. This trend is more significant for Gauge 28 compared to Gauge 30. Similarly, the trend is slightly more pronounced when the water level is closer to the gauges.

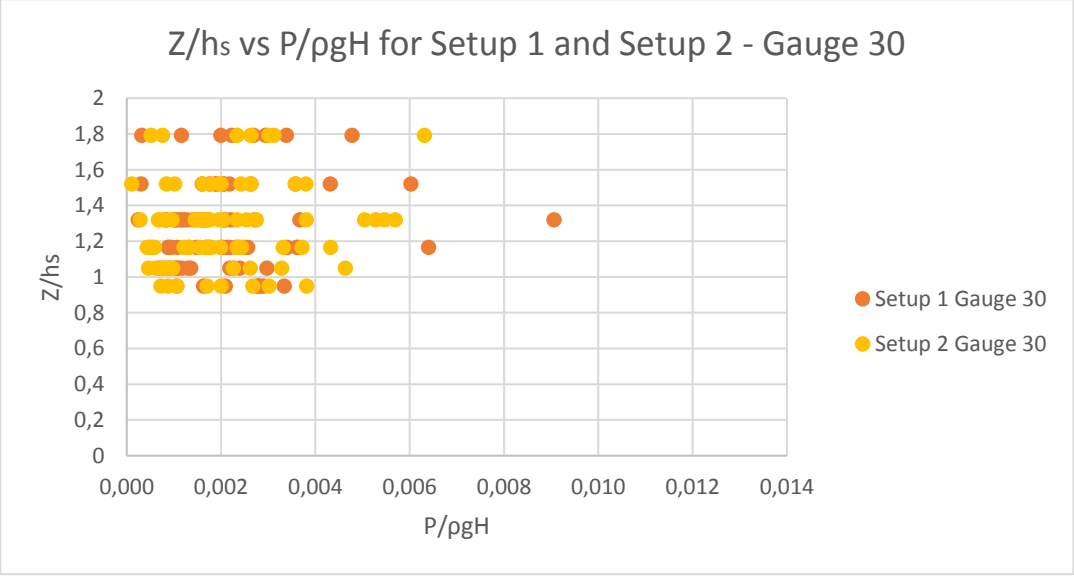

Figure 5.8: Z/hs vs P/ρgH for setup 1 and setup 2's gauge 30

It is also expected that the pressure values for gauge 27 and gauge 29 which are right and left edge pressure gauges are similar to Gauge 28. These pressure values are graphed with respect to relative wave height. The growth in the pressure values caused by bullnose is also observed especially for non-breaking wave conditions (higher water depths) compared to water depths closer to wave heights (impulsive load conditions).

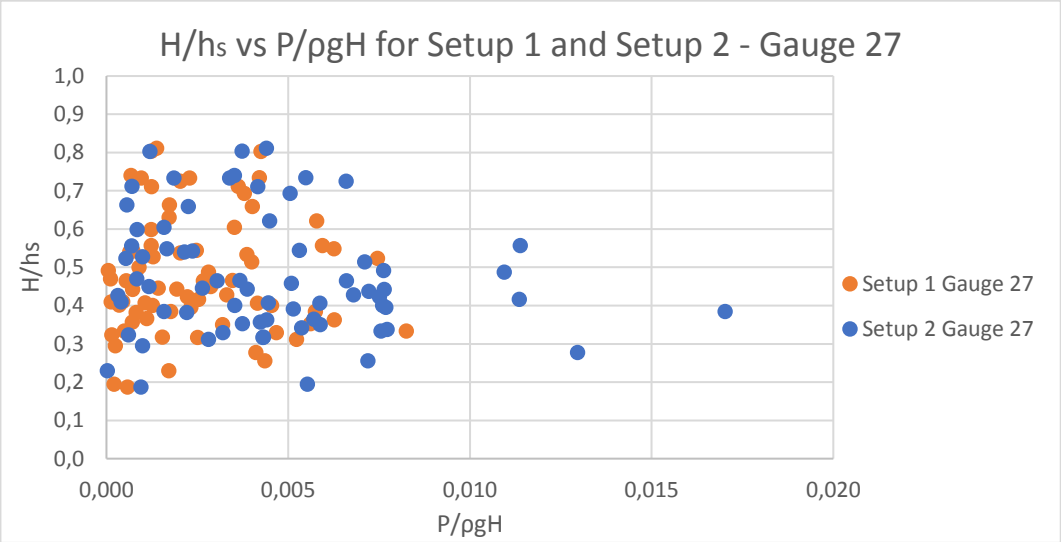

Figure 5.9: H/hs vs P/ρgH for setup 1 and setup 2's gauge 27

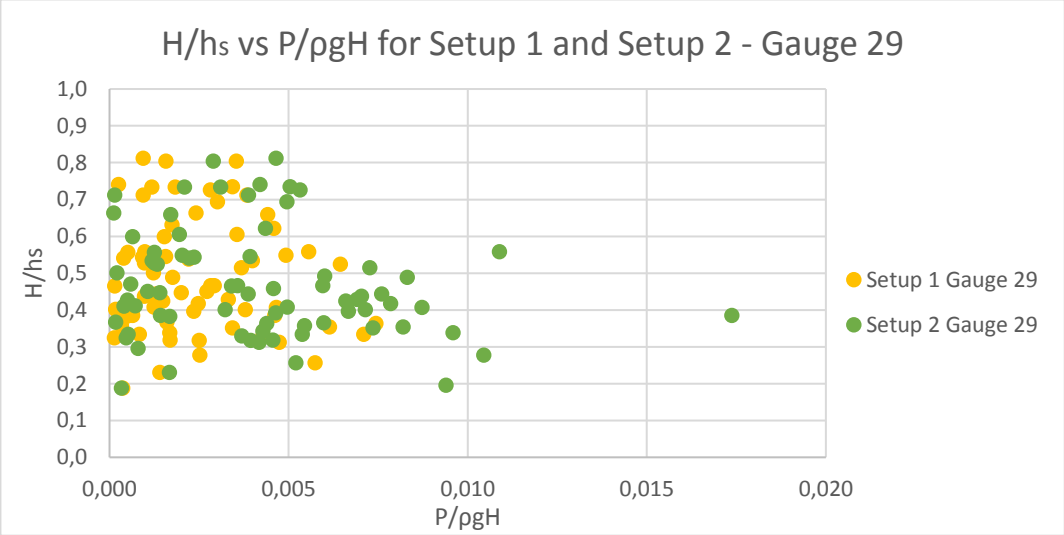

Figure 5.10: H/hs vs P/ρgH for setup 1 and setup 2's gauge 29

These inferences support the comparison made between different shaped seawalls by Anand et al. (2011). In that study, the flaring shaped seawall similar to the component bullnose was also measured bigger pressure values than the vertical wall. This is also coherent with the numerical analysis results of Castellino et al. (2018). They stated that "... a large and widespread pressure increase hits the recurved wall extending its influence on part of the vertical wall with a maximum value right under the recurve."

5.4 Case 4 – Discussion of the Bullnose at the Landward Side Storm Wall

In the case 4, bullnose effect is investigated to evaluate the landward storm wall without bullnose (Setup 7) and landward storm wall with bullnose (Setup 8). Both promenades have not any superstructure or component on the seaward side. In this case, gauge 29 is examined for both setups since it is located at the middle of landward storm wall for both setups. Figure 5.11 shows that the effect of the bullnose is not as significant as the front side observed in case 3 and the distribution of the pressure values are balanced. In the Figure 5.11, although the growth in the pressure for setup 8, can be seen slightly with respect to different water depths, it is not as much as in the case 2, seaward.

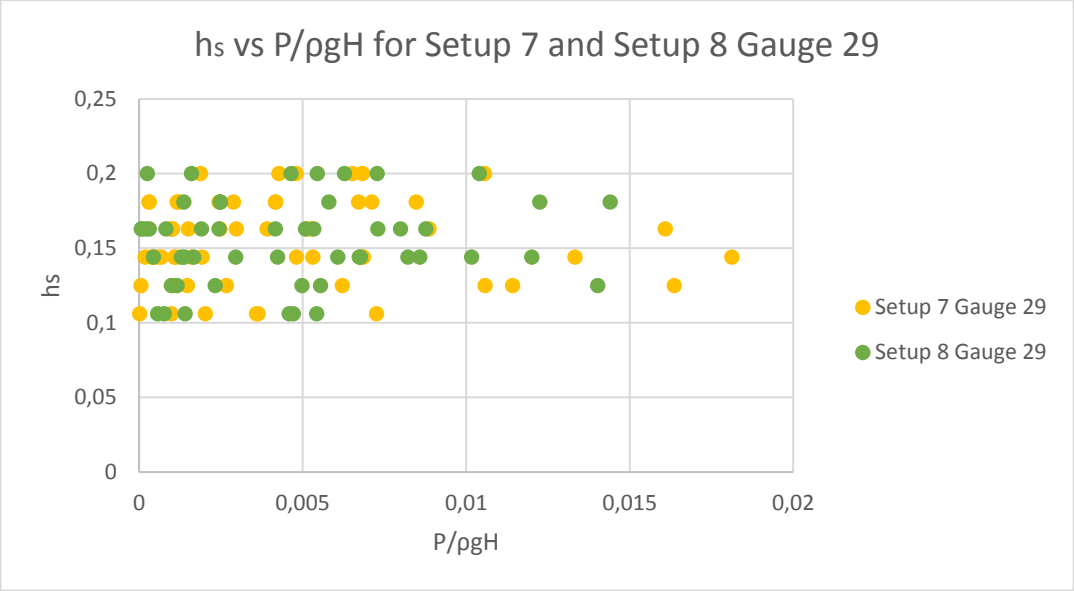

Figure 5.11: hs vs P/ρgH for setup 7 and setup 8 gauge 29

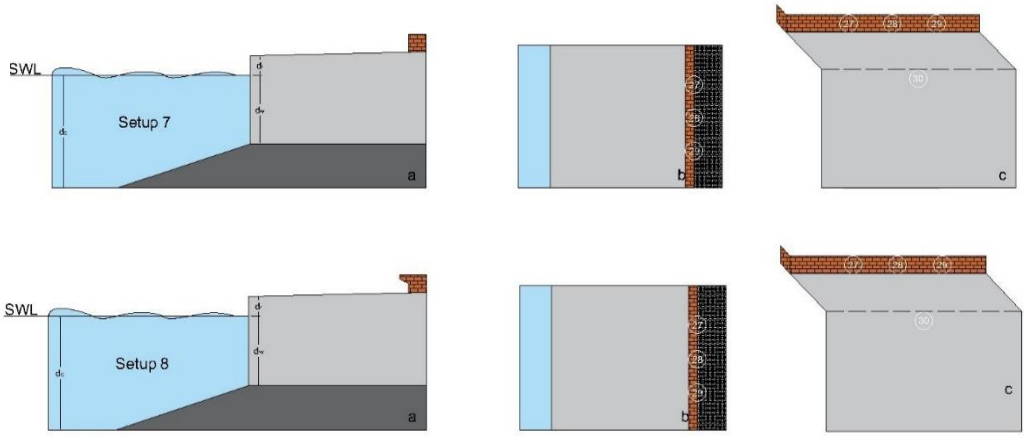

Figure 5.12: Setup 7 and setup 8, **a)** side view **b)** top view and **c)** front view

One to one comparisons of pressure data of all three pressure gauges along the storm wall are plotted in figure 5.13. The scatter among the three gauges is higher possibly due to promenade changing the wave characteristics to broken conditions which introduces higher randomness to the overall process. Still, the scatter diagram shows that the measured pressure values for the same wave for setup 8 are slightly larger compared to Setup 7 (without the bullnose).

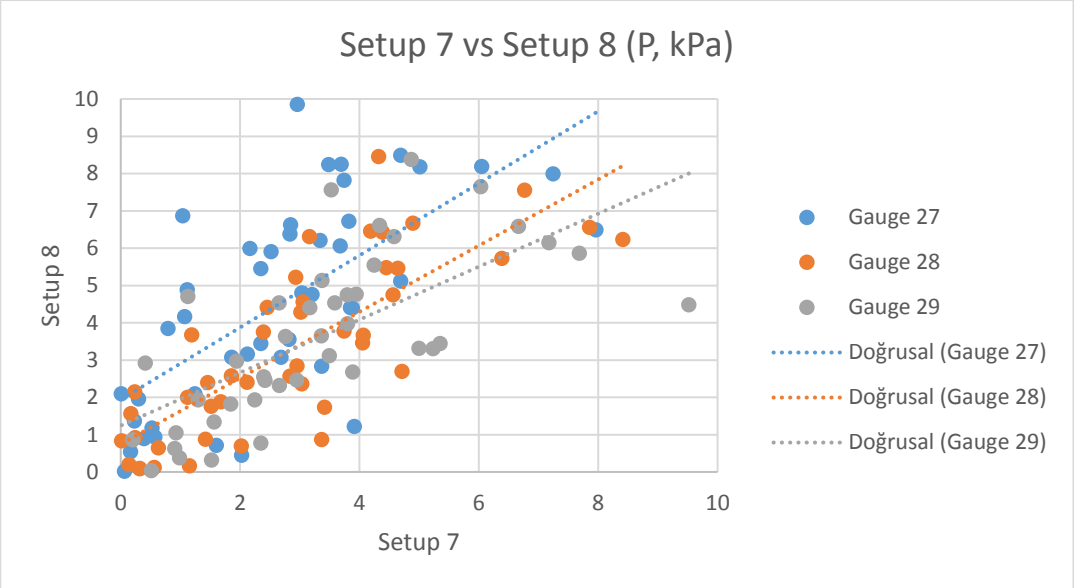

Figure 5.13: Setup 7 vs setup 8 in pressure

5.5 Case 5 – Discussion of Seaward Superstructure Effect at the Landward Side

In case 5, the effect of SWB configuration (shifted double row storm walls with gaps on the seaside) on the wave pressure at the landward storm wall is discussed. There are two setups with this configuration with bullnose (Setup 4) and without bullnose (Setup 6). These setups were compared to Setup 7 which is the configuration without any superstructure on the seaside. It is aimed to observe the effect of both gapped superstructure at the seaward and also bullnose for the landward. The evaluation is performed for the same water depth (h_s) (Figure 5.14).

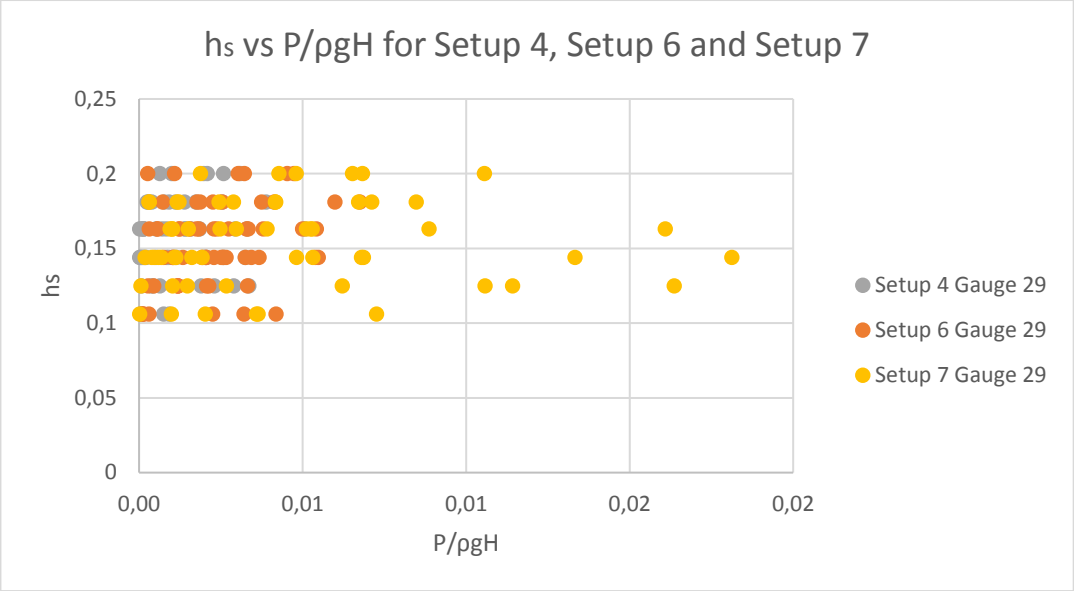

Figure 5.14: hs vs P/ρgH for setup 4, setup 6 and setup 7

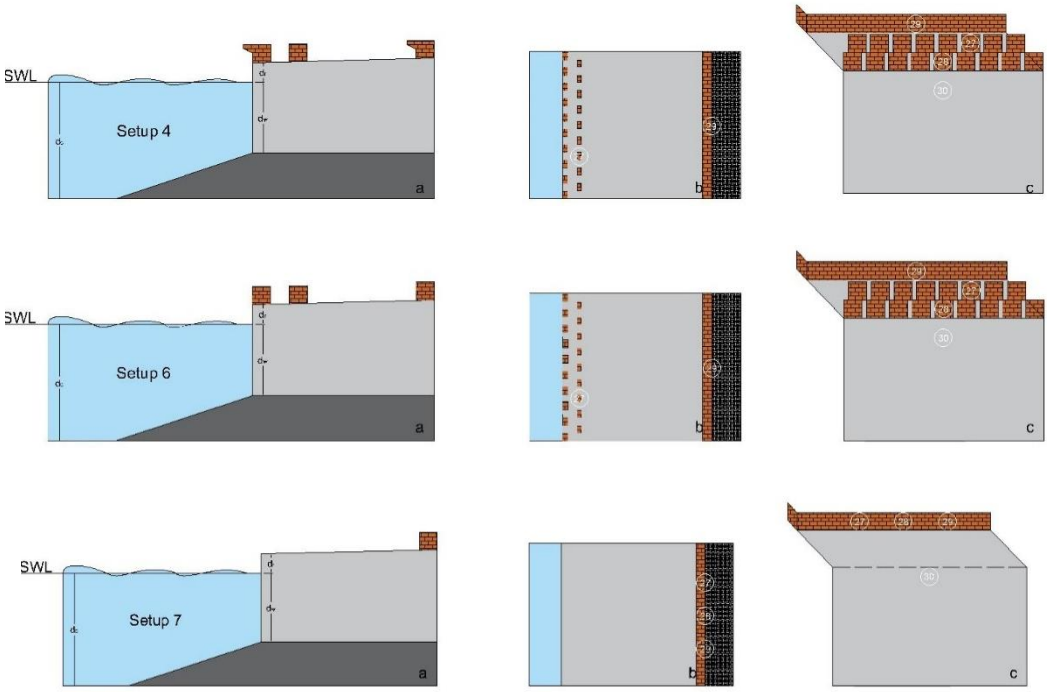

Figure 5.15: Setup 4, setup 6 and setup 7, **a)** side view **b)** top view and **c)** front view

As expected, the first observation for this case is the high pressure values are obtained for the no seaward superstructure (Setup 7) since there is not any

component to block any wave at the seaward. Another observation is noted that the pressure at the landward storm wall for the superstructure with bullnose is less than without bullnose which is probably due to the bullnose on the seaside decreasing the overtopping more than Setup 6, therefore the wave energy is more absorbed initially compared to Setup 6. This result directly supports the inferences of Ravindar & Sriram (2021) as the superstructures are efficient at reducing the impact pressure at the landward storm wall. It can be concluded that for the landward storm wall, the design of the seaside superstructure is more critical than its own configuration (bullnose attached or not). Figures 5.16-18 demonstrate the impact of seaside superstructure configuration on the overtopping process. Direct impact is observed for Setup 7, very low amount of water has reached for Setup 4 and a lot of the energy is absorbed in Setup 6 but still higher amount of water has overtopped.

Figure 5.16: During the experiment of setup 4 wave 5 (Hs0 = 0.088m and Tm-1,0 = 1.37s)

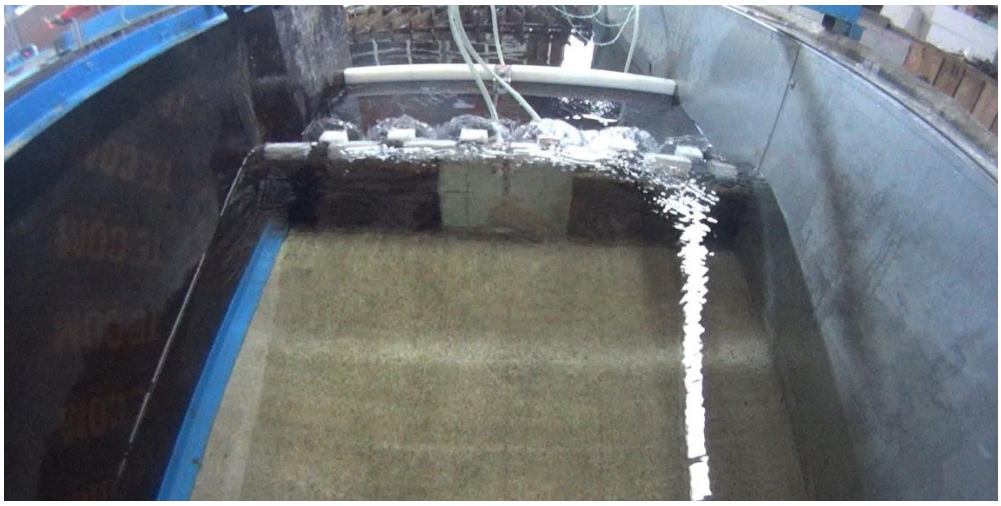

Figure 5.17: During the experiment of setup 6 wave 5 (H_{s0} = 0.088m and $T_{m-1,0}$ = 1.37s)

Figure 5.18: During the experiment of setup 7 wave 5 (H_{s0} = 0.088m and $T_{m-1,0}$ = 1.37s)

5.6 Case 6 – Discussion of Pressure Distribution on SWB Configuration With Respect to Its Components

Setup 4 and Setup 6 are the SWB configurations with and without bullnose attached to first row of seaward storm wall and continuous landward storm wall. The pressure gauges were located at the individual components for both setups. In this case, the

comparison of these two setups is presented to discuss the effect of mainly bullnose placement on the individual components.

Figure 5.19 and 5.20 presents the pressure data based on the relative location of the components in the x axis (distance to the vertical seawall with respect to wavelength). In the discussions, wavelength (L) is used the graphs calculated by equation 5.1.

$$L = 1.56T^2 \qquad (5.1)$$

To use this formula, the wave period values for gauge 11 located in the deep water is used. It was shown in the results sections that the change in wave period is very minimal.

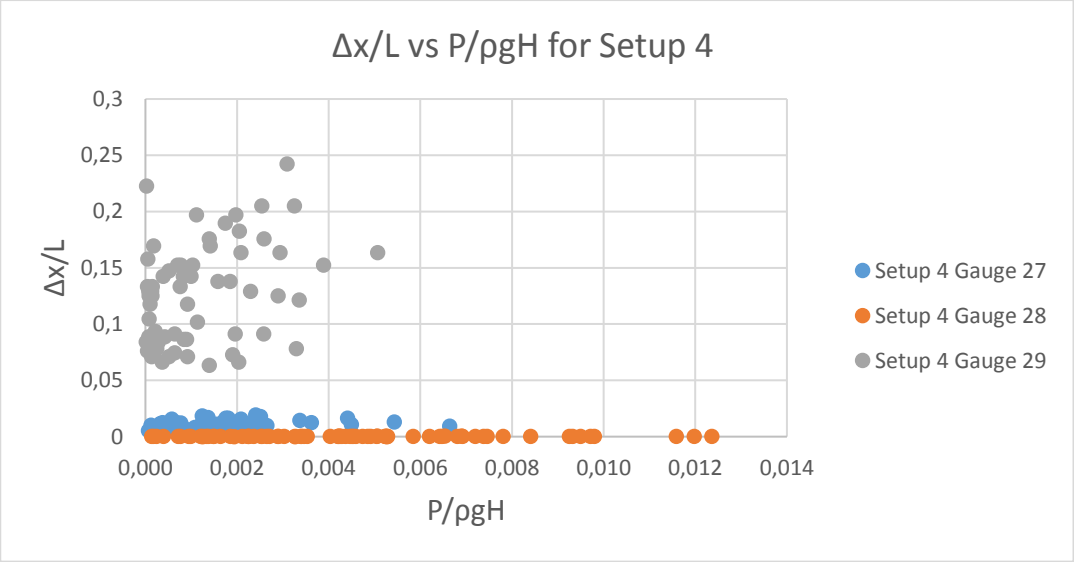

Figure 5.19: Δx/L vs P/ρgH for setup 4

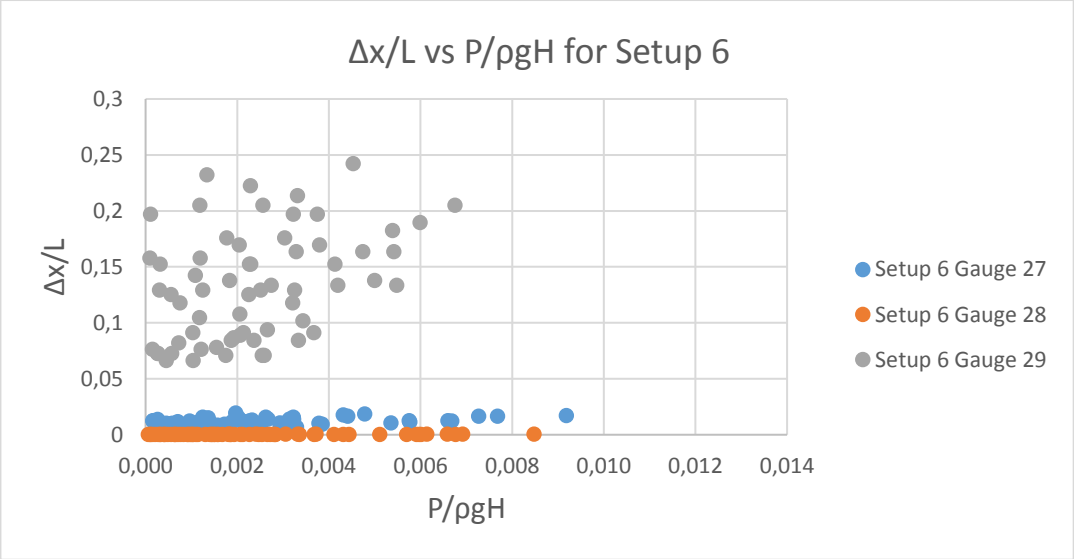

Figure 5.20: Δx/L vs P/ρgH for setup 6

As seen in the Figure 5.19 and Figure 5.20, the storm wall with bullnose of Setup 4 holds pressure at the seaward more than the storm wall without bullnose at the front side (setup 6). The graphs help to make interesting comparisons between the two setups. Gauge 28 located on the first row has the highest-pressure values when there is bullnose (Setup 4) but then the pressure values significantly decrease for second row (Gauge 27) and finally on the landward storm wall (Gauge 29). For setup 6, the higher pressures are both on first and second row of storm walls, higher pressures are observed at second row rather than first row. This is the case without bullnose. There is slight decrease in pressure for the landward storm wall however compared to Setup 4, the pressure distribution over the basin and components are more balanced. Individual components can experience similar pressure values for a range of hydrodynamic conditions for Setup 6. However, landward storm wall, the influence of the bullnose cannot be obviously observed as the others. This is probably due to significant change in the wave characteristics after the first two rows and bullnose effect of the seaside (Figure 5.22).

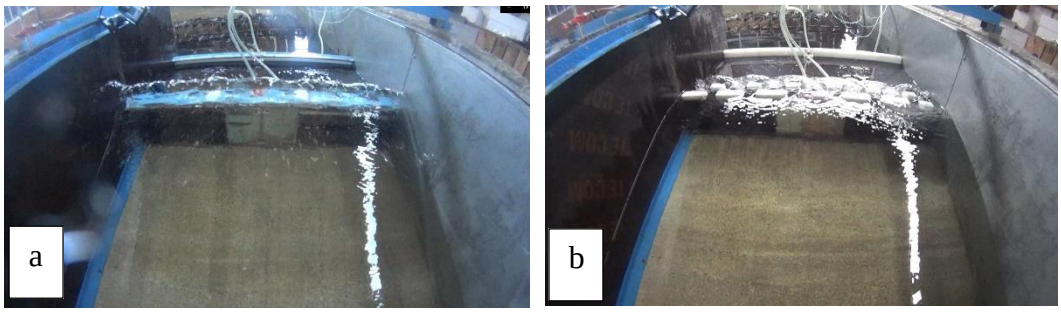

Figure 5.21: Photographs during the experiment **a)** first wave hit on the setup 4 **b)** first wave hit on the setup 6

On the other hand, the effect of the bullnose is discussed for the second row of the storm wall. Simply, the effect of the bullnose was expected to decrease in the measured wave pressure on the gauge 27 which is located at the second row of the storm wall. In Figure 5.22, this expectation is met. In this case, putting bullnose on the top of the superstructure on the seaward storm wall causes pressure increase on front structure but decrease on the landward structures.

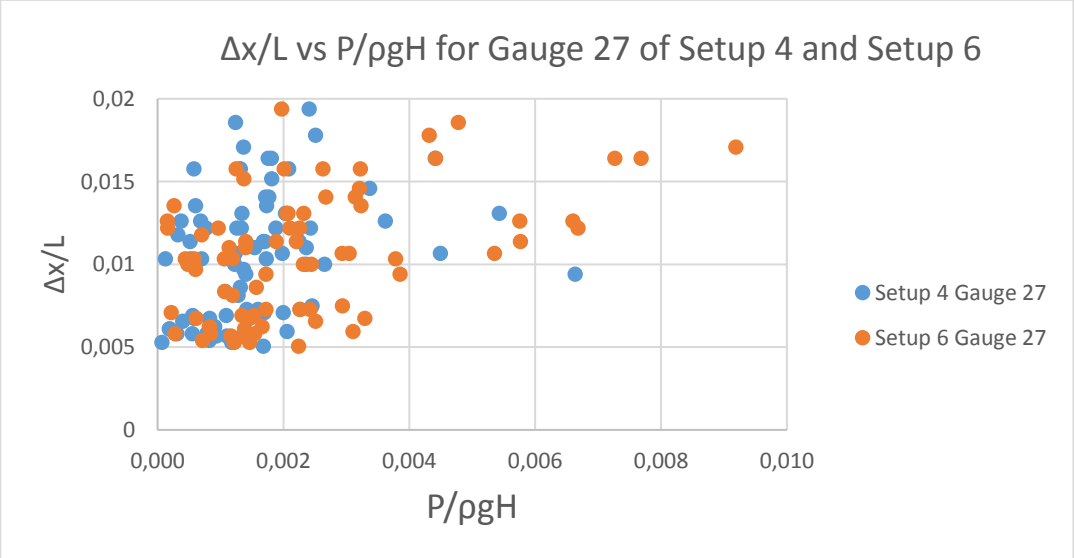

Figure 5.22: Δx/L vs P/ρgH for Gauge 27 of Setup 4 and Setup 6

5.7 Case 7 – Discussion of the Effect of the Wavelength at the Landward Side

In case 6, both Figure 5.23 and 5.24 hints at a possible effect of wave period on the pressure distribution observed at the components especially for the setup 6 which do not have bullnose. Therefore, the effect of wave period (wave length) is discussed to determine if a significant relationship exists or not. To discuss this effect, the landward pressure gauge data of Setup 4, 6 and 7 was analyzed.

As seen in the Figure 5.23, the parameter L is effective on the wave pressure for Setup 6. As wavelength increases, the pressure maximum pressure for the wavelength is decreasing for the gauge at the landward storm wall behind the promenade. This observation is not as clear for Setup 4 which has a bullnose on the seaward storm wall (Figure 5.24).

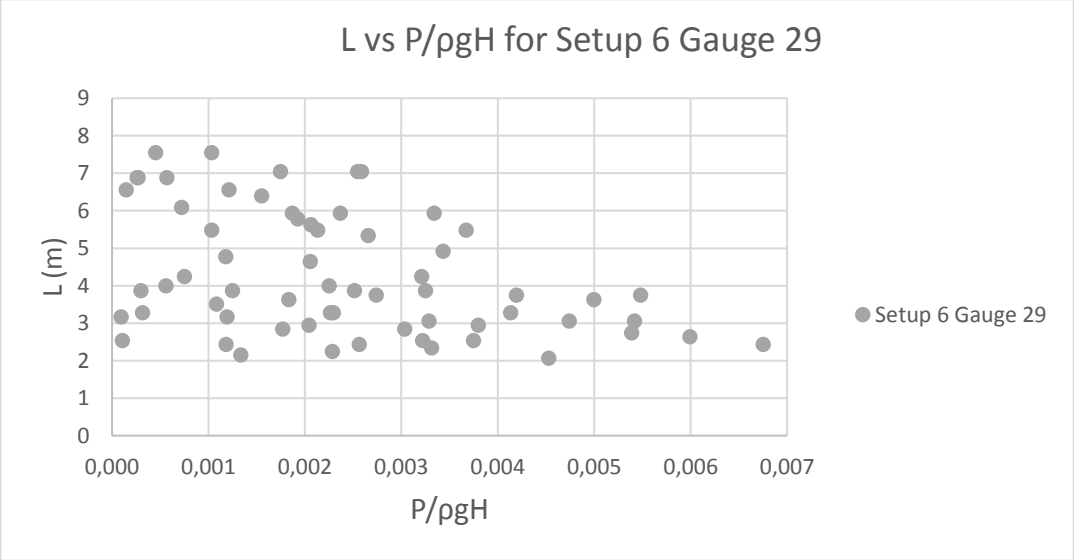

Figure 5.23: L vs P/ρgH for setup 6 gauge 29

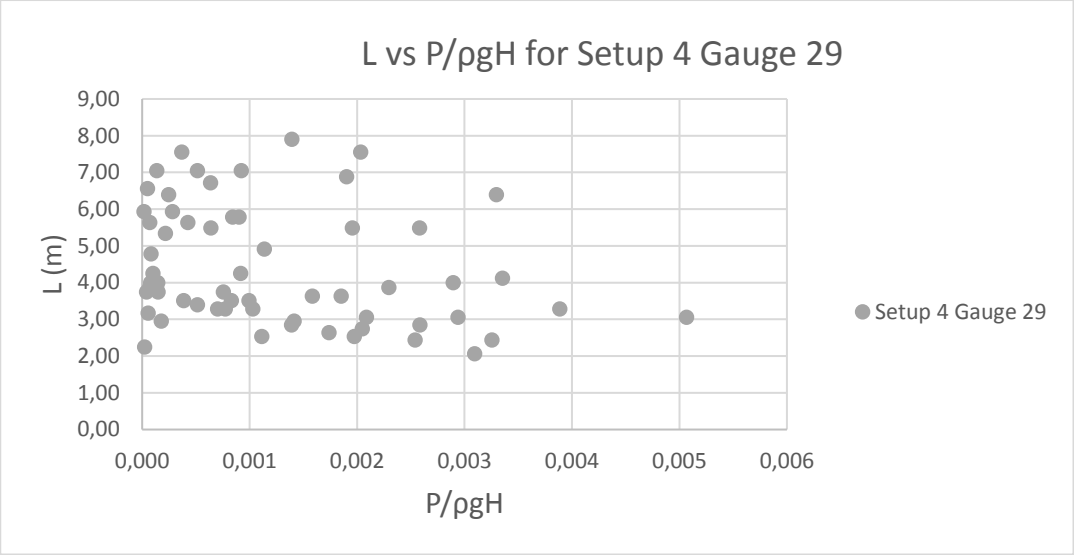

Figure 5.24: L vs P/ρgH for setup 4 gauge 29

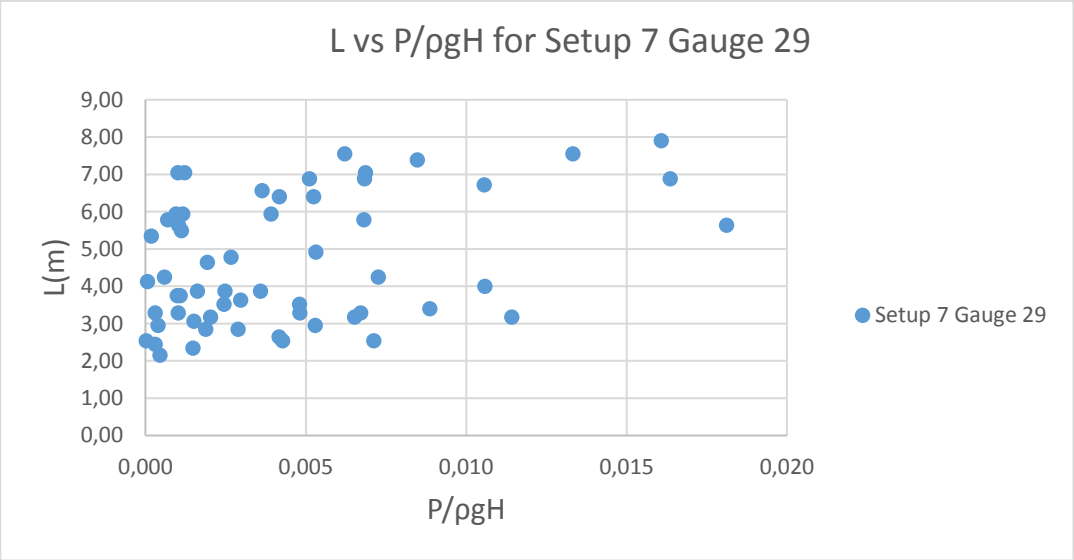

Figure 5.25: L vs P/ρgH for setup 7 gauge 29

On the contrary, in the setup 7 which has no superstructure on the seawall, the wavelength effect is again much clear to observe however the behavior is different than the other two setups stated previously in Figure 5.23 and Figure 5.24. Here as wavelength increases, measured pressures are higher. This reverse behavior is presented much clearly in Figure 5.25 which compares the same pressure gauge data with respect to SWB configuration (Setup 6) without bullnose and no seaside

superstructure (Setup 7). It is possible that with SWB configuration present, waves with larger wavelength are broken down between the gaps and the two rows thus decreasing the overall pressure exerted on the landward storm.

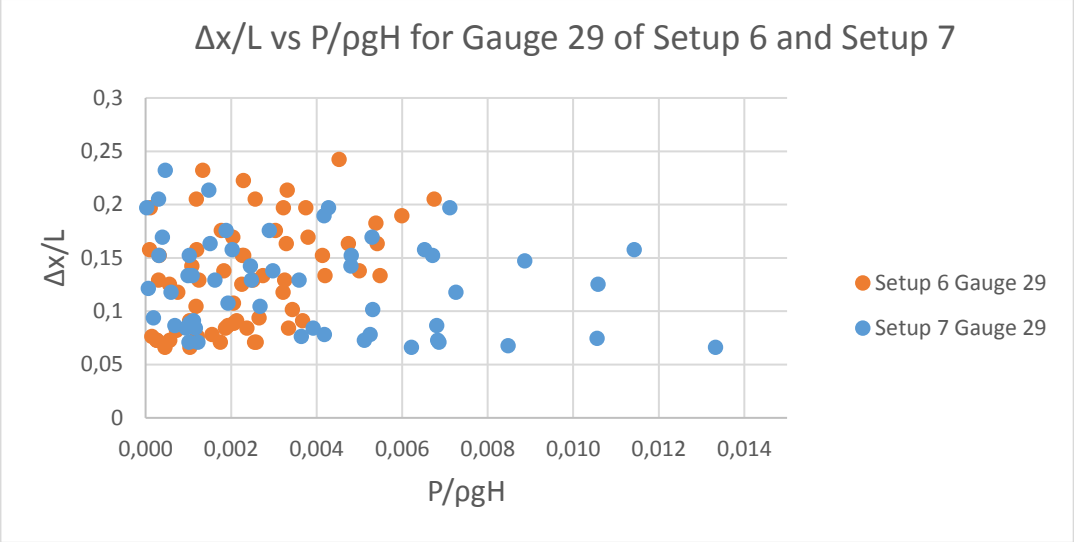

Figure 5.26: Δx/L vs P/ρgH for Gauge 29 of Setup 6 and Setup 7

5.8 Performance of Empirical Formulations - Goda (2010)

In this study, a comparison between Goda (2010) formula and experimental results has been performed for the Setup 11 which is actually not affected by bullnose and any additional superstructure. The comparison of the experimental data and computed data performed for each gauge in setup 11 since pressure values depend on the placement of the gauges. The pressure gauge placements of setup 11 is represented in Figure 5.27 as a reminder.

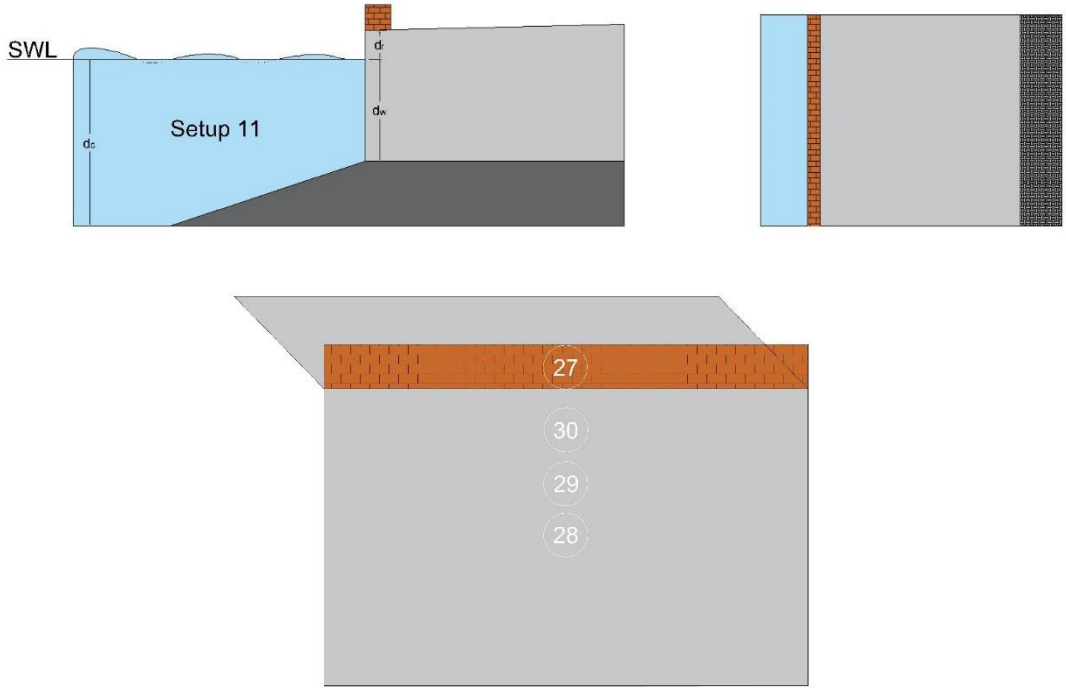

Figure 5.27: Setup 11

Additionally, the comparison is performed for both pressure and impulsive pressure formulas of Goda (2010), presented as equations 3.4 and 3.11. The pressure values are shown in different colors if they are caused by a quasi-static (conventional formula) or an impact load (impulsive formulation) in Figures 5.28 – 5.31. The comparisons show that the empirical formula for impact pressure significantly underestimates the pressure for the gauge located on the storm wall where most of the impact happens (Figure 5.28). This trend is less dominant for the rest of the gauges. In terms of quasi-static loads, Goda (2010) formula performs much better for all the gauges.

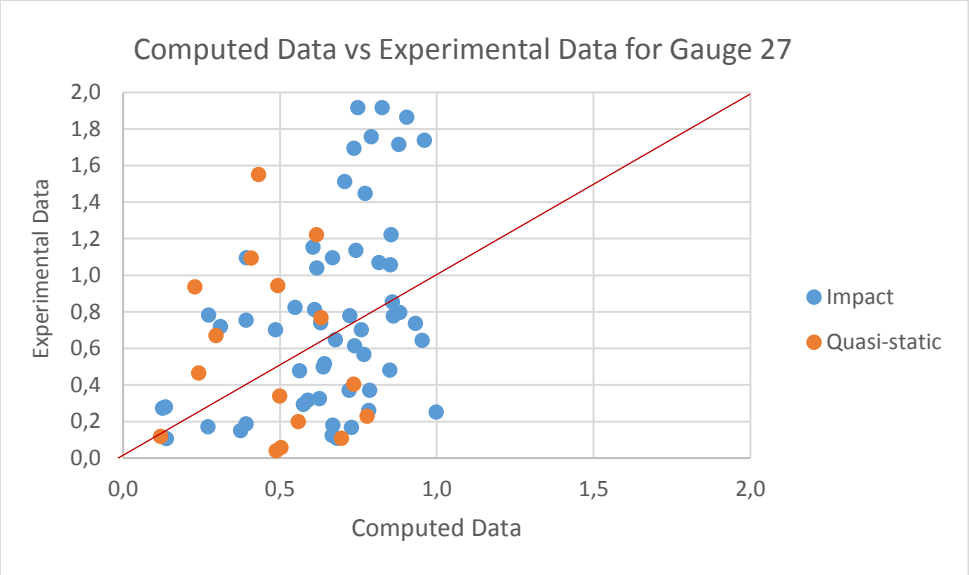

Figure 5.28: Computed data vs experimental data for gauge 27

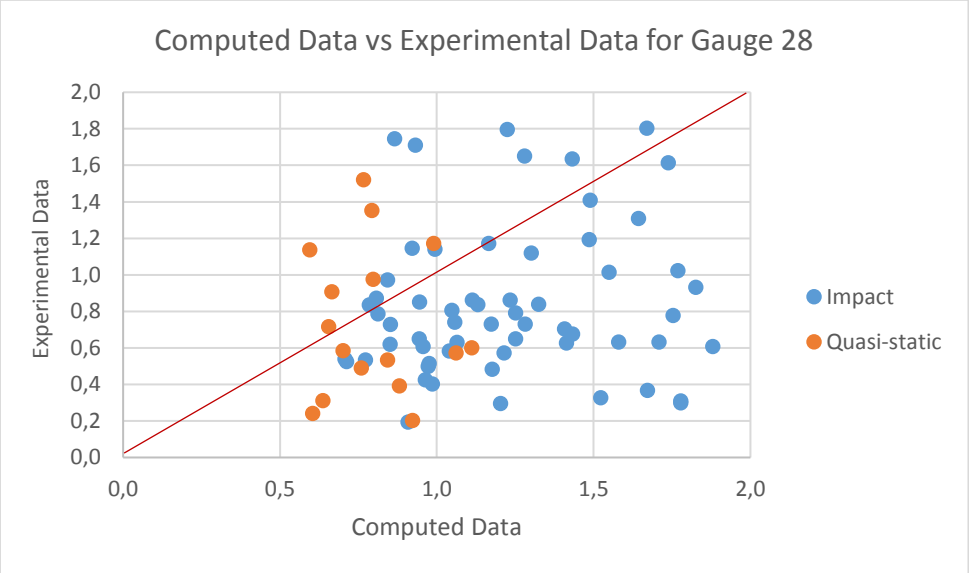

Figure 5.29: Computed data vs experimental data for gauge 28

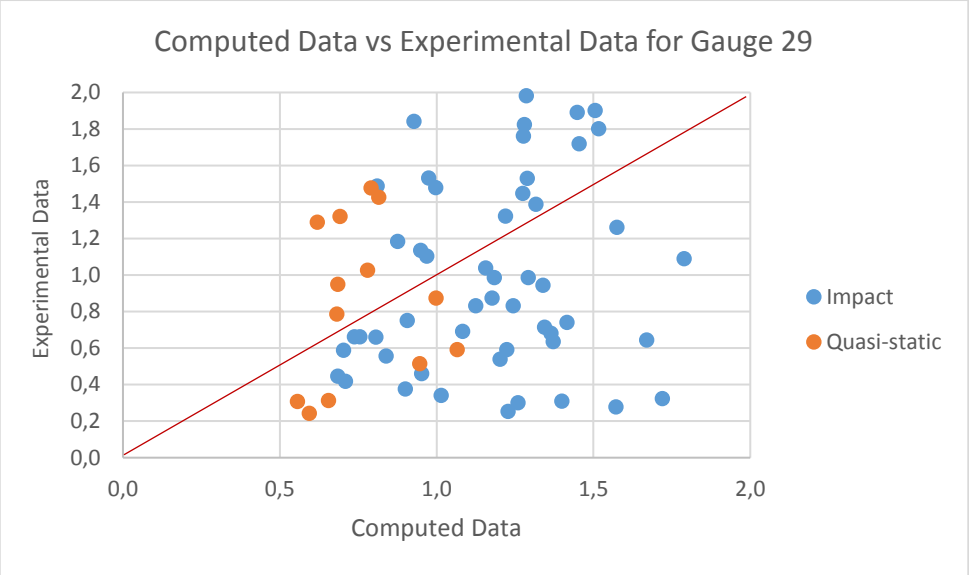

Figure 5.30: Computed data vs experimental data for gauge 29

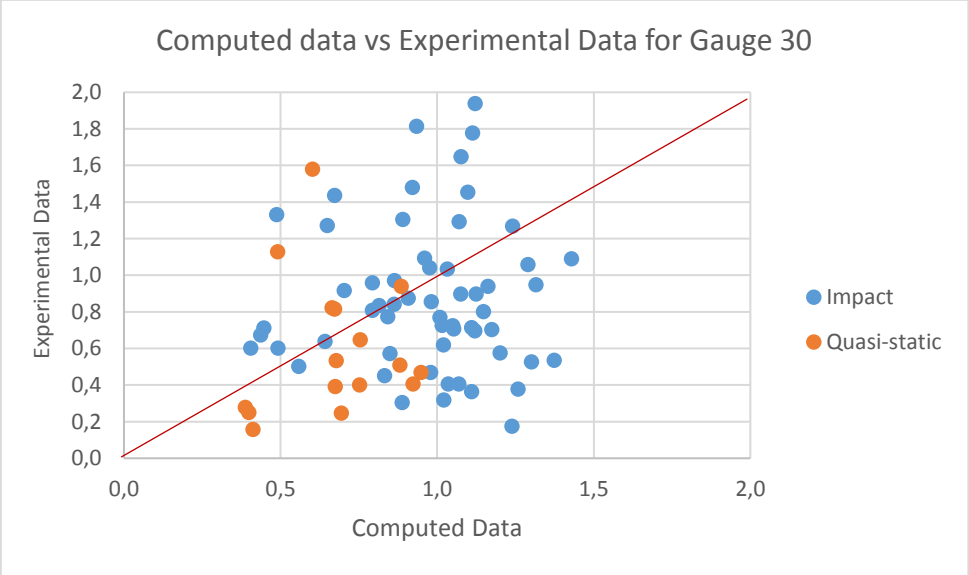

Figure 5.31: Computed data vs experimental data for gauge 30

For the experimental data and Goda (2010) computed data results, Mean Absolute Error (MAE) is calculated for each setup. MAE is a model evaluation for regression models. The MAE of a model with respect to a test set and data is the mean of the absolute values of the errors on all instances in the data. MAE is calculated by:

$$\mathrm{MAE} = \sum_{i=1}^{n} \frac{|y_i - x_i|}{n} \tag{5.1}$$

where x_i is true value, y_i is predicted value and n is total number of the data set. The results of the MAE for each setup are tabulated in the Table 5.

Table 5: Mean absolute error of experimental data and computed data for impact loads

Mean Absolute Error for Impact Loads			
Gauge 27	Gauge 28	Gauge 29	Gauge 30
0.5385	0.5510	0.6238	0.5687

At the end, although there are some related and similar values exist in the comparison between experimental data and Goda (2010) computed data, the error is almost homogenous across the vertical wall.

Table 6: Mean absolute error of experimental data and computed data for quasi-static loads

Mean Absolute Error for Quasistatic Loads			
Gauge 27	Gauge 28	Gauge 29	Gauge 30
0.4491	0.3818	0.5870	0.3238

On the other hand, the mean absolute error for quasi-static loads of the experimental data and computed data is smaller than impact loads for each gauge. For both wave conditions, the performance of the formulas is worse for Gauge 29.

Additionally, the Root Mean Square Error (RMSE) is calculated for the same data set. The RMSE is a way to assess how "good" the model fits the data set, which is a metric that tells us how far apart the predicted values are from the observed values in average.

$$\mathrm{RMSE} = \sqrt{\frac{\sum_{i=1}^{N}(x_i - \hat{x}_i)^2}{N}} \tag{5.5}$$

Table 7: Root mean square error of experimental data and computed data for impact loads

RMSE for Impact Loads			
Gauge 27	Gauge 28	Gauge 29	Gauge 30
0.7483	0.6875	0.7651	0.8684

Table 8: Root mean square error of experimental data and computed data for quasi-static loads

RMSE for Quasistatic Loads			
Gauge 27	Gauge 28	Gauge 29	Gauge 30
0.5190	0.4315	0.7355	0.4016

At the end, all statistical performance analysis shows that the experimental data and computed data with the Goda (2010) are not perfectly fit each other. There is significant scatter especially in the case of impact loads although certain amount to scatter is expected as pressure measurements, especially impact pressure is a very random process. However, this scatter might be differed due to the results of the following limitations. The first reason that why experimental data and computed data do not fit well each other might be the difference in the setup for Goda (2010) and this study. This study does not have any berm geometry due to rubble mound base that exists for vertical breakwaters. This rubble mound base influences the wave hydrodynamics in front of the structure which could have an impact on the comparisons.

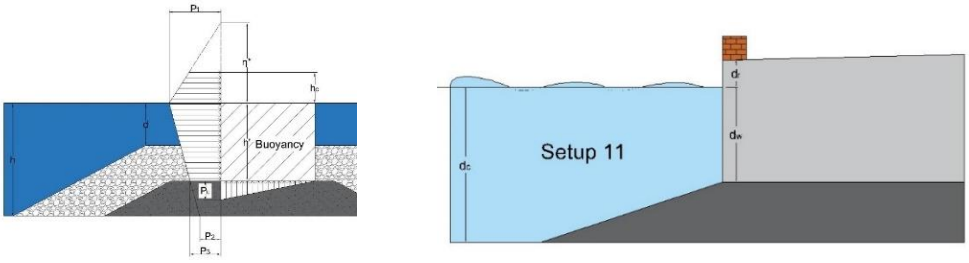

Figure 5.32: Comparison of Goda (2010) setup and experimental setup

Secondly, the results are the maximum pressure values but Goda (2010) represent a pressure value at the time of maximum horizontal force. Therefore, most of the measurement data are expected to be higher than the values of the computed data by Goda (2010). In addition, Goda (2010) does not consider larger impact forces since these forces cause local failures and represents a case for overall failures like structure sliding or overturning. In this study, some of the experimental data are less than the computed values by Goda (2010), which might mean the location of the sensors used in the experiment might not be at the place for that impact to record the higher values. In this case, the places and number of the sensors might limit to represent accurate results.

CHAPTER 6

CONCLUSION

In this chapter, the major and minor findings from the analyses and possible further required studies are presented.

This study analyzes the obtained data from the previously performed experiments belongs to BAP project, BAP-08-11-2015-036 "Assessment of Coastal Floods in Inner Bay of Izmir and A Solution Strategy: Stilling Wave Basin (İzmir İç Körfezde Yaşanan Fırtına Taşkınlarının Araştırılması ve Taşkınların Önlenmesi İçin Bir Öneri: Durgun Dalga Havuzu Modeli)". In this study, the experimental data of BAP project are analyzed focusing on wave pressure for a variety of superstructures located on a vertical seawall. In the experiment, setups differ for investigating the effect and behavior of the wave pressure on the components of the stilling wave basin. Also, the experiments were performed with different hydrodynamic parameters to also see effect and behavior of the wave pressure. This study analyzed the wave pressure data on the seaward, single and doubled rows, and the landward storm wall as individual components as well as the whole SWB structure to determine the magnitude and type of wave pressures.

First, the wave classification is performed by considering the analyzed data outputs based on relative wave height and structure geometry used in PROVERBS (2001) to describe the expected load on the structure and based on the pressure signal to describe the breaking type of the wave. The results show that with PROVERBS definitions, majority of the expected loads are impact. However, based on the pressure sensor, even for similar waves, a variety of pressure signals describing different types of wave breaking is observed. This could be caused by randomness and superstructures on the seaside effecting the pressure profile. However, this requires further studies.

After that, the wave pressure results and discussions are presented. To analyze the research questions, seven different cases are investigated. At the end, the below outcomes are obtained based on the range of the experiment data:

- In the configurations of additional superstructures on the seaside of the SWB, the pressure measurement of the landward storm wall decreases remarkably.
- Storm wall with gaps on the seaside causes more pressure in front of the storm wall.
- Additional superstructure on the seaside of the SWB increases the measured pressure on the front side of the vertical seawall.
- Bullnoses increase the pressure exerted both in front of the vertical structure and seaward storm wall.
- Bullnoses slightly increase the pressure exerted on the landward storm wall but this is not as significant as the seaward storm wall. This effect also might be reduced by SWB configuration.
- Bullnoses located on the seaside decrease the wave pressure on the superstructures that are located behind.

Basically, placing bullnoses as a superstructure on top of the storm wall causes pressure increase on seaward storm wall structure but decrease on the landward structures.

- Increase on the wavelength causes remarkably decrease on the wave pressure unless the waves are not already broken when approached to the pressure sensor.
- The experimental data for the vertical wall setup (Setup 11) is compared with the calculated data by empirical formulations of Goda (2010) including maximum pressures. The results show that the formulas usually underpredict the pressures. However, the scatter is much higher for the maximum pressure dataset. This is due to the limitations structural dissimilarity between experimental setup and Goda (2010), the experimental results are the maximum pressure values at a point while Goda (2010) calculates the

pressure when maximum horizontal forces are observed and Goda (2010) does not consider the high impact forces. At the end, the number of sensors can be increased to have accurate results in further studies.

Overall, the behavior of the wave pressure under different parameters, structures and places are investigated. With this study, also the behavior of the wave pressure under without sloped structure condition for a vertical wall also investigated. At the end, considering the wave pressure at different parts of SWB, the usage of components of the SWB resulted as beneficial in every case except the use of bullnose on the seaside.

At the end, the milestone of the study was to perform the filtering of the pressure signal. Although the pressure measurements have been taken by good technology pressure sensors, the air that generated through the waves affected the sensor and caused noises in the pressure signal. Moreover, the breaking classifications has been performed without the air trap considerations.

In general, the bigger wave pressures are occurred in setup 7 and setup 8. It might be caused as there is no superstructure on the seaward (only promenade exists). However, the effect of the promenade width should be considered as an extended further study. Additionally, the pressure on the landward storm wall of wave pressure should be studied further considering the double storm wall with gaps considering the gap width and second row placement. The absolute effect of the bullnose at the landward storm wall might be determined with the optimization in experiment setups. Lastly, the experimental results and empirical formula results are not matched. This is another topic to be studied further since they are not matched as much as expected. The present study may be addressed for the further studies for the components and applications of SWB.

REFERENCES

Altomare, C., Verwaest, T., Suzuki, T., & Trouw, K. (2014). Characterization of wave impacts on curve faced storm return walls within a stilling wave basin concept. Coastal Engineering Proceedings.

Anand, K. V., Sundar, V., & Sannasiraj, S. A. (2011). Hydrodynamic characteristics of curved-front seawall models compared with vertical seawall under regular waves. Journal of Coastal Research, 27(6), 1103-1112.

Castellino, M., Sammarco, P., Romano, A., Martinelli, L., Ruol, P., Franco, L., & de Girolamo, P. (2018). Large impulsive forces on recurved parapets under non-breaking waves. A numerical study. Coastal Engineering, 136, 1–15. https://doi.org/10.1016/j.coastaleng.2018.01.012

EurOtop, (2016): Van der Meer, J.W., Allsop, N.W.H., Bruce, T., De Rouck, J., Kortenhaus, A., Pullen, T., Schüttrumpf, H., Troch, P., Zanuttigh, B. (Eds.), Manual on Wave Overtopping of Sea Defences and Related Structures. An Overtopping Manual Largely Based on European Research, but for Worldwide Application. www.overtopping-manual.com.

Geeraerts, J., De Rouck, J., Beels, C., Gysens, S., De Wolf, P. (2006). Reduction of wave overtopping at seadikes: stilling wave basin (SWB). Proc. 30th Int. Conf. On Coastal Engineering. World Scientific, 4680–4691. https://doi.org/10.1142/9789812709554_0392.

Goda, Y. (2010). Random seas and design of maritime structures, second edition. World Scientific Publishing Company.

Hattori, M., Arami, A., & Yui, T. (1994). Wave impact pressure on vertical walls under breaking waves of various types. Coastal Engineering, 22(1-2), 79-114.

Hiroi, I. (1919). On a method of estimating the force of waves. Memoirs of Engineering Facility, Imperial University of Tokyo, 10(1), 19.

Hull, P., & Müller, G. (2002). An investigation of breaker heights, shapes and pressures. Ocean Engineering, 29(1), 59-79.

Kirkgöz, M. S. (1991). Impact pressure of breaking waves on vertical and sloping walls. Ocean Engineering, 18(1-2), 45-59.

Kisacik, D., Ozyurt Tarakcioglu, G., & Cappietti, L. (2022). Adaptation measures for seawalls to withstand sea-level rise. Ocean Engineering, 250. https://doi.org/10.1016/j.oceaneng.2022.110958

Kisacik, D., Ozyurt Tarakcioglu, G., & Baykal, C. (2019). Stilling wave basins for overtopping reduction at an urban vertical seawall – The Kordon seawall at Izmir. Ocean Engineering, 185, 82–99. https://doi.org/10.1016/j.oceaneng.2019.05.033

Kisacik, D., Troch, P., & van Bogaert, P. (2012). Description of loading conditions due to violent wave impacts on a vertical structure with an overhanging horizontal cantilever slab. Coastal Engineering, 60(1), 201–226. https://doi.org/10.1016/j.coastaleng.2011.10.001

Kortenhaus, A., Oumeraci, H., Allsop, N. W. H., McConnell, K. J., Van Gelder, P. H. A. J. M., Hewson, P. J., ... & Vicinanza, D. (1999). Wave impact loads-pressures and forces. Final Proceedings, MAST III, PROVERBS-Project: Vol. IIa: Hydrodynamic Aspects.

Molines, J., Bayon, A., Gómez-Martín, M. E., & Medina, J. R. (2019). Influence of Parapets on Wave Overtopping on Mound Breakwaters with Crown Walls. Sustainability (Switzerland), 11(24). https://doi.org/10.3390/su11247109

Marukami, K., Irie, I., & Kamikubo, Y. (1996). Experiments on a non-wave overtopping type of seawall. Coastal Engineering Proceedings, (25).

Oumeraci, H., Kortenhaus, A., Allsop, W., de Groot, M., Crouch, R. O. G. E. R., Vrijling, H., & Voortman, H. (2001). Probabilistic design tools for vertical breakwaters. CRC Press.

Oumeraci, H., Klammer, P., & Partenscky, H. W. (1993). Classification of breaking wave loads on vertical structures. Journal of waterway, port, coastal, and ocean engineering, 119(4), 381-397.

Ozyurt Tarakcioglu, G., Baykal, C., & Kisacik, D. (2015). İzmir İç Körfezde yaşanan fırtına taşkınlarının araştırılması ve taşkınların önlenmesi için bir öneri: Durgun Dalga Havuzu modeli. (Issue https://hdl.handle.net/11511/62012).

Ravindar, R. & Sriram, V. (2021). Impact pressure and forces on a vertical wall with different types of parapet. Journal of Waterway, Port, Coastal, and Ocean Engineering, 147(3), 04021007.

Ravindar, R., Sriram, V., Schimmels, S., & Stagonas, D. (2019). Characterization of breaking wave impact on vertical wall with recurve. ISH Journal of Hydraulic Engineering, 25(2), 153-161.

Sainflou, G. (1928). Essai sur les digues maritimes verticales. Annales de ponts et chaussées, vol 98, tome II, 1928 (4) pp 5-48.

Takahashi, S. (2002). Design of vertical breakwaters. PHRI reference document nr. 34.

Viriyakijja, K., & Chinnarasri, C. (2015). Wave Flume Measurement Using Image Analysis. Aquatic Procedia, 4, 522–531. https://doi.org/10.1016/j.aqpro.2015.02.068

Zanuttigh, B., & Formentin, S. M. (2018). Reduction of the wave overtopping discharge at dikes in presence of crown walls with bullnoses. Coastal Engineering Proceedings, (36), 110-110.

APPENDICES

A. Wave Classification Table for Wave Loadings

Table 9: Oumeraci et al. (2001) classification

		Oumeraci (2001) Classification	
		H/hs	Status
1	Wave 1	0.1877	Quasistatic
	Wave 2	0.2302	Quasistatic
	Wave 3	0.4004	Impact
	Wave 4	0.3960	Impact
2	Wave 1	0.4268	Impact
	Wave 2	0.5565	Impact
	Wave 3	0.4375	Impact
	Wave 4	0.3379	Quasistatic
3	Wave 1	0.4016	Impact
	Wave 2	0.5575	Impact
	Wave 3	0.6313	Impact
	Wave 4	0.5379	Impact
4	Wave 1	0.4103	Impact
	Wave 2	0.5278	Impact
	Wave 3	0.4433	Impact
	Wave 4	0.4006	Impact
5	Wave 1	0.3238	Quasistatic
	Wave 2	0.4501	Impact
	Wave 3	0.4238	Impact
	Wave 4	0.3508	Impact
6	Wave 1	0.2957	Quasistatic
	Wave 2	0.3851	Impact
	Wave 3	0.3168	Quasistatic
	Wave 4	0.2560	Quasistatic
7	Wave 1	0.4700	Impact
	Wave 2	0.5405	Impact
	Wave 3	0.4654	Impact
	Wave 4	0.3633	Impact
8	Wave 1	0.4079	Impact
	Wave 2	0.8039	Impact
	Wave 3	0.6635	Impact
	Wave 4	0.7339	Impact
9	Wave 1	0.3574	Impact
	Wave 2	0.7337	Impact
	Wave 3	0.7253	Impact
	Wave 4	0.7120	Impact

Table 9: Oumeraci et al. (2001) classification (cont'd)

10	Wave 1	0.5432	Impact
	Wave 2	0.4463	Impact
	Wave 3	0.3668	Impact
	Wave 4	0.3338	Quasistatic
11	Wave 1	0.3179	Quasistatic
	Wave 2	0.5990	Impact
	Wave 3	0.5005	Impact
	Wave 4	0.4106	Impact
12	Wave 1	0.1951	Quasistatic
	Wave 2	0.3652	Impact
	Wave 3	0.5449	Impact
	Wave 4	0.3534	Impact
13	Wave 1	0.0081	Quasistatic
	Wave 2	0.2774	Quasistatic
	Wave 3	0.3340	Quasistatic
	Wave 4	0.5237	Impact
14	Wave 1	0.7402	Impact
	Wave 2	0.6936	Impact
	Wave 3	0.5577	Impact
	Wave 4	0.8036	Impact
15	Wave 1	0.4649	Impact
	Wave 2	0.4659	Impact
	Wave 3	0.4070	Impact
	Wave 4	0.5145	Impact
16	Wave 1	0.3916	Impact
	Wave 2	0.7116	Impact
	Wave 3	0.5335	Impact
	Wave 4	0.6217	Impact
17	Wave 1	0.4582	Impact
	Wave 2	0.8113	Impact
	Wave 3	0.6051	Impact
	Wave 4	0.7344	Impact
18	Wave 1	0.3419	Quasistatic
	Wave 2	0.4286	Impact
	Wave 3	0.6590	Impact
	Wave 4	0.5486	Impact
19	Wave 1	0.3826	Impact
	Wave 2	0.4428	Impact
	Wave 3	0.3118	Quasistatic
	Wave 4	0.3295	Quasistatic
20	Wave 1	0.4919	Impact
	Wave 2	0.4880	Impact
	Wave 3	0.3851	Impact
	Wave 4	0.4169	Impact

B. Wave Heights Table

Table 10: Wave heights

Wave Heights (m)					
Wave	**Dimension**	**Gauge 2**	**Wave**	**Dimension**	**Gauge 2**
1	H_1	0.0375	11	H_1	0.0518
	H_2	0.0460		H_2	0.0976
	H_3	0.08		H_3	0.08
	H_4	0.08		H_4	0.07
2	H_1	0.0772	12	H_1	0.0281
	H_2	0.1007		H_2	0.0526
	H_3	0.08		H_3	0.08
	H_4	0.06		H_4	0.05
3	H_1	0.0655	13	H_1	0.0010
	H_2	0.0909		H_2	0.0347
	H_3	0.10		H_3	0.04
	H_4	0.09		H_4	0.07
4	H_1	0.0591	14	H_1	0.0785
	H_2	0.0760		H_2	0.0735
	H_3	0.06		H_3	0.06
	H_4	0.06		H_4	0.09
5	H_1	0.0648	15	H_1	0.0758
	H_2	0.0900		H_2	0.0759
	H_3	0.08		H_3	0.07
	H_4	0.07		H_4	0.08
6	H_1	0.0535	16	H_1	0.0564
	H_2	0.0697		H_2	0.1025
	H_3	0.06		H_3	0.08
	H_4	0.05		H_4	0.09
7	H_1	0.0766	17	H_1	0.0573
	H_2	0.0881		H_2	0.1014
	H_3	0.08		H_3	0.08
	H_4	0.06		H_4	0.09
8	H_1	0.0587	18	H_1	0.0362
	H_2	0.1158		H_2	0.0454
	H_3	0.10		H_3	0.07
	H_4	0.11		H_4	0.06
9	H_1	0.0447	19	H_1	0.0624
	H_2	0.0917		H_2	0.0722
	H_3	0.09		H_3	0.05
	H_4	0.09		H_4	0.05
10	H_1	0.0983	20	H_1	0.0708
	H_2	0.0808		H_2	0.0703
	H_3	0.07		H_3	0.06
	H_4	0.06		H_4	0.06

C. Wave Periods Table

Table 11: Wave periods

Wave Periods (s)					
Wave	**Dimension**	**Gauge 2**	**Wave**	**Dimension**	**Gauge 2**
1	T_1	1.6	11	T_1	2.6
	T_2	1.3		T_2	2.2
	T_3	1.2		T_3	2.2
	T_4	1.3		T_4	2.1
2	T_1	1.6	12	T_1	1.4
	T_2	1.4		T_2	1.2
	T_3	1.5		T_3	1.2
	T_4	1.3		T_4	1.2
3	T_1	1.6	13	T_1	0.4
	T_2	1.5		T_2	2.4
	T_3	1.5		T_3	1.4
	T_4	1.5		T_4	1.2
4	T_1	1.5	14	T_1	1.7
	T_2	1.2		T_2	1.6
	T_3	1.3		T_3	1.6
	T_4	1.2		T_4	1.7
5	T_1	1.6	15	T_1	1.7
	T_2	1.4		T_2	1.6
	T_3	1.4		T_3	1.6
	T_4	1.3		T_4	1.7
6	T_1	1.5	16	T_1	2.4
	T_2	1.2		T_2	1.9
	T_3	1.3		T_3	1.7
	T_4	1.3		T_4	1.9
7	T_1	1.5	17	T_1	2.5
	T_2	1.4		T_2	1.9
	T_3	1.4		T_3	1.7
	T_4	1.3		T_4	1.9
8	T_1	2.5	18	T_1	2.4
	T_2	2.0		T_2	1.4
	T_3	1.8		T_3	1.2
	T_4	1.9		T_4	1.4
9	T_1	2.6	19	T_1	1.5
	T_2	1.7		T_2	1.5
	T_3	1.6		T_3	1.5
	T_4	1.6		T_4	1.4
10	T_1	2.2	20	T_1	1.6
	T_2	2.2		T_2	1.6
	T_3	2.1		T_3	1.6
	T_4	2.2		T_4	1.7

D. Wave Classification Table for Breaking Cases

Table 12: Wave classification table for breaking cases according to gauge 30

Wave	SETUP 1	SETUP 2	SETUP 4	SETUP 6	SETUP 7	SETUP 11
1	NB	NB	NB	NB	NB	NB
	NB	NB	NB	NB	NB	NB
	NB	BW	NB	NB	NB	NB
	NB	BW	BW	SBW	NB	NB
2	NB	NB	NB	NB	NB	NB
	NB	NB	NB	NB	NB	NB
	NB	BW	NB	NB	NB	NB
	SBW	BW	BW	NB	NB	SBW
3	NB		NB	NB	NB	NB
	NB		NB	NB	NB	NB
	SBW		SBW	NB	NB	SBW
	SBW		SBW	SBW	SBW	SBW
4	NB	NB	NB	NB	NB	NB
	NB	NB	NB	NB	NB	NB
	SBW	SBW	SBW	NB	NB	NB
	SBW	SBW	SBW	BW	NB	SBW
5	NB	NB	NB	NB	NB	NB
	NB	NB	NB	NB	NB	NB
	SBW	BW	BW	NB	NB	NB
	SBW	SBW	BW	BW	NB	SBW
6	NB	NB	NB	NB	NB	NB
	NB	NB	NB	NB	NB	NB
	SBW	SBW	SBW	SBW	NB	NB
	SBW	SBW	SBW	SBW	NB	SBW
7	NB	NB	NB	NB	NB	NB
	NB	NB	SBW	NB	NB	NB
	SBW	SBW	SBW	BW	NB	SBW
	SBW	SBW	SBW	BW	BW	BW
8	NB	SBW	NB	NB	NB	NB
	NB	BW	SBW	SBW	NB	SBW
	NB	SBW	NB	SBW	NB	SBW
	NB	BW	SBW	SBW	NB	SBW
9	NB	NB	NB	NB	NB	NB
	NB	SBW	SBW	NB	NB	NB
	SBW	BW	BW	NB	NB	SBW
	NB	SBW	SBW	NB	NB	BW

Table 12: Wave classification table for breaking cases according to gauge 30 (cont'd)

10	NB	NB	NB	NB	NB	NB
	NB	NB	NB	NB	NB	NB
	NB	NB	NB	NB	NB	NB
	NB	NB	NB	NB	NB	NB
11	NB	NB	NB	NB	NB	NB
	NB	NB	NB	NB	NB	NB
	NB	NB	NB	NB	NB	NB
	NB	NB	NB	NB	NB	NB
12	NB	NB	NB	NB	NB	NB
	SBW	NB	BW	NB	NB	NB
	SBW	SBW	BW	BW	NB	SBW
	BW	SBW	BW	BW	NB	BW
13	NB	NB	NB	NB		NB
	SBW	NB	NB	NB		NB
	SBW	SBW	SBW	SBW		SBW
	SBW	SBW	NB	BW		BW
14	SBW	NB	NB	NB	NB	NB
	BW	SBW	BW	SBW	NB	NB
	SBW	BW	BW	SBW	SBW	SBW
	SBW	SBW	SBW	SBW	NB	BW
15	SBW	NB	NB	NB	NB	NB
	BW	NB	SBW	BW	NB	NB
	SBW	SBW	BW	BW	BW	BW
	SBW	BW	BW	SBW	BW	BW
16	NB	NB	SBW	NB	NB	NB
	SBW	SBW	SBW	SBW	NB	SBW
	SBW	SBW	SBW	NB	SBW	SBW
	SBW	SBW	SBW	SBW	NB	SBW
17	NB	NB	SBW	NB	NB	NB
	SBW	SBW	SBW	BW	NB	SBW
	SBW	SBW	SBW	SBW	SBW	SBW
	SBW	SBW	SBW	SBW	NB	SBW
18	NB	NB	NB	NB	NB	NB
	SBW	NB	NB	SBW	NB	NB
	SBW	NB	NB	SBW	NB	NB
	SBW	NB	NB	SBW	NB	SBW
19	SBW	NB	NB	SBW	SBW	NB
	BOW	BW	BW	NB	NB	SBW
	BOW	BOW	NB	NB	SBW	NB
	BOW	BOW	SBW	NB	SBW	SBW

Table 12: Wave classification table for breaking cases according to gauge 30 (cont'd)

20		BW	SBW	BW	BOW	NB
	NB	BOW	BW		BOW	BW
	SBW	BOW	BOW	BW	BOW	SBW
	BOW	BOW	BOW	SBW	BOW	BOW